A PRECISION STUDY OF THE MOLYBDENUM AND TUNGSTEN $K\alpha_1$ X-RAY LINES, AND A MEASUREMENT OF THE REFLECTING PROPERTIES OF THE (310) PLANES OF QUARTZ; BY THE METHOD OF THE TWO CRYSTAL X-RAY SPECTROMETER

Thesis by

William Junius West

In Partial Fulfillment of the Requirements

For the Degree of

Doctor of Philosophy

California Institute of Technology

Pasadena, California

1949

ACKNOWLEDGMENTS

The success in achieving the high accuracy of the measurements obtained in this study was made possible by the high precision two crystal x-ray spectrometer designed and built by Professor J. W. M. DuMond assisted by Mr. Douglas Marlow.

It is with great preasure that I acknowledge my indebtedness to Professor DuMond for his advice and guidance on many of the experimental techniques developed in this study. I appreciate his interest and his suggestion of this thesis topic and the opportunity it has given me of associating with him.

Mr. Leon Shenfil assisted in obtaining part of the experimental data.

ABSTRACT

Using a precision two crystal x-ray spectrometer, the $K\alpha_1$ lines of molybdenum and tungsten and the (310) planes of quartz were studied primarily for the purpose of calibrating the curved crystal gamma ray spectrometer, designed and built by J. W. M. DuMond, so as to help provide a precision linkage between the gamma and x-ray regions. Absolute determinations of the Bragg angles for $MoK\alpha_1$ and $WK\alpha_1$ reflected from the (310) planes of quartz are described. These were undertaken (1) to standardize the tungsten K spectrum with higher accuracy in terms of the Siegbahn x-ray scale of wavelengths, and (2) to yield on this scale a precision determination of the grating constant of the quartz (310) planes. The wavelength for the $WK\alpha_1$ line was found to be

$$\lambda_{K\alpha_1} = 208.575 \pm 0.008 \text{ x.u. (Siegbahn scale)}$$

The grating constant of the quartz (310) planes was determined as

$$d_{18^\circ} = 1177.637 \pm 0.020 \text{ x.u. (Siegbahn scale)}$$

The reflecting properties of the (310) planes of quartz in the unstressed condition were measured experimentally in the wavelength range $0.123\text{Å} \leq \lambda \leq 0.710\text{Å}$ and a comparison made to the results calculated from the theoretical diffraction patterns for the particular quartz crystals used. It was found that the integrated reflecting power did not decrease with the first power of the wavelength (as predicted by theory), but to a power slightly less than unity. This result differs from the work of David A. Lind who found that the integrated reflecting power decreased as λ^2 for an identical quartz plate to the ones used here, but in the stressed condition as found in the curved crystal spectrometer.

The development of a xenon filled Geiger counter is presented. This counter was used as a highly efficient detector of the x-rays.

TABLE OF CONTENTS

TITLE

PART I

INTRODUCTION

The accuracy of a curved crystal focussing spectrometer is determined, in part, by the accuracy of the wavelength standard used to calibrate the instrument, or the grating constant of the crystal planes used. Generally both are desired.

The two meter curved crystal focussing spectrometer designed and built by J. W. M. DuMond[1] for use in the gamma ray region employs the (310) planes of quartz. These quartz planes are three inches square and 1 mm thick; they were chosen because of their strength, and because their (310) planes have moderately good reflecting power and a lattice spacing of only 1.177Å. This small spacing gives large dispersion, which is desirable when the spectrometer is used in the gamma ray region. Because of the large dispersion it is not mechanically desirable to build the instrument large enough to include the MoK_{α_1} line, which is very accurately known, for a wavelength standard. The WK_{α_1} line is used instead.

This study is concerned with (1) an accurate determination of the WK_{α_1} line and the (310) grating spacing of quartz for calibrating the curved crystal gamma ray spectrometer; and (2) a measurement of the properties of the diffraction pattern from the (310) planes of quartz (in the unstressed condition) in the wavelength range $0.123\text{Å} \leq \lambda \leq 0.710\text{Å}$. The reflecting power of a crystal in important when the problem of intensities is considered for the curved crystal spectrometer used in the gamma ray region. These quartities are determined by the method of the two crystal x-ray spectrometer. The crystal

plates tested are presumably identical to the ones used in the gamma ray spectrometer, having been cut from the same block of quartz. The reflecting power vs. λ of one of the plates has been measured by David A. Lind[2] in the stressed condition as found in the curved crystal spectrometer. The reflecting power vs. λ studied here is to give additional information to the curved crystal study to help determine whether or not the mechanism of reflection is altered when the crystal is curved.

Part II will treat the theory of reflection from plane, unstressed, perfect crystals; and also plane, unstressed crystals with one disorder, the mosaic crystal; this is usually the most important type of disorder.

Part III will treat the theory of the two crystal x-ray spectrometer. As will be shown there, it is impossible, with the method used, to obtain the single crystal diffraction pattern from the result of the two crystal x-ray spectrometer. The method will be to use the theoretical diffraction patterns of a single crystal and from these derive the theoretical results for the two crystal x-ray spectrometer. These will be compared to the experimental results.

Part IV treats the experimental apparatus and method.

Part V discusses the results for wavelength determination of the Tungsten K_{α_1} line, and the determination of the grating constant for the (310) planes of quartz.

Part VI discusses the two crystal x-ray diffraction patterns obtained and gives a comparison to the diffraction patterns expected from theory.

PART II

X-RAY DIFFRACTION IN CRYSTALS

It has been shown by many investigators that crystals vary considerably in the degree to which they approach a perfect crystal. By a perfect crystal is meant one in which the atomic periodicity is continued with no interruptions over the extent of the crystal. The degree of perfectness of a crystal can be determined by comparing its x-ray diffraction pattern with theory. Investigations have found only a few crystals that show good agreement[3],[4] and then only for λ greater than 0.710Å. The accepted reason for the majority of nonconformity with the theory of a perfect crystal is that disorders exist within the crystal. These disorders are usually classified as substitution or displacement. By substitution is meant the change of the scattering power of a given atomic site, generally by occupation by a foreign atom. By displacement is meant that the scattering sites are not periodic but are displaced. Small differences of electronic configuration from atom to atom are neglected. Thermal motion adds with Compton scattering to increase background scattering. The disorder that is ascribed to most of the discrepancy is that of the mosaic structure. This type of crystal is composed of many small perfect crystal blocks whose directions deviate slightly from the mean.

The diffraction of x-rays from perfect and mosaic crystals will be considered here. The method will follow essentially that of Zachariasen,[5] M. v. Laue,[6] and Brillouin.[7]

The development will not be rigorous as this is found in the texts cited. The method will be to outline the steps so that the

terms in the resulting diffraction equation will be defined and can be used. The perfect crystal is treated first and then extended to the mosaic structure.

RECIPROCAL LATTICE

It has been found that the use of a reciprocal lattice greatly simplifies the problem of diffraction. In the direct lattice

$$\bar{A}_L = L_1\bar{a}_1 + L_2\bar{a}_2 + L_3\bar{a}_3$$

gives the position of the lattice points where L_1, L_2, L_3 are integers and $\bar{a}_1$, $\bar{a}_2$, $\bar{a}_3$ give the directions of the three oblique coordinates and their magnitude gives the length of the sides of the parallelopiped forming the unit cell. A point within the unit cell is given by

$$\bar{r} = x_1\bar{a}_1 + x_2\bar{a}_2 + x_3\bar{a}_3$$

where $|x_j| < 1$. The equation of a crystal face is given by

$$h_1x_1 + h_2x_2 + h_3x_3 - k = 0$$

where the ratios $h_1:h_2:h_3$ are called the Miller indices written $(h_1\ h_2\ h_3)$. The unit normal to this face, drawn outwards is given by

$$\bar{u}_h = \frac{\bar{B}_h}{|\bar{B}_h|}\ ;\ \text{where}\ \bar{B}_h = h_1\bar{b}_1 + h_2\bar{b}_2 + h_3\bar{b}_3 \qquad 2.1$$

which defines the set of reciprocal vectors $\bar{b}_1$, $\bar{b}_2$, $\bar{b}_3$ where

$$\bar{b}_1 = \frac{\bar{a}_2 \times \bar{a}_3}{(\bar{a}_1\bar{a}_2\bar{a}_3)},\ \bar{b}_2 = \frac{\bar{a}_3 \times \bar{a}_1}{(\bar{a}_1\bar{a}_2\bar{a}_3)},\ \bar{b}_3 = \frac{\bar{a}_1 \times \bar{a}_3}{(\bar{a}_1\bar{a}_2\bar{a}_3)}$$

$(\bar{a}_1\bar{a}_2\bar{a}_3)$ is the volume of the unit cell, and

$$a_j \cdot b_k = \delta_{jk}\begin{cases} 0 & j \neq k \\ 1 & j = k \end{cases}$$

For the particular sequences of planes (H_1 H_2 H_3) the normal to this sequence is $\bar{B}_H = H_1\bar{b}_1 + H_2\bar{b}_2 + H_3\bar{b}_3$ and the spacing between planes is $d_H = \frac{1}{|\bar{B}_H|}$. Thus for each sequence of planes in the direct lattice there exists a vector $\bar{B}_H$ based on the reciprocal vectors $\bar{b}_1$, $\bar{b}_2$, $\bar{b}_3$. The assembly of points given by the vectors $\bar{B}_H$ corresponding to all the sequences of planes in the direct lattice is called the reciprocal lattice.

PERIODIC FUNCTIONS

Because the variation of a physical property from point to point in a crystal is periodic, a function representing such a property must satisfy

$$\Omega(x_1x_2x_3) = \Omega(x_1 + L_1, x_2 + L_2, x_3 + L_3) \qquad 2.2$$

A convenient method of representation is by expanding the function in a Fourier series

$$\Omega(x_1x_2x_3) = \sum_{-\infty}^{\infty}\sum\sum \Omega_{H_1H_2H_3} e^{-i2\pi(H_1x_1 + H_2x_2 + H_3x_3)}$$

where Ω_H is usually complex. Because $\bar{a}_j \cdot \bar{b}_k = \delta_{jk}$ this can be written

$$\Omega(\bar{r}) = \Omega_H e^{-i2\pi(\bar{B}_H \cdot \bar{r})} \qquad 2.3$$

For $\bar{r}' = \bar{r} + L_1\bar{a}_1 + L_2\bar{a}_2 + L_3\bar{a}_3$

$$\bar{B}_H \cdot \bar{r}' = \bar{B}_H \cdot \bar{r} + L_1H_1 + L_2H_2 + L_3H_3 = \bar{B}_H \cdot \bar{r} + \text{integer}$$

and the condition of Eq. 2.2 is satisfied.

The coefficients of the Fourier series are determined by multiplying Eq. 2.3 by $e^{i2\pi\bar{B}_H' \cdot \bar{r}}$ and integrating over the unit cell. This is possible because of the orthogonality of the exponential functions.

$$\mathcal{Q}_H = \frac{1}{V}\int_v \mathcal{Q} e^{i2\pi(\bar{B}_H \cdot \bar{r})} dv \qquad 2.4$$

If the function that is expanded by the Fourier series is real, then from Eq. 2.4 $\mathcal{Q}_{\bar{H}} = \mathcal{Q}_H^*$ where $\bar{H}$ means $-H_1$, $-H_2$, $-H_3$ and $\mathcal{Q}_H^*$ is the complex conjugate of $\mathcal{Q}_H$.

LAUE VECTOR EQUATION

For a one dimensional grating the condition for diffraction expressed in vector form is $\bar{a}_1 \cdot (\bar{k}_{H_1} - \bar{k}_o) = H_1$ where $\bar{a}_1$ is the spacing, $\bar{k}_o = \frac{1}{\lambda}\bar{u}_o$ is incident wave vector, and $\bar{k}_H = \frac{1}{\lambda}\bar{u}_H$ the diffracted wave vector and H_1 is an integer. For a three dimensional grating there are three such equations, where the general form is given by

$$\bar{k}_H - \bar{k}_o = \bar{B}_H \qquad 2.5$$

$\bar{B}_H = H_1\bar{b}_1 + H_2\bar{b}_2 + H_3\bar{b}_3$, and is the normal to the diffracting planes. This is called the Laue vector equation. As $|\bar{k}_H| = |\bar{k}_o| = \frac{1}{\lambda}$, $\bar{B}_H$ bisects the obtuse angle between the two wave vectors; and as $\bar{B}_H$ is normal to the diffracting planes, then each wave vector makes equal angles with the diffracting planes. Taking the absolute magnitude of each side of Eq. 2.5 gives Bragg's equation

$$n\lambda = 2d \sin \theta$$

If the closed triangle defined by Eq. 2.5 is constructed in the reciprocal lattice, a sphere can be constructed with radius $|\bar{k}_o| = \frac{1}{\lambda}$ with the vector $\bar{k}_o$ terminating at the origin of the reciprocal lattice; see Fig. 1 (p. 7). If the sphere passes through a reciprocal lattice point, there is a corresponding $\bar{B}_H$ for that point and Eq. 2.5 is satisfied. A diffraction maximum then exists. There are many variations

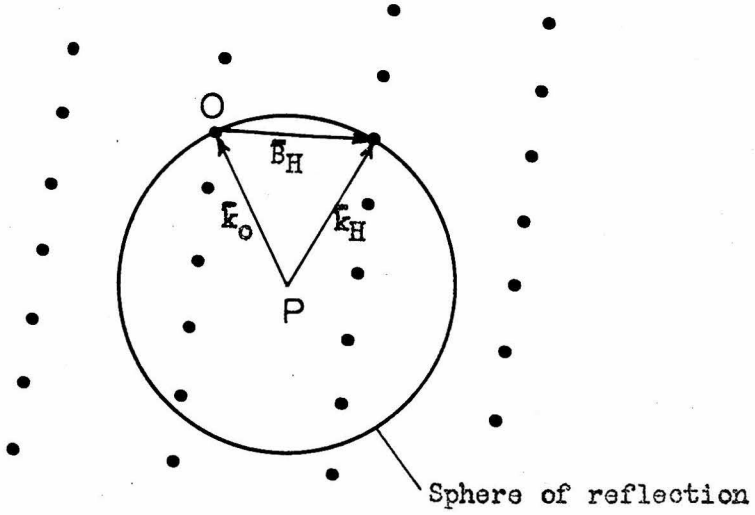

Fig. 1. A section of the reciprocal lattice with origin at O, and with the direction of the incident x-ray beam as $\bar{PO}$. When the sphere of reflection passes through a lattice point as shown, a diffraction maximum exists.

possible to get diffraction maxima. The sphere of reflection can be increased or decreased in size by changing the wavelength, for its radius is $|\bar{K}_o| = \frac{1}{\lambda}$, or the position of the sphere can be rotated about the origin of the reciprocal lattice by changing the direction of $\bar{K}_o$. In either case a diffraction maximum will occur when the sphere passes through a reciprocal lattice point. In this study the magnitude of $\bar{K}_o$ is held constant and its direction will have only one degree of freedom.

SCATTERING OF X-RAYS

Before discussing the interference produced by the crystal, the scattering by the elementary processes will be outlined. There are many types of scattering of x-rays by substances, but the only type of interest here is that scattering done coherently. If an electron which is held to an atom is caused to oscillate by a plane wave of monochromatic x-rays, the scattered intensity is given by the classical J. J. Thomson formula

$$I_\theta = I_o \frac{e^2}{mc^2} \frac{1 + \cos^2\theta}{R}$$

The polarizability α_θ, which is the dipole moment induced per unit field, is

$$\alpha_\theta = - \frac{e^2}{m\omega_o^2}$$

where θ is the scattering angle and R is that distance from electron to the point of observation.

If the entire atom is considered, and the restoring forces and interaction between electrons neglected, then the instantaneous amplitude of scattering is given by

$$\overline{E}_{atom} = \overline{E}_e \sum_j e^{i\overline{s}\cdot\overline{r}_j} \qquad 2.6$$

where $\overline{E}_e$ is the scattered amplitude of a single electron and the summation adds up the phases from the electrons in the atom. The phase is important as the wavelength of x-rays is of the order of magnitude of the size of the atom. But, as the electrons are in continual motion in the atom, to obtain the coherent term of the scattering Eq. 2.6 must be averaged over the variable positions of the electrons giving the mean amplitude of scattering as $E_{coh} = E_e \sum_j \phi_j$

where $$\phi_j = \int \sigma_j e^{i\overline{s}\cdot\overline{r}_j} dv$$

and $\sigma_j dv$ is the probability of finding the jth electron in volume element dv; and $$I_{coh} = I_e \left| \sum_j \phi_j \right|^2$$

The atomic scattering power is defined as

$$f^o = \sum_j \phi_j$$

When the binding force and a damping term are taken into consideration these results are modified to

$$f = \sum_j \frac{\phi_j}{1 - \left(\frac{\omega_j}{\omega_o}\right)^2 - i\frac{k_j}{\omega_o}}$$

where $\omega_o = 2\pi\nu_o$, ν_o is the impressed frequency; and $\omega_j = 2\pi\nu_j$ where ν_j is the characteristic frequency for the jth electron. This classical picture needs modification to satisfy the quantum mechanical picture of the atom. This adaptation has been carried out by H. Hönl[8] giving

$$f = \sum_j \phi_j(1 + \chi_j + i\eta_j) = f^o + \sum_j (\chi_j + i\eta_j) \qquad 2.7$$

where χ and η are the contributions from anomalous scattering and their importance depends on the nearness of the frequency of the incident x-rays to the critical x-rays absorption edges of the atom.

The explicit form of ξ_j and η_j as developed by Hönl will be presented later.

STRUCTURE FACTOR

The structure factor, F, is defined in terms of the unit cell. It is the ratio of the resulting amplitude of scattering from the atoms in the unit cell in a given direction to that of a single electron.

$$F = \sum_k f_k e^{i\bar{s}\cdot\bar{r}_k} \qquad 2.8$$

f_k is the structure factor per atom as defined by Eq. 2.7, and the exponential term gives the proper phase for each kth atom when scattering is observed at a particular direction; $\bar{s} = 2\pi(\bar{k} - k_o)$ and is the bisector of the obtuse angle between incident and scattering wave vector; $\bar{r}_k$ is the position vector of each atom in the unit cell. When calculating the structure factor F_H for a particular set of diffracting planes $\bar{s} = 2\pi\bar{B}_H$. The polarizability is now given by

$$\alpha = -\frac{e}{m\omega_o^2}\quad (1 + \xi_j + i\eta_j)\mathfrak{S}_j \qquad 2.9$$

where $(1 + \xi_j + i\eta_j)$ is the term due to anomalous dispersion and is the same as in Eq. 2.7 and

$$\mathfrak{S}_j(\bar{r}) = \sum \sigma_j^k(\bar{r} - \bar{r}_k) \qquad 2.10$$

is the electron distribution function of type j in the unit cell, and σ_j^k is the distribution function for type j electron in the kth atom.

DYNAMICAL THEORY OF X-RAY DIFFRACTION

The dynamical theory of x-ray scattering includes the effects of

absorption and the interaction between the incident and scattered radiation which are neglected in the simple theory of diffraction. It is to be pointed out that there is a distinct difference in the system where no diffraction takes place and when there is diffraction. In the second case the internal incident wave and the diffracted waves form a coupled system, and the solution for this coupled system results in a set of linear equations (the number depending on the number of diffracted waves); the simultaneous solution of these equations defines the possible "modes" due to the coupling; that is, the permitted values for (1) the index of refraction for the internal incident and diffracted waves and (2) the corresponding ratio of the amplitudes of the internal incident and diffracted waves.

The method of solving the problem of finding the energy in the diffracted wave as a function of the direction of the incident wave requires three steps; (1) joining the phase of the internal and external incident waves at the incident boundary, (2) finding the permitted values for the index of refraction and the corresponding amplitude ratios for the internal incident and diffracted waves consistent with the coupled system, and (3) applying the boundary conditions for the particular use and shape of the crystal. Let the external incident wave vector be $\bar{K}_0^e$, and the internal incident and diffracted wave vectors be $\bar{\beta}_0$ and $\bar{\beta}_H$. Joining the incident waves at a plane boundary gives

$$\bar{\beta}_0 = \bar{K}_0^e + \frac{k_0 \delta_0}{\gamma_0} \bar{n}$$

where the magnitudes of $\bar{\beta}_0$ and $\bar{K}_0^e$ are related by the index of re-

fraction $1 + \delta_o$. $\beta_o = k_o(1 + \delta_o)$. $\bar{n}$ is the unit vector normal to the crystal face pointing in, and γ_o is the direction cosine of the external incident wave vector $\bar{K}_o^e$. Inside the crystal Laue's vector equation is $\bar{\beta}_H = \bar{\beta}_o + \bar{B}_H$; combining this equation with the one for β_o above gives

$$\bar{\beta}_H = \bar{K}_o^e + \frac{k_o \delta_o}{\gamma_o} \bar{n} + \bar{B}_H \qquad 2.11$$

Thus when the permitted values of δ_o are known the internal diffracted wave vector is determined.

When no diffraction takes place $\delta_o = \frac{1}{2}\psi_o$ (see Eq. 2.13) where $1 + \frac{1}{2}\psi_o$ is the average measured index of refraction. When diffraction takes place the possible values of δ_o are determined by the conditions of self consistency between internal incident and diffracted waves.

Inside the crystal the differential equation for the displacement vector obtained from Maxwell's equation is

$$\bar{\nabla} \times \left(\bar{\nabla} \times \frac{\bar{D}}{\varepsilon}\right) = -\frac{1}{c^2} \frac{\partial^2 \bar{D}}{\partial t^2} \qquad 2.12$$

where the magnetic permeability is assumed to be unity and the current density is zero. The dielectric constant, ε, is related to the polarizability per unit volume, α, by

$$\varepsilon = 1 + \frac{4\pi\alpha}{1 - \frac{4\pi}{3}\alpha} \approx 1 + 4\pi\alpha$$

where α is small. As α is periodic, having the same period as the lattice, $4\pi\alpha$ is expanded in the Fourier series

$$\psi = 4\pi\alpha = \sum_H \psi_H e^{-i2\pi \bar{B}_H \cdot \bar{r}} \qquad 2.13$$

and $\frac{1}{\varepsilon} \approx 1 - \psi$. The displacement vector can also be expanded into

a Fourier series which represents the internal incident wave and any number of diffracted waves.

$$\bar{D} = \sum_H \bar{D}_H e^{i\omega_0 t - i2\pi \bar{\beta}_H \cdot \bar{r}} \qquad 2.14$$

Substitution of Eqs. 2.13 and 2.14 in Eq. 2.12 gives a set of linear homogeneous equations which represent the self consistency between incident and diffracted waves. When there is only one $\bar{E}_H$ satisfied in the Laue vector equation this set reduces to two equations. For a non-trivial solution of the ratio of amplitudes to exist requires

$$(2\delta_0 - \psi_0)(2\delta_H - \psi_0) = \psi_H \psi_{\bar{H}} \sin^2 \chi \qquad 2.15$$

and the non-trivial solution is

$$\frac{D_H}{D_0} = \frac{2\delta_0 - \psi_0}{\psi_{\bar{H}} \sin \chi}$$

where $1 + \delta_0$ and $1 + \delta_H$ are the refractive indices of incident and diffracted waves and are related by Eq. 2.11. Eq. 2.15 is quadratic in δ_0 and gives

$$\left.\begin{matrix} \delta_0' \\ \delta_0'' \end{matrix}\right\} = \frac{1}{2}\left\{\psi_0 - z \pm \sqrt{q + z^2}\right\}$$

q and z are defined later and $\delta_0 = \frac{1}{2}\psi_0$ for no diffraction. χ is the angle between $\bar{D}_0$ and $\bar{\beta}_H$. $\chi = \frac{\pi}{2}$ when $\bar{D}_0$ is normal to the plane containing $\bar{\beta}_0$ and $\bar{\beta}_H$ (normal polarization) and $\chi = \frac{\pi}{2} - 2\theta$ when in the plane of $\bar{\beta}_0$ and $\bar{\beta}_H$ (parallel polarization).

There are, then, possible two incident and two diffracted waves. Suppose the boundaries are plane and parallel, and the diffracted wave leaves the face opposite the face the incident wave enters. The boundary conditions are: At $\bar{n} \cdot \bar{r} = 0$ the normal components of the displacement vectors and tangential components of the electric vectors must be continuous across the boundary. As the dielectric constant

is approximately unity

$$D_o' + D_o'' = E_o^e \qquad \bar{n}\cdot\bar{r} = 0$$

The diffracted wave must vanish at the incident boundary

$$D_H' + D_H'' = 0 \qquad \bar{n}\cdot\bar{r} = 0$$

At the exit boundary the intensities are equated going across.

Satisfying these conditions the diffraction equation obtained is

$$\frac{I_H}{I_o^e} = b^2 \left|\psi_H\right|^2 K e^{-\mu_o t} \frac{\sin^2(av) + \sinh^2(aw)}{\left|q + s^2\right|} \qquad 2.16$$

I_H is the intensity of the external diffracted wave and I_o^e is the intensity of the external incident wave.

$$\frac{1}{b} = 1 + \frac{\bar{n}\cdot\bar{E}_H}{\bar{n}\cdot\bar{k}_o^e}\ ;\ b \approx \frac{\gamma_o}{\gamma_H}$$

γ_o and γ_H are the direction cosines of incident and diffracted waves.

$b = +1$ for the diffracting planes normal to the crystal face.

$b = -1$ for the diffracting planes parallel to the face.

$K = 1$ for normal polarization

$K = \cos 2\theta$ for parallel polarization

$u + iw \equiv \sqrt{q + s^2}$ $\qquad a \equiv \pi k_o \frac{t_o}{\gamma_o}$

$q = bK^2\psi_H\psi_{\bar{H}}$ $\qquad t = \frac{1}{2}\left(\frac{1}{\gamma_o} + \frac{1}{\gamma_H}\right)t_o$

$s = \frac{1 - b\psi_o}{2} + \frac{b}{2}\alpha$ $\qquad t_o$ = thickness of crystal plate

$\alpha \approx 2(\theta_B - \theta)\sin 2\theta_B$ $\qquad \theta_B$ is the Bragg angle for reflection

ψ_H and $\psi_{\bar{H}}$ are determined by the method of Eq. 2.4 from Eqs. 2.13 and 2.9.

DIFFRACTION EQUATION FOR THE (310) PLANES OF QUARTZ

The crystals are optically flat plates 1 mm thick and the (310) diffracting planes are normal to the face (b = +1). For crystals that have an inversion center $\psi_H^* = \psi_{\bar{H}}$ and $\psi_H\psi_{\bar{H}} = |\psi_H|^2$, whereby the calculations are somewhat simplified; quartz does not have an inversion center and so both terms must be calculated. The contributions due to anomalous scattering are included. For these crystals the variables in the diffraction equation are

$$q = K^2\psi_H\psi_{\bar{H}}$$

$$s = (\theta_B - \theta)\sin 2\theta_B$$

At each wavelength q is constant and the diffraction pattern is measured using as the independent variable the angular deviation $(\theta_B - \theta)$ of the incident wave vector from the position given by Bragg's condition of reflection. To be able to compare theory with experiment ψ_H and $\psi_{\bar{H}}$ must be calculated for each wavelength. This is done in the following:

When anomalous dispersion is present

$$\psi = -\frac{4\pi e^2}{m\omega_0^2}\sum (1 + \xi_j + i\eta_j)\Omega_j \qquad 2.17$$

from Eq. 2.9. So ψ can be written $\psi = \psi' + i\psi''$ where both ψ' and ψ'' are real and can be represented by Fourier series

$$\psi' = \sum_H \psi_H' e^{-i2\pi \mathbf{B}_H \cdot \mathbf{r}}$$

$$\psi'' = \sum_H \psi_H'' e^{-i2\pi \mathbf{B}_H \cdot \mathbf{r}}$$

and ψ_H' and ψ_H'' are both complex, thus

$$\psi_H = (\psi_{Hr}' + i\psi_{Hi}') + i(\psi_{Hr}'' + i\psi_{Hi}'')$$

$$\psi_{\overline{H}} = (\psi_{Hr}' - i\psi_{Hi}') + i(\psi_{Hr}'' - i\psi_{Hi}'')$$

where the condition that if ψ' and ψ'' are real $\psi_{\overline{H}}' = \psi_H'^*$, $\psi_{\overline{H}}'' = \psi_H''^*$ and $\overline{H}$ means $-H_1, -H_2, -H_3$ is used. So

$$\psi_H\psi_{\overline{H}} = |\psi_H'|^2 - |\psi_H''|^2 + 2i\left[\psi_{Hr}'\psi_{Hr}'' + \psi_{Hi}'\psi_{Hi}''\right]$$

$$= |\psi_H'|^2\left\{1 - \left|\frac{\psi_H''}{\psi_H'}\right|^2 + 2i\,\frac{\left[\psi_{Hr}'\psi_{Hr}'' + \psi_{Hi}'\psi_{Hi}''\right]}{|\psi_H'|^2}\right\} \qquad 2.18$$

$$= |\psi_H'|^2\left\{1 - \varkappa^2 + 2ic\right\}$$

where $\varkappa$ and c are defined by comparing to the preceding equation. Using the method of Eq. 2.4 and substituting for the values of ψ' and ψ'' from Eqs. 2.13 and 2.9 the values for ψ_H' and ψ_H'' are

$$\psi_H' = -\frac{1}{V}\frac{4\pi e^2}{m\omega_0^2}\int\sum(1 + \mathcal{F}_j)\Omega_j e^{i2\pi\overline{B}_H\cdot\overline{r}}dv$$

$$\psi_H'' = -\frac{1}{V}\frac{4\pi e^2}{m\omega_0^2}\int\sum\eta_j\Omega_j e^{i2\pi\overline{B}_H\cdot\overline{r}}dv$$

Substituting for Ω_j defined by Eq. 2.10

$$\psi_H' = -\frac{1}{V}\frac{4\pi e^2}{m\omega_0^2}\sum_j(1 + \mathcal{F}_j)\int\sum_k\sigma_j^k(\overline{r} - \overline{r}_k)e^{i2\pi\overline{B}_H\cdot\overline{r}}dv$$

$$\psi_H'' = -\frac{1}{V}\frac{4\pi e^2}{m\omega_0^2}\sum_j\eta_j\int\sum_k\sigma_j^k(\overline{r} - \overline{r}_k)e^{i2\pi\overline{B}_H\cdot\overline{r}}dv$$

Multiplying the integrand of each by $e^{-i2\pi\overline{B}_H\overline{r}_k}e^{i2\pi\overline{B}_H\overline{r}_k}$ and interchanging the order of the two finite summations gives

$$\psi_H' = \frac{-4\pi e^2}{Vm\omega_0^2}\sum_k\left[\sum_j(1 + \mathcal{F}_j)\,\phi_j^k\right]e^{i2\pi\overline{B}_H\cdot\overline{r}_k}$$

$$\psi_H'' = \frac{-4\pi e^2}{Vm\omega_0^2}\sum_k\left[\sum_j\eta_j\phi_j^k\right]e^{i2\pi\overline{B}_H\cdot\overline{r}_k}$$

where $\phi_j^k = \int \sigma_j^k(\bar{r} - \bar{r}_k) e^{i2\pi \bar{S}_H (\bar{r} - \bar{r}_k)} dv$.

The magnitude of the terms $(1 + \xi_j)\phi_j^k$ and $\eta_j \phi_j^k$ are calculated using the results of Hönl[8], who has derived the expressions for ξ_j and η_j for the two electrons in the K shell as

$$2\xi_K = \frac{2^7 e^{-4}}{9}\left\{\frac{4}{(1-\Delta)^2}\left(x^2 \log\left|1 - \frac{1}{x^2}\right|\right) - \frac{1}{(1-\Delta)^3}\left(2x^2 + x^3 \log\left|\frac{1-x}{1+x}\right|\right)\right\}$$

$$2\eta_K = \frac{\pi 2^7 e^{-4}}{9}\left\{\frac{4x^2}{(1-\Delta)^2} - \frac{x^3}{(1-\Delta)^3}\right\}$$

where $x = \frac{\lambda}{\lambda_K}$ and Δ depends on the kind of atom and has been determined by Hönl.

In Appendix B $2\xi_K$ and $2\eta_K$ have been calculated for the range of wavelength $0.123\text{Å} \leq \lambda \leq 0.710\text{Å}$. Both $2\xi_K$ and $2\eta_K$ decrease with decreasing wavelength.

For $\lambda = 0.710\text{Å}$, $2\eta_K = 0.067$ and $2\xi_K = 0.091$. As $2\xi_K$ is small compared to f_k^o the ξ_j terms are dropped. The anomalous terms are very much less for the L type electron and so only the contribution from the K electrons need be considered. Thus

$$\xi_j = 0 \qquad j = K, L, M \text{ etc.}$$

$$\eta_j = \begin{cases} \eta_K & j = K \\ 0 & j = L, M \ldots \text{etc.} \end{cases}$$

and the values for ψ_H' and ψ_H'' become

$$\psi_H' = \frac{-4\pi e^2}{Vm\lambda_o^2} \sum_k f_k^o \, e^{i2\pi \bar{S}_H \cdot \bar{r}_k}$$

$$\psi_H'' = \frac{-4\pi e^2}{Vm\lambda_o^2} \sum 2\eta_K \phi_K^k e^{i2\pi \bar{S}_H \cdot \bar{r}_k}$$

where $\sum \phi_j^k = f_k^o$. The maximum value of ϕ_K^k will be when λ is large compared to the radii of the K shell electrons, and the contribution of the two electrons add in phase so $\phi_K^k = \int \sigma_K^k dv = 1$. $\phi_K^k < 1$

for shorter wavelengths. Using the maximum value, which is a fairly good approximation for the wavelength used, there results:

$$\psi_H' = \frac{-4\pi e^2}{Vm\omega_o^2} \sum_k f_k^o e^{i2\pi \bar{B}_H \cdot \bar{r}_k}$$

$$\psi_H'' = \frac{-4\pi e^2}{Vm\omega_o^2} \sum_k 2\eta_K k e^{i2\pi \bar{B}_H \cdot \bar{r}_k}$$

These summations are calculated in Appendix B, giving for $\lambda = 0.710\text{Å}$

$$\psi_H' = \frac{-4\pi e^2}{m\omega_o^2} \frac{1}{V} \left\{ -10.49 + i\ 18.68 \right\}$$

$$\psi_H'' = \frac{-4\pi e^2}{m\omega_o^2} \frac{1}{V} \left\{ -0.077 + i\ 0.112 \right\}$$

and

$$\psi_H = \frac{-4\pi e^2}{m\omega_o^2} \frac{1}{V} \left\{ -10.60 + i\ 18.60 \right\}$$

$$\psi_{\bar{H}} = \frac{-4\pi e^2}{m\omega_o^2} \frac{1}{V} \left\{ -10.38 - i\ 18.76 \right\}$$

Referring to Eqs. 2.18

$$\chi = 6.99 \times 10^{-2}$$

$$c = 6.98 \times 10^{-3}$$

χ and c both decrease as λ decreases. So

$$1 - |\chi|^2 \approx 1$$

and then

$$\psi_H \psi_{\bar{H}} = K^2 |\psi_H'|^2 \{1 + 2ic\} \qquad 2.19$$

Referring now to the variables contained in the diffraction Eq. 2.16 and defining y as $y \equiv \frac{s}{b^{\frac{1}{2}} K |\psi_H'|}$

$$v + iw = \sqrt{K^2 b |\psi_H'|^2 \{1 + 2ic\} + y^2 b K^2 |\psi_H'|^2}$$

$$\approx K b^{\frac{1}{2}} |\psi_H'| \sqrt{1 + y^2} \left\{ 1 + i \frac{c}{1 + y^2} \right\}$$

where c has been shown to be small, and defining A as

$$A = aK\,|\psi_H'|\,\overline{b^2} = \pi k_o K\,|\psi_H'|\,\frac{t_o}{\gamma_o} \qquad 2.20$$

$$v + iw = \frac{A}{a}\sqrt{1+y^2}\left\{1 + i\frac{c}{1+y^2}\right\}$$

$$av = A\sqrt{1+y^2}$$

$$aw = \frac{cA}{\sqrt{1+y^2}}$$

Eq. 2.16 now becomes

$$\frac{I_H}{I_o^e} = e^{-\frac{\mu_o t_o}{\gamma_o}}\,\frac{\sin^2 A\sqrt{1+y^2} + \sinh^2\frac{cA}{\sqrt{1+y^2}}}{(1+y^2)} \qquad 2.21$$

The variation of A with the thickness of the crystal is given by $\frac{\Delta A}{A} = \frac{\Delta t}{t}$. Thus for A large the corresponding change in Δt for a $\frac{\pi}{2}$ change in A will be of the order of the irregularities in the crystal thickness from point to point. The crystal plates used in this experiment were 1 mm thick and for $\lambda = 0.710\text{Å}$, $A = 40$. The term $\sin^2 A\sqrt{1+y^2}$ in Eq. 2.21 changes from 0 to 1 when $A = \frac{\pi}{2}$. The corresponding change in the crystal thickness would be $\Delta t_o = 3 \times 10^{-3}$ cm, which is of the order of magnitude of the irregularities in the crystal faces. Since $\sin^2 A\sqrt{1+y^2}$ oscillates rapidly between 0 and 1 from point to point on the crystal face, it is replaced by its average value $\frac{1}{2}$.

When cA is small $\sinh^2\frac{cA}{\sqrt{1+y^2}}$ can be replaced by the first term in its series expansion. For the quartz crystals used in this experiment at $\lambda = 0.710\text{Å}$, $cA = 0.277$ and at $\lambda = 0.208\text{Å}$, $cA = 0.00676$. With an error of 1 per cent and less in the wavelength range $0.123 \leq \lambda \leq 0.710\text{Å}$

$$\sinh^2\frac{cA}{\sqrt{1+y^2}} = \frac{c^2A^2}{1+y^2}$$

With these approximations the diffraction equation (Eq. 2.21)

for the particular crystals used in this experiment becomes

$$\frac{I_H}{I_o^e} = \frac{e^{-\frac{\mu_o t_o}{\gamma_o}}}{2(1+y^2)}\left(1 + \frac{2c^2A^2}{1+y^2}\right) \qquad 2.22$$

The exponential term gives the true absorption of the beam in passing through the crystal. The term in cA gives the effect of the anomalous scattering on the diffraction pattern. When $\mu_o = 0$ and cA = 0 the diffraction pattern is just that of a witch. The change in the shape of the diffraction pattern when the value of cA is changed from 0 to 0.277 (the maximum value for the wavelength range used in this study) is illustrated in Fig. 2 (p. 21). The peak values of the curves differ by only 15.4 per cent. As y increases the two curves rapidly approach each other. A useful feature of this diffraction curve, that will be used later, is that it is symmetrical about y = 0.

PROPERTIES OF THE DIFFRACTION PATTERN TO BE COMPARED TO EXPERIMENT

At any one wavelength the detector (counter) that measures the x-ray diffraction from the crystal measures the power received, $P_H = I_H S_H$, where S_H is the crossectional area of the beam, and the external incident power is $P_o = I_o^e S_o$. So

$$\frac{P_H}{P_o} = \frac{I_H}{I_o^e}\frac{S_H}{S_o} = \frac{I_H \gamma_H}{I_o^e \gamma_o} = \frac{I_H}{I_o^e}\frac{1}{b} = \frac{I_H}{I_o^e}$$

for b = 1 (diffraction planes normal to faces of the crystal). The area under the curves of $\frac{P_H}{P_o}$ vs. $\varepsilon = (\theta_B - \theta)$, where ε is the angular deviation from the Bragg angle, is called the integrated reflecting power and is given by

$$R_H^o = \int \frac{P_H}{P_o}\, d(\theta_B - \theta) \qquad 2.23$$

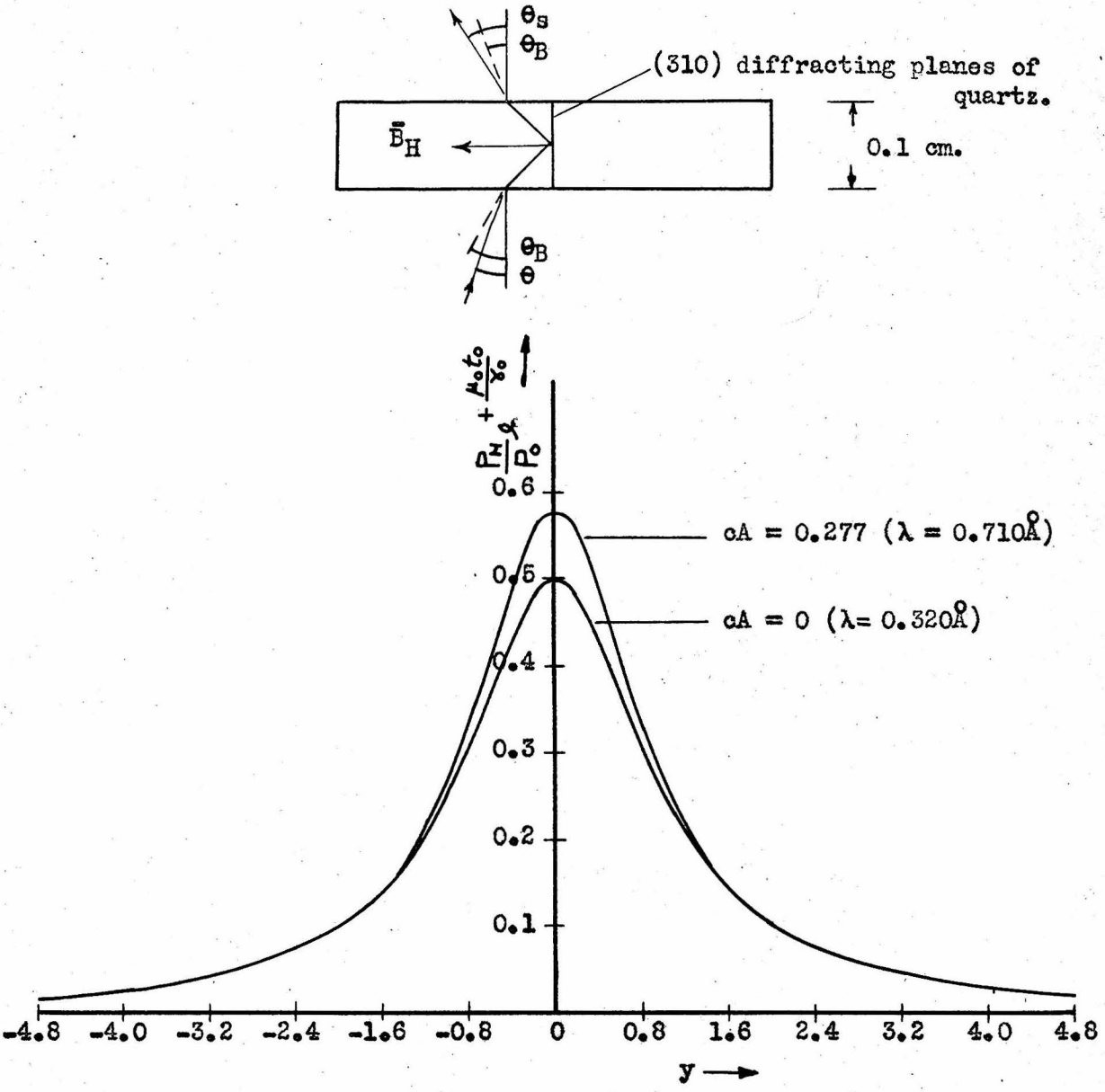

Fig. 2. The top illustration shows schematically the diffraction of an x-ray beam for the transmission case and for the crystals used in this study. The lower illustration shows the ratio of the power of the diffracted beam to that of the incident beam as a function of the angular deviation of the incident ray from Bragg's angle, θ_B, ($y = (\theta_B - \theta) \sin 2\theta_B / K|\psi_H|$) for the particular crystals and range of wavelengths used in this study.

This, with the half width at half max, w_θ; and $\frac{P_H(0)}{P_o}$, the ratio of the peak value of the diffraction equation to the power in the incident beam, are the usual quantities compared with experiment.

The variable y defined by

$$y = \frac{\theta}{K|\Psi_H'|} = \frac{(\theta_B - \theta)\sin 2\theta_B}{K|\Psi_H'|} \qquad 2.24$$

is used in place of ξ for calculations because of its convenience, so

$$R_H^y = R_H^0 \frac{\sin 2\theta_B}{K|\Psi_H'|} \qquad 2.25$$

From Eq. 2.22

$$R_H^y = \int_{-\infty}^{\infty} e^{-\frac{\mu_o t_o}{\gamma_o}\frac{1}{2(1+y^2)}(1+\frac{2c^2A^2}{1+y^2})}\,dy$$

$$R_H^y = e^{-\frac{\mu_o t_o}{\gamma_o}\frac{\pi}{2}(1+c^2A^2)} \qquad 2.26$$

For the wavelength range $0.120\text{Å} \leq \lambda \leq 0.710\text{Å}$, c^2A^2 has a maximum value of 0.0767 at $\lambda = 0.710\text{Å}$. The ratio of the power received by the detector at the peak of diffraction curve to that of the incident beam is given by

$$\frac{P_H(0)}{P_o} = e^{-\frac{\mu_o t_o}{\gamma_o}\frac{1}{2}(1+2c^2A^2)}$$

$$= e^{-\frac{\mu_o t_o}{\gamma_o}} \begin{cases} 0.564 & \lambda = 0.710\text{Å} \\ 0.500 & \lambda = 0.208\text{Å} \end{cases} \qquad 2.27$$

The half width at half maximum w_y (measured in the same dimensionless units as y) is given by

$$\frac{P_H(w_y)}{P_o} = \frac{1}{2}\frac{P_H(0)}{P_o}$$

$$w_y \approx \sqrt{\frac{2}{1+2c^2A^2}\left(1+\frac{2c^2A^2}{1+w_y'^2}\right) - 1} \qquad 2.28$$

where w_y' is the solution for $\sigma A = 0$;

$$w_y = \begin{cases} 0.94 & \text{for } \lambda = 0.710\text{Å} \\ 0.9995 & \text{for } \lambda = 0.208\text{Å} \end{cases}$$

These results are used in Part III in calculating the theoretical rocking curves for the two crystal x-ray spectrometer.

MOSAIC CRYSTAL

For the two quartz crystals described here, the width of the experimental diffraction curves obtained by the two crystal spectrometer are only about twice that predicted by the theory. Then if a mosaic structure is to be considered the distribution function for the directions of these blocks must have a half width of the order of magnitude of the width of the diffraction pattern. Let

$$W(\Delta) = \frac{1}{\eta\sqrt{2\pi}} e^{-\frac{\Delta^2}{2\eta^2}} \qquad 2.29$$

be the distribution function for the direction of the small crystal blocks from the mean, and let the reflecting power of a layer dT in the crystal be σdT. For a given incident angle θ with the crystal face, the glancing angle will be different for each of the small blocks, say $\theta + \Delta$. Thus for a single layer of blocks of thickness t_o inside the crystal

$$\sigma = \frac{1}{t_o}\int_{-\infty}^{\infty} W(\Delta)\,\frac{P_H}{P_o}(\theta - \theta_B + \Delta)\,d\Delta \qquad 2.30$$

where $\frac{P_H}{P_o}$ is the diffraction pattern for a single crystal.

As the beam travels through the crystal it is continually losing energy by true absorption and diffraction, and gaining energy from multi-reflection. At a distance T in the crystal, the equations giving the increase or loss in power for the incident and diffracted beams are

$$d\mathcal{P}_o = -\mu_o \mathcal{P}_o \frac{dT}{\gamma_o} - \sigma \mathcal{P}_o dT + \sigma \mathcal{P}_H dT$$

$$d\mathcal{P}_H = -\mu_o \mathcal{P}_H \frac{dT}{\gamma_H} - \sigma \mathcal{P}_H dT + \sigma \mathcal{P}_o dT$$

The boundary conditions are

$$\mathcal{P}_o(T) = \mathcal{P}_o(0) \qquad T = 0$$

$$\mathcal{P}_H(0) = 0 \qquad T = 0$$

The solution is

$$\frac{\mathcal{P}_H(T)}{\mathcal{P}_o(0)} = e^{-\left(\frac{\mu_o}{\gamma_o} + \sigma\right)T_o} \sinh(\sigma T_o) \qquad 2.31$$

T_o is the thickness of the crystal. Eq. 2.31 can be expanded into the form

$$\frac{\mathcal{P}_H(T)}{\mathcal{P}_o(0)} = e^{-\frac{\mu_o T_o}{\gamma_o}} \sigma T_o \left(1 - \sigma T_o + \frac{2}{3}(\sigma T_o)^2 - \frac{1}{3}(\sigma T_o)^3 + \ldots\right) \qquad 2.32$$

The integrated reflecting power for the entire crystal is then

$$\mathcal{R}_H = \int \frac{\mathcal{P}_H}{\mathcal{P}_o} d(\theta_B - \theta) \qquad 2.33$$

which can be calculated when σ given by Eq. 2.30 is known. When the thickness (t_o) of the small blocks is small so that $A = \frac{\pi}{\lambda} \frac{K |\psi_H'| t_o}{\gamma_o} \ll 1$ the diffraction Eq. 2.21 becomes

$$\frac{P_H}{P_o} \approx A^2 \frac{\sin^2 Ay}{(Ay)^2} \qquad 2.34$$

To smooth out the interference fringes this is replaced by a function having the same area and the same value at $y = 0$

$$\frac{P_H}{P_o} \approx A^2 e^{-\frac{A^2 y^2}{\pi}} \qquad 2.35$$

Substituting Eqs. 2.35 and 2.29 in Eq. 2.30 gives

$$\sigma = \frac{1}{t_o \eta} \frac{A^2}{\sqrt{2\pi}} \int_{-\infty}^{\infty} e^{-h^2 \Delta^2} e^{-\ell^2(\varepsilon + \Delta)^2} d\Delta$$

where $$h^2 = \frac{1}{2\eta^2} \; ; \; \ell^2 = \frac{A^2}{\pi} \left(\frac{\sin 2\theta_B}{K\,|\psi_H|}\right)^2$$

By the method of completing the square of the exponent

$$\sigma = Be^{-\frac{\epsilon^2 \ell^2 h^2}{h^2 + \ell^2}} \qquad 2.36$$

where

$$B = \frac{A^2(t_o)}{t_o \eta \sqrt{2}\,\sqrt{h^2 + \ell^2}}$$

Substituting this in Eq. 2.32 and the result in Eq. 2.33 and performing the integration gives for the integrated reflecting power of the mosaic crystal

$$\mathcal{R}_H^{\theta} = e^{-\frac{A_o T_o}{\gamma_o}} \left\{ \frac{T_o d\, K^2}{\cos^2\theta_B} \left(\frac{e^2}{mc^2} \frac{|F_H|}{V}\right)^2 \lambda^2 \right\} \left(1 - \frac{T_o B}{2} + \frac{2T^2B^2}{9} - \frac{1}{12} T_o{}^3 B^3 + \ldots\right) \qquad 2.37$$

where

$$T_o B = \frac{T_o t_o \lambda^2 K^2}{\cos^2\theta_B} \left\{\frac{e^2}{mc^2} \frac{|F_H|}{V}\right\}^2 \frac{1}{\sqrt{1 + 2\eta^2 \pi^2 t_o^2}}$$

T_oB increases linearly with t_o. For T_oB small compared to 1, so that only the first term of Eq. 2.37 is needed, $\mathcal{R}_H^{\theta}$ is independent of thickness of the mosaic blocks, t_o, and of the standard deviation, η, of the distribution function $W(\Delta)$, but is proportional to λ^2. As t_o is increased, T_oB becomes larger and the dependence of $\mathcal{R}_H^{\theta}$ on t_o, η, and higher power of λ^2 enter. Eq. 2.37 is good as long as $A = \frac{\pi}{\lambda} |\psi_H| \frac{t_o}{\gamma_o} << 1$; that is, small primary extinction. Primary extinction is the loss of energy in passing through a single block. For the case $A \simeq 1$ the solution becomes rather complicated. For a single crystal Zachariasen[5] shows that R_H^y increases almost linearly with A until $A \simeq 1$ where it has the value of 2 (same dimensionless units as y) and then oscillates about $R_H^y = 1.6$ as A increases. The

amplitudes of the first oscillation are about 50 per cent of the mean but decrease fairly rapidly as A increases. For $A > 1$ the diffraction pattern, Eq. 2.22, must be used for the blocks, and results approach that for a perfect crystal.

As $|\psi_H|$ is proportional to λ^2, A is proportional to λ. Thus primary extinction decreases with λ or t_o. Depending on the other constants Eq. 2.37 should become more valid as λ decreases.

The above results show a marked difference between a perfect crystal and an ideal mosaic crystal ($T_oB << 1$). The integrated reflecting power, R_H^o, for a perfect crystal varies as λ; for an ideal mosaic crystal the integrated reflecting power, $\mathcal{R}_H^o$, varies as λ^2. But if $A \approx 1$ or greater (larger blocks) the theory for a mosaic crystal is complicated; therefore, by comparing the width and peak values of the diffraction pattern with perfect crystal theory, one can obtain an estimate of the perfectness of the crystals.

PART III

THEORY OF THE TWO CRYSTAL X-RAY SPECTROMETER

The theory of the two crystal x-ray spectrometer has been worked out by Schwarzschild,[9] Spencer,[10] Laue,[11] Smith,[12] and DuMond.[13] The texts by Compton and Allison[14] and Zachariasen[5] have also been used extensively in presenting the theory of the two crystal spectrometer. The present work involves the transmission of the diffracted beam through the crystal and is slightly different from the usual case of reflection from cleavage planes.

Fig. 3 (p. 28) shows a schematic arrangement of the x-ray tube, the two crystals with their diffracting planes normal to the faces (greatly exaggerated) mounted on the spectrometer, and the detector. When crystal A is set for Bragg reflection for a particular wavelength, crystal B can be set in two positions for Bragg reflection (see Fig. 3). These two positions have an angular separation of 2θ, where θ is the glancing angle for Bragg reflection that the incident beam makes with the diffracting planes.

The case where the diffracting planes are parallel or nearly parallel is called the "parallel" position. It will be shown that when crystal A is stationary and crystal B is rotated off parallelism, the resulting plot of the power received by the detector vs. the angular setting of crystal B is dependent only on the properties of the crystals and not on the spectral distribution of the radiation or the geometry of the slit system. This curve is called a two crystal "parallel" rocking curve.

As the single crystal diffraction pattern cannot be derived from

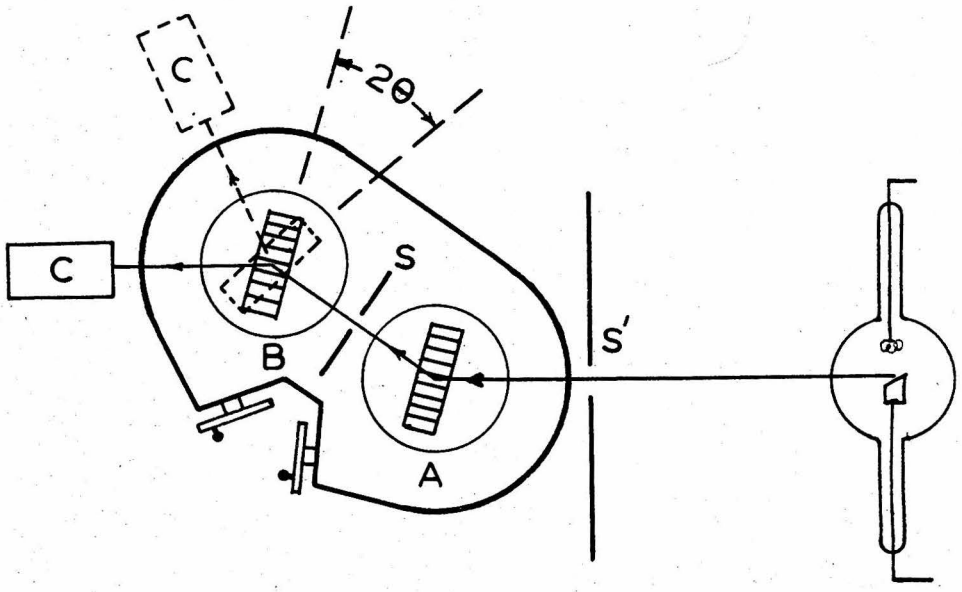

Fig. 3. Schematic illustration of the two crystal x-ray spectrometer employing the (310) planes (transmission case) of two identical quarts plates, 1 mm. thick. The full lines show the general position for the parallel rocking curve. The dotted lines show the position for the antiparallel rocking curve. The slits or stops are at S and S'. The xenon-filled counter is at C.

the two crystal experimental "parallel" rocking curve, the perfectness of the crystals can be determined by comparing the experimental two crystal "parallel" curve with the two crystal "parallel" rocking curves calculated from the single crystal theoretical diffraction pattern.

Rotating crystal B through 2θ from parallelism with crystal A gives the position of crystal B called the antiparallel position. It will be shown that the power received by the detector as crystal B is rotated through small angles for this arrangement, is a function primarily of the spectral distribution of the x-rays and requires only a minor correction due to the diffraction patterns of the crystals and the vertical divergence of the x-ray beam.

When crystal A is set to diffract a particular wavelength such as the $K_{\alpha 1}$ line, 2θ for this line can be determined by measuring angular separation of the settings of crystal B for the parallel and antiparallel positions. If the value of 2θ for two lines is determined, using the same crystals in each case, and the wavelength of one of the lines is known accurately, then an accurate determination can be made of the unknown wavelength. This is done in this study by using the $MoK_{\alpha 1}$ line as a standard and determining the $WK_{\alpha 1}$ line. Using an accurately known wavelength and 2θ as measured above, the grating spacing of the diffracting crystal can be measured using Bragg's law of reflection.

GENERAL THEORY OF THE TWO CRYSTAL SPECTROMETER

The case that will be considered is for perfect crystals, where the x-ray source is far enough away from the crystals so that the incident waves are plane waves, and the diffracting area of crystal

(of diameter D measured normal to the diffracting planes) is large compared to the wavelength so that $\frac{\lambda}{D}$ (the angular measure of the Fraunhofer diffraction pattern from the finite region of scattering) is very much less than the diffraction pattern of the crystals. With these conditions the method of rays will be used.

Let the central ray for Figs. 4 (p. 31) and 5 (p. 32) satisfy Bragg's law at crystal A

$$\lambda_0 = 2d \sin \theta_B \qquad 3.1$$

Since slits are used to confine the beam, there is consequently vertical and horizontal divergence in the beam. If a neighboring ray makes an angle $d\theta$ with the central ray (it may have both horizontal and vertical divergence), it will be Bragg reflected only if its wavelength differs from the central ray by

$$d\lambda = 2d \cos \theta_B d\theta$$

Thus if this ray of wavelength λ is to be Bragg reflected, it must make a glancing angle, measured normal to the diffracting planes, of

$$\theta_B + \frac{\lambda - \lambda_0}{\lambda_0} \tan \theta_B \qquad 3.2$$

Consider now a ray that has horizontal divergence α and vertical divergence ϕ measured with reference to the central ray. It has been shown[13],[15] that for ϕ and α small, the glancing angle measured in a plane normal to the lattice planes and including the ray is

$$\theta_B + \alpha - \frac{\phi^2}{2} \tan \theta_B \qquad 3.3$$

In Part II it was shown that the diffraction pattern of a crystal is a function of the deviation of the glancing angle from Bragg's condition of reflection. This deviation at crystal A, for the ray having vertical and horizontal divergence, is just the difference between

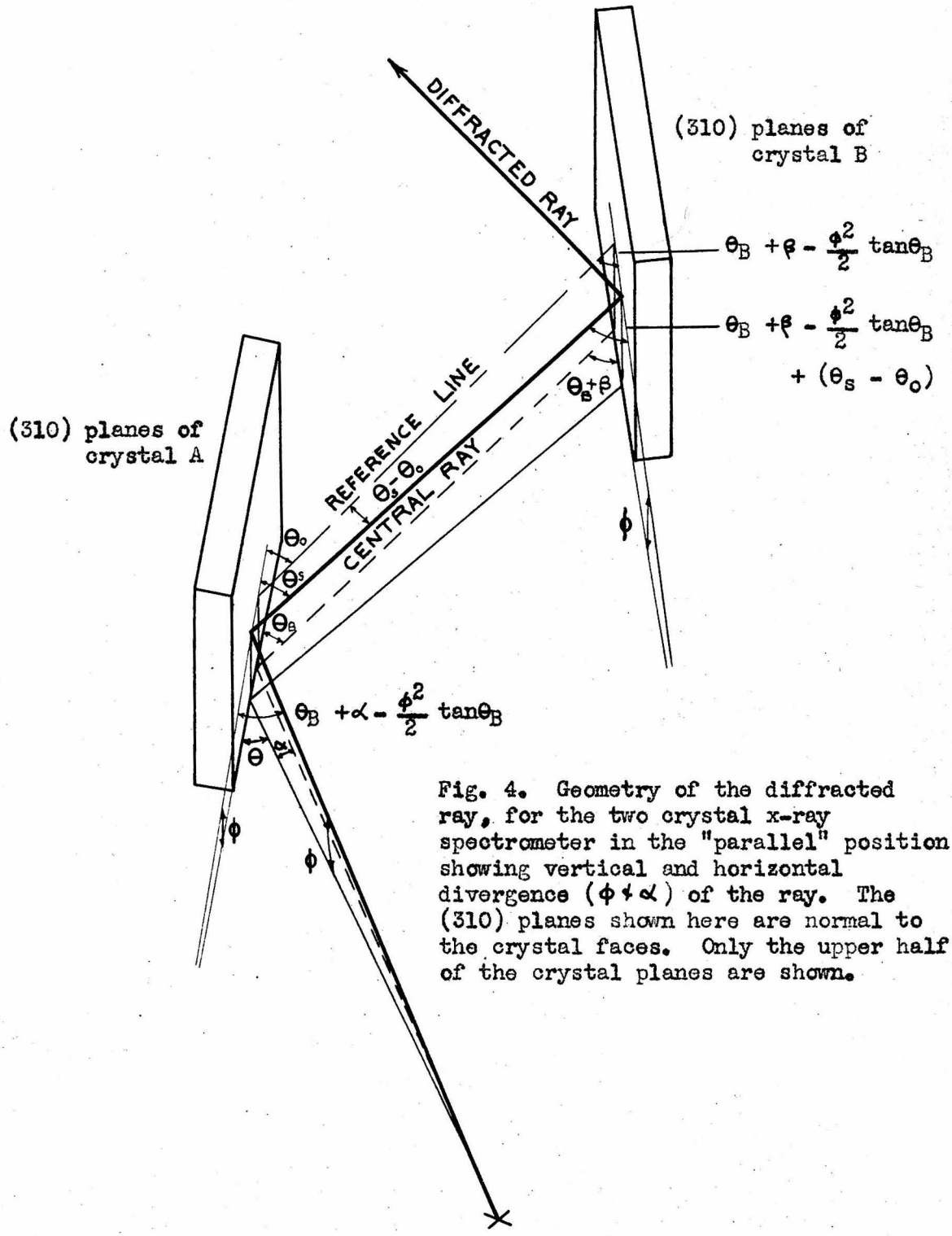

Fig. 4. Geometry of the diffracted ray, for the two crystal x-ray spectrometer in the "parallel" position showing vertical and horizontal divergence (ϕ & α) of the ray. The (310) planes shown here are normal to the crystal faces. Only the upper half of the crystal planes are shown.

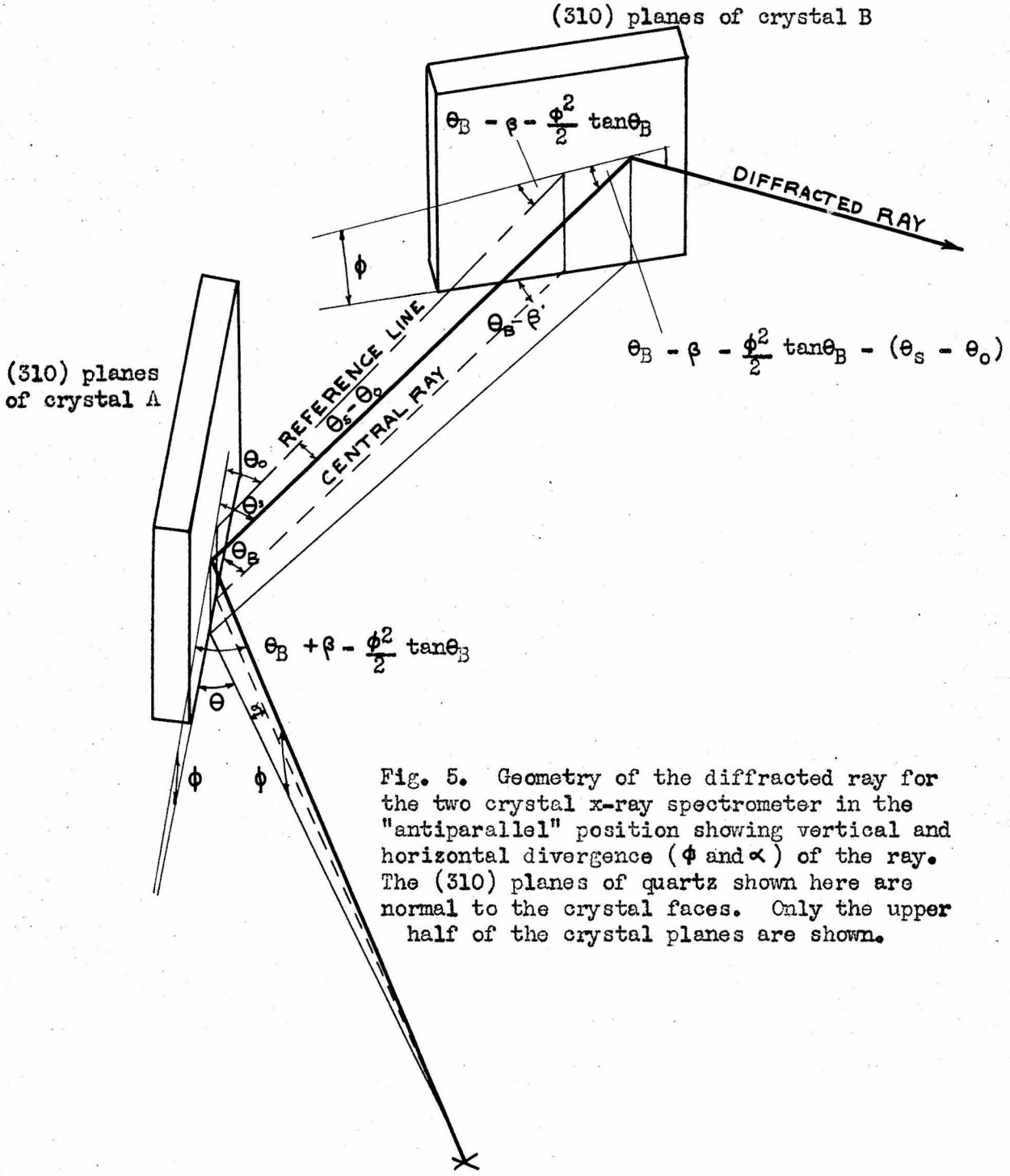

Fig. 5. Geometry of the diffracted ray for the two crystal x-ray spectrometer in the "antiparallel" position showing vertical and horizontal divergence (ϕ and α) of the ray. The (310) planes of quartz shown here are normal to the crystal faces. Only the upper half of the crystal planes are shown.

Eqs. 3.3 and 3.2, which is

$$\alpha = \frac{\phi^2}{2} \tan \theta_B - \frac{\lambda - \lambda_o}{\lambda_o} \tan \theta_B \qquad 3.4$$

The intensity of this ray after diffraction from crystal A is then

$$I_o(\lambda - \lambda_o) \frac{I_H}{I_o} \left(\alpha - \frac{\phi^2}{2} \tan \theta_B - \frac{\lambda - \lambda_o}{\lambda_o} \tan \theta_B\right) \qquad 3.5$$

The glancing angle of scattering, θ_s, is related to the glancing incident angle, θ, measured from the diffracting planes as follows:*

$$\theta_s = \theta_B(\lambda) - b\left[\theta - \theta_B\right] \quad (\lambda) \qquad 3.6$$

Let crystal B deviate by an angle β from satisfying Bragg's condition of reflection for the central ray ($\lambda = \lambda_o$, $\alpha = \phi = 0$); β is positive for clockwise rotation.

The glancing angle of scattering, θ_s, of the ray leaving the lattice planes of crystal A of wavelength λ and vertical and horizontal divergence ϕ and α is

$$\theta_s = \left(\theta_B + \frac{\lambda - \lambda_o}{\lambda_o} \tan \theta_B\right) - b\left(\alpha - \frac{\phi^2}{2} \tan \theta_B - \frac{\lambda - \lambda_o}{\lambda_o} \tan \theta_B\right) \qquad 3.7$$

Let a reference line (see Figs. 4 (p. 31) and 5 (p. 32)) be drawn for which $\alpha = 0$, $\phi = \phi$. It will make a glancing angle θ_o, measured in a plane normal to the lattice planes and including the ray, of

$$\theta_o = \theta_B - \frac{\phi^2}{2} \tan \theta_B \qquad 3.8$$

The deviation of the general ray from this reference line will be

$$\theta_s - \theta_o = \frac{\lambda - \lambda_o}{\lambda_o} \tan \theta_B + \frac{\phi^2}{2} \tan \theta_B - b\left[\alpha - \frac{\phi^2}{2} \tan \theta_B - \frac{\lambda - \lambda_o}{\lambda_o} \tan \theta_B\right] \qquad 3.9$$

Referring to Figs. 4 (p. 31) and 5 (p. 32) it is seen that the glancing angle this scattered ray from crystal A makes with the lattice planes of crystal B will be different for the parallel and antiparallel case. For the parallel case:

---

*See Appendix C.

Referring to Fig. 4 (p. 31), for a rotation φ of crystal B the reference line will make a glancing angle of

$$\theta_B - \varphi - \frac{\phi^2}{2} \tan \theta_B \qquad 3.10$$

with the planes of crystal B. Thus the glancing angle for the particular ray under consideration on crystal B will be

$$\theta_B - \beta - \frac{\phi^2}{2} \tan \theta_B + (\theta_s - \theta_o) \qquad 3.11$$

which is

$$\theta_B - \beta - \frac{\phi^2}{2} \tan \theta_B + \left[\frac{\lambda - \lambda_o}{\lambda_o} \tan \theta_B + \frac{\phi^2}{2} \tan \theta_B - b\left(\alpha - \frac{\phi^2}{2} \tan \theta_B - \frac{\lambda - \lambda_o}{\lambda_o} \tan \theta_B\right)\right] \qquad 3.12$$

For the antiparallel case:

Referring to Fig. 5 (p. 32), the reference line will make a glancing angle of

$$\theta_B + \beta - \frac{\phi^2}{2} \tan \theta_B \qquad 3.13$$

with the planes of crystal B. The ray in question now makes a glancing angle of

$$\theta_B + \beta - \frac{\phi^2}{2} \tan \theta_B - (\theta_s - \theta_o) \qquad 3.14$$

which is

$$\theta_B + \beta - \frac{\phi^2}{2} \tan \theta_B - \left[\frac{\lambda - \lambda_o}{\lambda_o} \tan \theta_B + \frac{\phi^2}{2} \tan \theta_B - b\left(\alpha - \frac{\phi^2}{2} \tan \theta_B - \frac{\lambda - \lambda_o}{\lambda_o} \tan \theta_B\right)\right] \qquad 3.15$$

Thus the general result is obtained for the glancing angle with the planes of crystal B of this ray of wavelength λ_o with vertical and horizontal divergence ϕ and α, and for either parallel or antiparallel case (crystal B is rotated through angle β from angular setting for Bragg's law of reflection for the central ray):

$$\theta_B \mp \beta - \frac{\phi^2}{2}\tan\theta_B \pm \left[\frac{\lambda-\lambda_o}{\lambda_o}\tan\theta_B + \frac{\phi^2}{2}\tan\theta_B - b\left(\alpha - \frac{\phi^2}{2}\tan\theta_B - \frac{\lambda-\lambda_o}{\lambda_o}\tan\theta_B\right)\right] \qquad 3.16$$

where the upper signs are for the "parallel" case and the lower for the "antiparallel". If this ray of wavelength λ is to satisfy Bragg's condition of reflection it must make a glancing angle of

$$\theta_B + \frac{\lambda - \lambda_o}{\lambda_o}\tan\theta_B \qquad 3.17$$

with the planes of crystal B. The angular deviation of the ray of wavelength λ from condition of Bragg reflection is just the difference between Eqs. 3.16 and 3.17 which is

$$\mp\beta - \frac{\phi^2}{2}\tan\theta_B - \frac{\lambda-\lambda_o}{\lambda_o}\tan\theta_B \pm \left[\frac{\lambda-\lambda_o}{\lambda_o}\tan\theta_B + \frac{\phi^2}{2}\tan\theta_B - b\left(\alpha - \frac{\phi^2}{2}\tan\theta_B - \frac{\lambda-\lambda_o}{\lambda_o}\tan\theta_B\right)\right] \qquad 3.18$$

The intensity of this ray after reflection from crystal A and crystal B is then $I_o(\lambda - \lambda_o)\frac{I_H}{I_o}\left(\alpha - \frac{\phi^2}{2}\tan\theta_B - \frac{\lambda-\lambda_o}{\lambda_o}\tan\theta_B\right) \times$

$$\frac{I_H}{I_o}\left(\mp\beta - \frac{\phi^2}{2}\tan\theta_B - \frac{\lambda-\lambda_o}{\lambda_o}\tan\theta_B \pm \left\{\frac{\lambda-\lambda_o}{\lambda_o}\tan\theta_B + \frac{\phi^2}{2}\tan\theta_B - b\left(\alpha - \frac{\phi^2}{2}\tan\theta_B - \frac{\lambda-\lambda_o}{\lambda_o}\tan\theta_B\right)\right\}\right) \qquad 3.19$$

with the convention of signs as before.

PARALLEL CASE

The above case treats both crystals as being identical. If not, then diffraction pattern and θ_B will be different for each crystal in the derivation above. The case is general as the diffracting planes can make any angle with the two parallel faces of the crystal. The specific case for these planes to be normal to the crystal faces (b = +1)

will now be treated. For b = +1 Eq. 3.19 reduces to

$$I_o(\lambda - \lambda_o)\frac{I_H}{I_o}(\alpha - \frac{\phi^2}{2}\tan\theta_B - \frac{\lambda-\lambda_o}{\lambda_o}\tan\theta_B)\frac{I_H}{I_o}(-\beta-\alpha+\frac{\phi^2}{2}\tan\theta_B+\frac{\lambda-\lambda_o}{\lambda_o}\tan\theta_B) \qquad 3.20$$

For a particular setting β and for normal polarization of the incident beam, the ratio of the power diffracted from crystal B to that incident on crystal B will be

$$P(\beta) \qquad 3.21$$

$$= \frac{S_H' \int\int\int I_o(\lambda-\lambda_o)\frac{I_H}{I_o}(\alpha-\frac{\phi^2}{2}\tan\theta_B-\frac{\lambda-\lambda_o}{\lambda_o}\tan\theta_B)\frac{I_H}{I_o}(-\beta-\alpha+\frac{\phi^2}{2}\tan\theta_B+\frac{\lambda-\lambda_o}{\lambda_o}\tan\theta_B)\,d\lambda\,d\phi\,d\alpha}{S_H \int\int\int I_o(\lambda-\lambda_o)\frac{I_H}{I_o}(\alpha-\frac{\phi^2}{2}\tan\theta_B-\frac{\lambda-\lambda_o}{\lambda_o}\tan\theta_B)\,d\lambda\,d\phi\,d\alpha}$$

where S_H and S_H' are the crossectional area of the incident and diffracted beams at crystal B. It is assumed that the intensity is uniform in areal extent over the operation of the system defined by the slits. For b = 1, $S_H'/S_H = 1$. Let $\varepsilon = \alpha - \frac{\phi^2}{2}\tan\theta_B - \frac{\lambda-\lambda_o}{\lambda_o}\tan\theta_B$. Then

$$P(\beta) = \frac{\int\int I_o(\lambda-\lambda_o)\left[\int \frac{I_H}{I_o}(\varepsilon)\frac{I_H}{I_o}(-\beta-\varepsilon)\,d\varepsilon\right]d\lambda\,d\phi}{\int\int I_o(\lambda-\lambda_o)\left[\frac{I_H}{I_o}(\varepsilon)\,d\varepsilon\right]d\lambda\,d\phi} \qquad 3.22$$

As $\frac{I_H}{I_o}(\varepsilon) = 0$ except in a very short range, the limits of integration are extended to $\pm\infty$. As ϕ and λ are constant over the integration on α then $\int_{-\infty}^{\infty}\frac{I_H}{I_o}(\varepsilon)\frac{I_H}{I_o}(-\beta-\varepsilon)\,d\varepsilon$ and $\int_{-\infty}^{\infty}\frac{I_H}{I_o}(\varepsilon)\,d\varepsilon$ become independent of λ and ϕ, so

$$P(\beta) = \frac{\int_{-\infty}^{\infty}\frac{I_H}{I_o}(\varepsilon)\frac{I_H}{I_o}(-\beta-\varepsilon)\,d\varepsilon}{\int_{-\infty}^{\infty}\frac{I_H}{I_o}(\varepsilon)\,d\varepsilon} \qquad 3.23$$

Thus the $P(\beta)$ curve is independent of the height or width of the slits or the spectral distribution of the radiation employed. This assumes that the variation of the diffraction pattern with wavelength

is small over the range of wavelengths allowed to be transmitted by the slits.

QUANTITIES TO BE COMPARED TO EXPERIMENT

In the normal operation of the two crystal spectrometer as used here, both parallel and normal polarized components (represented by superscripts) of the x-ray beam enter the detector. The ratio of the power received by the detector to that incident on crystal B now becomes

$$P(\beta) = \frac{\int_{-\infty}^{\infty} \left[{}^{p}P_o \frac{{}^{p}I_H}{I_o}(\varepsilon) \frac{{}^{p}I_H}{I_o}(-\beta-\varepsilon) + {}^{n}P_o \frac{{}^{n}I_H}{I_o}(\varepsilon) \frac{{}^{n}I_H}{I_o}(-\beta-\varepsilon) \right] d\beta}{\int_{-\infty}^{\infty} \left[{}^{p}P_o \frac{{}^{p}I_H}{I_o}(\varepsilon) + {}^{n}P_o \frac{{}^{n}I_H}{I_o}(\varepsilon) \right] d\varepsilon} \qquad 3.24$$

The integrated reflecting power for the two crystal spectrometer is defined as

$$R = \int_{-\infty}^{\infty} P(\beta)\, d\beta$$

where R is the area under the "normalized" two crystal rocking curve as defined by Eq. 3.24. Thus

$$R = \frac{\int_{-\infty}^{\infty} \left[\int_{-\infty}^{\infty} \left\{ {}^{p}P_o \frac{{}^{p}I_H}{I_o}(\varepsilon) \frac{{}^{p}I_H}{I_o}(-\beta-\varepsilon) + {}^{n}P_o \frac{{}^{n}I_H}{I_o}(\varepsilon) \frac{{}^{n}I_H}{I_o}(-\beta-\varepsilon) \right\} d\varepsilon \right] d\beta}{\int_{-\infty}^{\infty} \left[{}^{p}P_o \frac{{}^{p}I_H}{I_o}(\varepsilon) + {}^{n}P_o \frac{{}^{n}I_H}{I_o}(\varepsilon) \right] d\varepsilon} \qquad 3.25$$

This can be simplified by examining the repeated integral in the numerator

$$\int_{-\infty}^{\infty} \left[\int_{-\infty}^{\infty} \frac{I_H}{I_o}(\varepsilon) \frac{I_H}{I_o}(-\beta-\varepsilon)\, d\varepsilon \right] d\beta$$

The order of integration can be interchanged as $\frac{I_H}{I_o} \approx \frac{1}{1+\varepsilon^2}$ and thus the integrand satisfies the conditions for such an interchange.

$$\int_{-\infty}^{\infty}\left[\int_{-\infty}^{\infty}\frac{I_H}{I_o}(\varepsilon)\,\frac{I_H}{I_o}(-\beta-\varepsilon)\,d\varepsilon\right]d\beta=\int_{-\infty}^{\infty}\frac{I_H}{I_o}(\varepsilon)\left[\int_{-\infty}^{\infty}\frac{I_H}{I_o}(-\beta-\varepsilon)\,d\varepsilon\right]d\beta$$

but $\int_{-\infty}^{\infty}\frac{I_H}{I_o}(-\beta-\varepsilon)\,d\varepsilon=\int_{-\infty}^{\infty}\frac{I_H}{I_o}(-\varepsilon)\,d\varepsilon$ and is independent of β

being the area under the diffraction curve. So

$$\int_{-\infty}^{\infty}\left[\int_{-\infty}^{\infty}\frac{I_H}{I_o}(\varepsilon)\,\frac{I_H}{I_o}(-\beta-\varepsilon)\,d\varepsilon\right]d\beta=\int_{-\infty}^{\infty}\frac{I_H}{I_o}(\varepsilon)\,d\varepsilon\cdot\int_{-\infty}^{\infty}\frac{I_H}{I_o}(-\varepsilon)\,d\varepsilon$$

and

$$R=\frac{{}^{p}P_o\left[{}^{p}R_H^{\theta}\right]^2+{}^{n}P_o\left[{}^{n}R_H^{\theta}\right]^2}{{}^{p}P_o\,{}^{p}R_H^{\theta}+{}^{n}P_o\,{}^{n}R_H^{\theta}} \qquad 3.26$$

where $R_H^{\theta}=\int_{-\infty}^{\infty}\frac{I_H}{I_o}(\varepsilon)\,d\varepsilon$ as defined by Eq. 2.23.

If the wavelength used is not too close to λ_{min}, defined by $\lambda_{min}=\frac{hc}{eV}$ (V is the voltage applied across the x-ray tube), the radiation can be considered unpolarized, and ${}^{n}P_o={}^{p}P_o=\frac{P_o}{2}$. Eq. 3.26 now becomes

$$R=\frac{\left[{}^{p}R_H^{\theta}\right]^2+\left[{}^{n}R_H^{\theta}\right]^2}{{}^{p}R_H^{\theta}+{}^{n}R_H^{\theta}} \qquad 3.27$$

From Eq. 2.25 this is written in terms of R_H^{y} as

$$R=\frac{|\psi_H'|\left\{\left[{}^{n}R_H^{y}\right]^2+\cos^2 2\theta_B\left[{}^{p}R_H^{y}\right]^2\right\}}{\sin 2\theta_B\left\{{}^{n}R_H^{y}+\cos 2\theta_B\,{}^{p}R_H^{y}\right\}} \qquad 3.28$$

From Eq. 2.26

$$R_H^{y}=e^{-\frac{\mu_o t_o}{\gamma_o}\frac{\pi}{2}\left[1+c^2a^2\right]}$$

and so for each polarization

$${}^{n}R_H^{y}=e^{-\frac{\mu_o t_o}{\gamma_o}\frac{\pi}{2}\left[1+\ell_o^2\right]};\quad {}^{p}R_H^{y}=e^{-\frac{\mu_o t_o}{\gamma_o}\frac{\pi}{2}\left[1+\ell_o^2\cos^2 2\theta_B\right]}$$

and

$$e^{\frac{\mu_o t_o}{\gamma_o}}R=\left\{\frac{e^2}{mc^2}\frac{d}{2}\frac{|F_H|}{V}\right\}\frac{\lambda}{\cos\theta_B}\left[\frac{1+\cos^2 2\theta_B+2\ell_o^2\left(1+\cos^4 2\theta_B\right)}{1+\cos 2\theta_B+\ell_o^2\left(1+\cos^3 2\theta_B\right)}\right] \qquad 3.29$$

where $\ell_o=cA\ (K=1)$ is defined by Eqs. 2.18 and 2.20 and is the term due to anomalous scattering.

The peak value of the $P(\beta)$ curve is

$$P(0) = \frac{\int_{-\infty}^{\infty} \left[\frac{n_{I_H}}{I_o} (\varepsilon) \right]^2 d\varepsilon + \int_{-\infty}^{\infty} \left[\frac{p_{I_H}}{I_o} (\varepsilon) \right]^2 d\varepsilon}{n_{R_H^\theta} + p_{R_H^\theta}} \qquad 3.30$$

since $\frac{I_H}{I_o} (\varepsilon)$ is symmetrical about $\varepsilon = 0$. From Eq. 2.25 this becomes in terms of the variable y

$$P(0) = \frac{\int_{-\infty}^{\infty} \left[\frac{n_{I_H}}{I_o} (y) \right]^2 dy + \cos 2\theta_B \int_{-\infty}^{\infty} \left[\frac{p_{I_H}}{I_o} (y) \right]^2 dy}{n_{R_H^y} + \cos 2\theta_B \; p_{R_H^y}}$$

Substituting for R_H^y and $\frac{I_H}{I_o} (y)$ from Eqs. 2.26 and 2.22

$$P(0) e^{\frac{\mu_o t_o}{\gamma_o}} = \frac{1}{4} \left[\frac{1 + \cos 2\theta_B + \frac{3}{4} \ell_o^2 (1 + \cos^3 2\theta_B)}{1 + \cos 2\theta_B + \ell_o^2 (1 + \cos^3 2\theta_B)} \right] \qquad 3.31$$

The half width at half maximum, W_θ, for the two crystal "parallel" rocking curve is determined by doubling the half width of the diffraction pattern for the case of a single crystal. This is justified because the theoretical diffraction pattern of the single crystal given by Eq. 2.22 deviates from a witch by only about 6 per cent at $\lambda = 0.710\text{Å}$ and a negligible amount at $\lambda = 0.210\text{Å}$. In Appendix D it is shown that the result of the fold of two witches is another witch whose half width at half maximum is the sum of the half width of the two witches being folded. Thus, let W_θ be the half width of the two crystal "parallel" rocking curve; then

$$W_\theta = 2w_\theta = \frac{|\overline{K}||\psi_H|}{\sin 2\theta_B} w_y$$

Substituting the value of w_y from Eq. 2.28

$$W_\theta = \left\{ \frac{2d}{\pi} \frac{e^2}{mc^2} \frac{|F_H|}{V} \right\} \cos \theta_B \lambda \left[\frac{2(1 + \ell_o^2 \cos^4 \theta_B)}{1 + 2\ell_o^2 \cos^4 \theta_B} - 1 \right]^{\frac{1}{2}} \qquad 3.32$$

$\text{Re} \frac{\mu_o t_o}{\gamma_o}$, $P(0) e^{\frac{\mu_o t_o}{\gamma_o}}$, and W_θ are calculated as a function of wave-

length in Appendix F. These three quantities are used in comparing the theoretical two crystal "parallel" rocking curves with the experimental "parallel" rocking curves. In Part VI the calculations for these three quantities are presented and compared with the experimental results.

ANTIPARALLEL CASE

Referring to Eq. 3.19 and the sign convention, in the antiparallel case the intensity of the beam after reflection from both crystals is

$$I_o(\lambda-\lambda_o)\frac{I_H}{I_o}\left(\alpha-\frac{\phi^2}{2}\tan\theta_B-\frac{\lambda-\lambda_o}{\lambda_o}\tan\theta_B\right)\frac{I_H}{I_o}\left(\beta-\alpha-3\left\{\frac{\phi^2}{2}\tan\theta_B+\frac{\lambda-\lambda_o}{\lambda_o}\tan\theta_B\right\}\right)$$

Let $a(\phi,\lambda)=\frac{\phi^2}{2}\tan\theta_B+\frac{\lambda-\lambda_o}{\lambda_o}\tan\theta_B$. The ratio of the power diffracted from crystal B to the incident power on it now becomes, for normal polarization,

$$P_{\#}(\beta)=\frac{\int\int\int I_o(\lambda-\lambda_o)\frac{I_H}{I_o}(\alpha-a(\phi,\lambda))\frac{I_H}{I_o}(\beta+\alpha-3a(\phi,\lambda))\,d\alpha\,d\phi\,d\lambda}{\int\int\int I_o(\lambda-\lambda_o)\frac{I_H}{I_o}(\alpha-a(\phi,\lambda))\,d\alpha\,d\phi\,d\lambda} \qquad 3.33$$

where $P_{\#}(\beta)$ means the antiparallel case. Here a single variable cannot be defined to include all terms in ϕ, α, and λ to be the same in both arguments of the numerator. The integration on α can be performed in the denominator, and the result is $\int_{-\infty}^{\infty}\frac{I_H}{I_o}(\varepsilon)\,d\varepsilon$ and is independent of $a(\phi,\lambda)$, which merely displaces the curve; its area remains essentially the same. Let

$$\varepsilon_1=\alpha-a(\phi,\lambda)$$

$$\varepsilon_2=\beta-2a(\phi,\lambda)$$

$$\varepsilon_2+\varepsilon_1=\beta+\alpha-3a(\phi,\lambda)$$

and Eq. 3.33, using the same argument as before to extend the integration limits to $\pm\infty$, becomes

$$P_H(\beta) = \frac{\int\int^{\lambda}\int^{\phi} I_o(\lambda-\lambda_o)\left[\int_{-\infty}^{\infty}\frac{I_H}{I_o}(\varepsilon_1)\frac{I_H}{I_o}(\varepsilon_2+\varepsilon_1)\,d\varepsilon_1\right]d\phi d\lambda}{\int\int^{\lambda}\int^{\phi} I_o(\lambda-\lambda_o)\,d\phi\,d\lambda\cdot\left[\int_{-\infty}^{\infty}\frac{I_H}{I_o}(\varepsilon_1)\,d\varepsilon_1\right]} \qquad 3.34$$

When $\frac{I_H}{I_o}$ is an even function, $\frac{I_H}{I_o}(\varepsilon) = \frac{I_H}{I_o}(-\varepsilon)$, (which is so for the case under consideration, see Eq. 2.22); the term in the brackets is just the two crystal "parallel" rocking curve (see Eq. 3.23). So

$$P_H(\beta) = \frac{\int_{-\phi}^{\phi}\left[\int_{-\lambda}^{\lambda} I_o(\lambda-\lambda_o)\,P(\beta-2a(\phi,\lambda))\,d\lambda\right]d\phi}{\int_{-\phi}^{\phi}\left[\int_{-\lambda}^{\lambda} I_o(\lambda-\lambda_o)\,d\lambda\right]d\phi} \qquad 3.35$$

where

$$\beta - 2a(\phi,\lambda) = \left\{\frac{\lambda_o}{2\tan\theta_B}(\beta-\phi^2\tan\theta_B)-(\lambda-\lambda_o)\right\}\frac{2\tan\theta_B}{\lambda_o}$$

$$\equiv \left\{\gamma-(\lambda-\lambda_o)\right\}\frac{2\tan\theta_B}{\lambda_o}$$

Let $I_o(\lambda-\lambda_o)$ be a spectral line and let the vertical slit jaws be wide enough so that $I_o(\lambda-\lambda_o)\to 0$ at the edges so that the limits of integration become $\pm\infty$. It has also been shown from experiment and theory that $I_o(\lambda-\lambda_o)$ for line spectra of the heavy elements is a witch. The parallel rocking curve is also a witch. The result of the integration of Eq. 3.35 gives another witch (see Appendix D). $I_o(\lambda-\lambda_o)$ and $P(\varepsilon_2)$ can be written in terms of quantities used above as

$$\frac{I_o(\lambda-\lambda_o)}{\int_{-\lambda}^{\lambda} I_o(\lambda-\lambda_o)\,d\lambda} = \frac{I_1}{1+\left(\frac{\lambda-\lambda_o}{a}\right)^2}$$

$$P(\varepsilon_2) = \frac{I_2}{1+\frac{\left(\beta-\frac{2\phi^2}{2}\tan\theta_B-\frac{2\lambda-\lambda_o}{\lambda_o}\tan\theta_B\right)^2}{g^2}}\;\frac{I_2}{1+\frac{((\lambda-\lambda_o)-\gamma)^2}{c^2}}$$

where $c = \frac{\varepsilon \lambda_0}{2 \tan \theta_B}$; $\gamma = (\beta - \phi^2 \tan \theta_B) \frac{\lambda_0}{2 \tan \theta_B}$.

So from Appendix D

$$P_{\mu}(\beta) = \int_{-\phi_{MAX.}}^{\phi_{MAX}} \frac{I_1 I_2 ac}{a+c} \frac{\pi}{1+\left(\frac{\gamma}{a+c}\right)^2} \frac{d\phi}{2\phi_{max}} = \frac{P_0}{2\phi_{max}} \int_{-\phi_m}^{\phi_{MAX.}} \frac{d\phi}{1+\frac{\beta^2 - 2\beta\phi^2 \tan\theta_B + \phi^4 \tan^2\theta_B}{(a+c)^2}}$$

Dropping the term in ϕ^4 in the integrand

$$P_{\mu}(\beta) = \frac{P_0}{1+\frac{\beta^2}{(a+c)^2}} \left\{ 1 + \phi^2 \left[\frac{2\beta \tan\theta_B}{1+\frac{\beta^2}{(a+c)^2}} \right]^{\frac{3}{2}} + \phi^4 \left[\frac{2\beta \tan\theta_B}{1+\frac{\beta^2}{(a+c)^2}} \right]^{\frac{5}{2}} + \cdots \right\} \qquad 3.37$$

Thus by making the assumption that the spectral distribution of an x-ray line is a witch, then the vertical divergence affects only the amplitude and not the shape of the antiparallel rocking curve, if terms in ϕ^2 can be dropped, where the crystals are used in transmission and the diffracting planes are normal to the crystal faces. The width of the $P_{\mu}(\beta)$ curve differs from the $I_0(\lambda - \lambda_0)$ curve by the half width being increased by the half width (g) of the parallel rocking curves.

PART IV

EXPERIMENTAL APPARATUS

Components of the experimental system are: the x-ray tube and its filament and high voltage supply, the two crystal spectrometer, and the detector of the x-rays.

X-RAY EQUIPMENT

The molybdenum and tungsten x-ray tubes used for the determination of the wavelength of the $WK\alpha_1$ line were also used to determine the characteristics of the two crystal "parallel" rocking curves in the wavelength range $0.120\text{Å} \leq \lambda \leq 0.710\text{Å}$. The high voltage for the molybdenum tube was supplied by a Wappler rectified, filtered high voltage supply. A Phillips rectified high voltage source was used with the tungsten tube.

In both the wavelength determination and the diffraction pattern characteristics vs. wavelength study, it is desirable to hold the power supply constant. From the Dushman thermionic emission equation it can be shown that a 1 per cent change in the filament current can cause a 10 per cent change in the emission current, which shows the desirability of holding filament voltage constant. The filament voltage was stabilized by a saturable core voltage stabilizer. This worked very well as long as no large abrupt voltage changes occurred in the supply line. The expense of stabilizing the high voltage supply was too great to justify use in this experiment. Maintaining the high voltage constant was done manually.

TWO CRYSTAL X-RAY SPECTROMETER

The success in achieving the high accuracy in the $WK\alpha_1$ wavelength determination, described in the next part, was made possible by the high precision of the two crystal x-ray spectrometer designed and built by DuMond.[16] It has the ability to reproduce angular settings to about 1/4 of a second of arc over as large angles of rotation as 180°. The instrument is capable of great flexibility. The instrument is shown in Fig. 6 (p. 45). The axis of the spectrometer table coincides with the axis for crystal holder, pivot A. The axis of crystal holder B moves with the spectrometer table about pivot A. The axis for the detector arm and cradle coincides with the axis of crystal holder B. The gears were so designed that when all four drives are coupled together the proper relationship for Bragg reflection is always satisfied. In this study the detector arm and crystal B were coupled together. Crystal A is stationary. Thus when a rocking curve was measured, the detector moved twice as fast as crystal B so as always to satisfy Bragg's condition of reflection. In the construction of the two crystal spectrometer, the worm gears driving the crystal pivots were lapped to reduce errors and the final errors in the readings were determined by optical methods.[16] The error graphs are shown in Fig. 7 (p. 46). As the widths of the rocking curves obtained in the parallel and antiparallel positions are of the magnitude of a minute of arc and less, it is seen from the correction curves that the variation of the correction over this range is very small. When measuring 2θ to determine $\lambda_{WK\alpha_1}$, the corrections were consequently made only to the center position of the observed rocking curves.

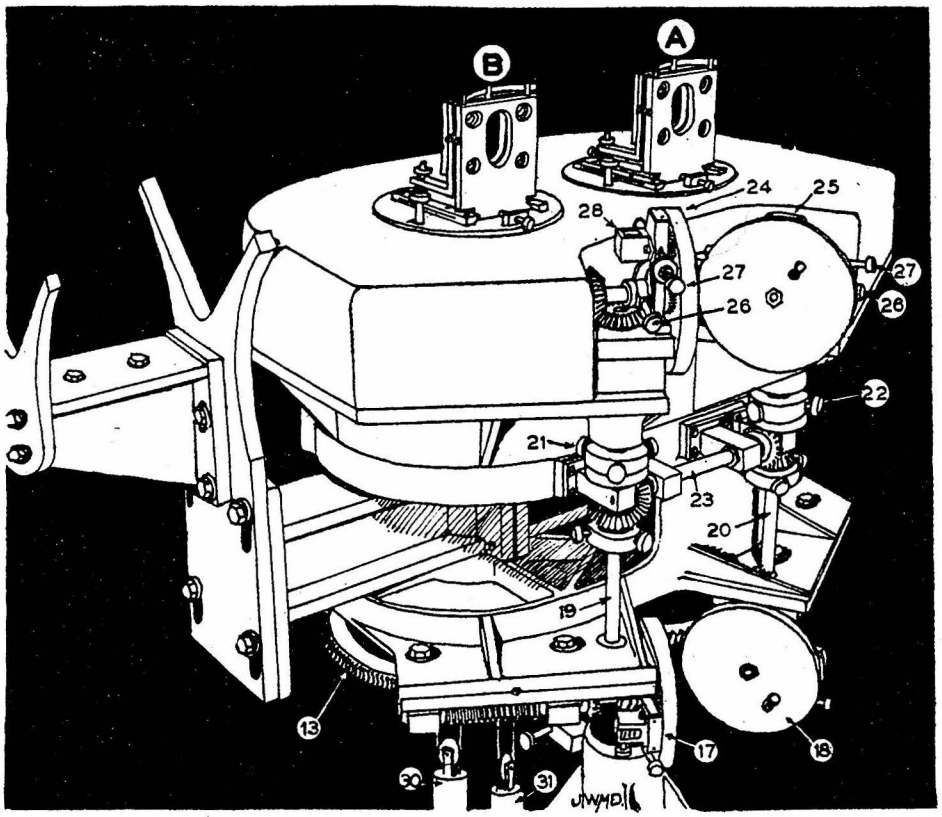

Fig. 6. Two crystal x-ray spectrometer showing crystal holders A and B, gear drives, clutches coupling the upper and lower worm wheel drives, and cradle for holding the detector. [Copied from DuMond and Marlow, R.S.I. 8, 112 (1937)]

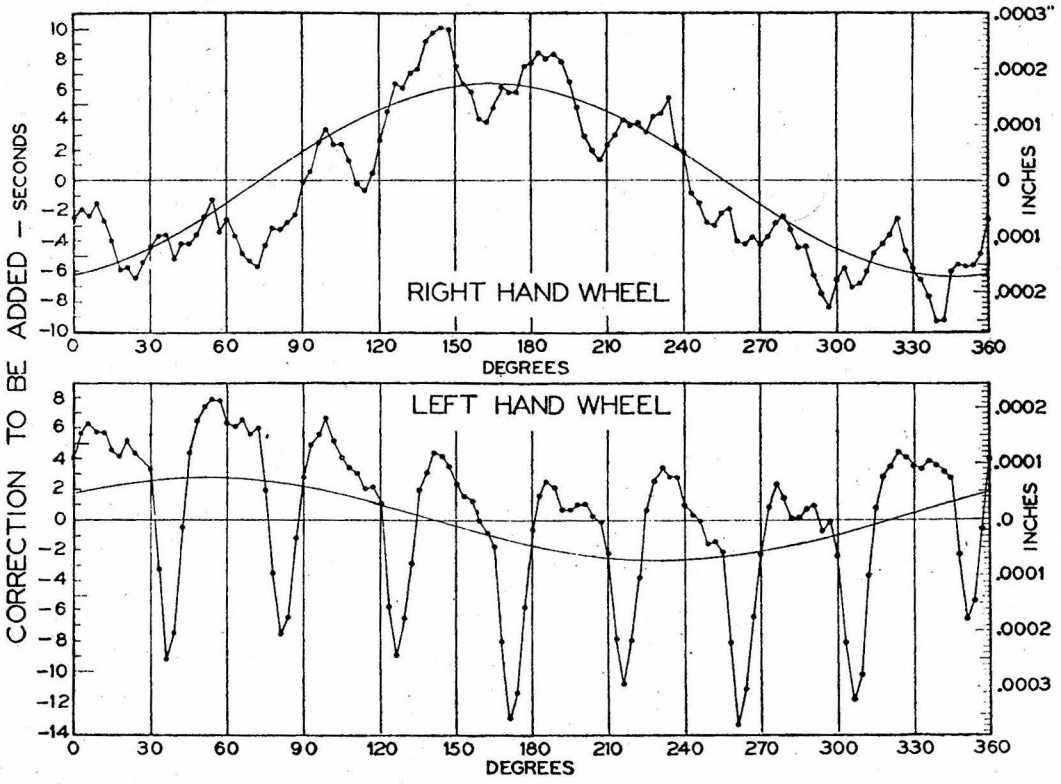

Fig. 7. Error graphs obtained by optical calibration of the two worm wheels in the two crystal x-ray spectrometer. [Copied from DuMond and Marlow, R.S.I. 8, 112 (1937)]

The quartz crystals used in this study were optically flat plates 1 mm thick with the (310) diffracting planes normal to the face. Great care was taken in mounting the crystals so that no mechanical strains would be introduced causing curvature of the crystals. This was done by a three point support. Small tension springs were used to maintain contact of the crystal with these three points.

The proper alignment of the spectrometer and x-ray beam is very important for this precision study. The spectrometer was conveniently constructed so that the flat top portion (see Fig. 6 (p. 45)) was machined fairly accurately perpendicular to the axes of the pivots A and B, which are very accurately parallel. Thus these axes are easily made vertical by the use of the leveling screws on the feet of the spectrometer and a high sensitive level on the table top. The faces of the crystals were made vertical by the use of a level telescope with a Gauss eyepiece. The centers of the crystals were then made to coincide with axes of the pivots A and B. To facilitate finding the positions of the crystals for Bragg reflection of the K_{α_1} line, the zero readings for the crystals, when their faces are parallel and when the x-ray beam passes over the crystal pivots, A and B, was determined. This was done by establishing by means of trammels and plumb-bobs a horizontal perpendicular bisector of the axes A and B. The telescope of an optical spectrometer which has a Gauss eyepiece was then adjusted so that its axis of rotation (adjusted to be vertical) was on this bisector. With the telescope pointed at each crystal face the angle which the normal to each crystal made with the bisector was determined. This was done by rotating both the telescope and crystal

until the cross hairs in the Gauss eyepiece were reflected back into the telescope. The angle of rotation of the telescope was read and the crystal rotated back through the same amount to its zero setting. The x-ray tube and slits were then adjusted so that the x-ray beam passed horizontally over the axes of both pivots A and B.

It is very important that the diffracting planes shall be parallel to their axes of rotation and vertical. In the present Laue or transmission case with a quartz lamina these planes are not optically accessible as reflecting surfaces. If they are not parallel to their axes of rotation, then for each vertically diverging ray a different setting of crystal B relative to crystal A is required for the ray to be Bragg reflected at both crystals. This has the effect of broadening the rocking curves. This fact was used in the process of making the diffracting planes parallel. The first step in this process was to take a Laue photograph of the diffracted beam from the (310) planes of the quartz crystals of a very small x-ray target with a narrow slit in front of the crystal, the film being placed 240 cms behind the crystal, then to rotate the crystal through 180° and take another photograph on the same film. The horizontal perpendicular distance of the photographic images from the projection of the incident beam (approximately 127 cm) and the vertical displacement of the photographic images (4-8 mm) from each other were measured. The angle that the crystal planes made with the vertical axis of rotation was then calculated. A lever arm and tangent screw connected to the crystal holder was used to correct the direction of the crystal planes. The amount of correction was determined by use of a telescope and scale, and a small mirror attached

to the crystal holders. The photographic images were about 3-4 mm in size and were not sharp, making it possible to locate the direction of the crystal planes only within several minutes of arc. The error in making the axes A and B vertical was also of the same magnitude. The second step was to run a parallel rocking curve and then rotate crystal B 180° and repeat the run. The narrower curve for crystal B in these two positions corresponded to the case where the diffracting planes for crystals A and B were more nearly parallel. Crystal B was then set in the position for the broader parallel-rocking curve, and the directions of the diffracting planes of both crystals A and B were then rotated by a small amount, but in opposite directions, so as to make both more nearly vertical and at the same time coincide with the pivot axis. The process was then repeated until the narrowest parallel-rocking curve was obtained.

The vertical slit jaws determine the range of wavelengths that are able to pass through the system in the "parallel position" rocking curve studies. As the diffraction pattern of the crystals is only of the order of two seconds of arc, each ray of wavelength λ from the x-ray tube must satisfy Bragg's law of reflection to be transmitted. If the central ray of wavelength λ_0 is Bragg reflected then the ray of wavelength λ must make an angle ε with the central ray to be Bragg reflected, where $\varepsilon = \frac{\lambda - \lambda_0}{\lambda_0} \tan \theta_0$. This is shown by Fig. 8 (p. 50). At each angle ε a different wavelength is Bragg reflected. As the angle of incidence equals the angle of reflection ($\theta = \theta_B$) all the rays from a given point T_0 at the target focal spot come to a focus at T_0''' where $OT_0 = OT_0'''$. The defining slits were located midway between

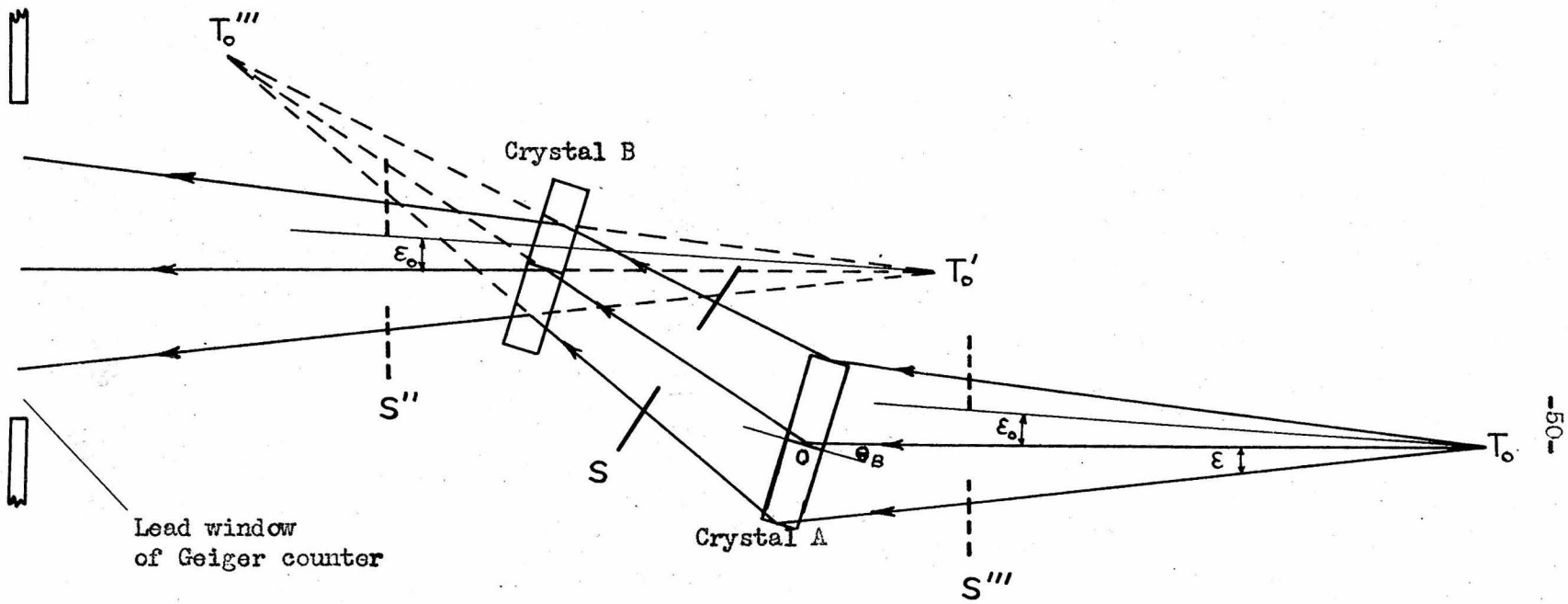

Fig. 8. Schematic illustration showing the horizontal divergence of the x-ray beam from a particular point (T_o) on the focal spot of the target of the x-ray tube. S is the defining slit system and has effective images at S" and S"'. The range in wavelengths transmitted by the system is determined by ε_o and is given by Bragg's law, $d\lambda = 2d \cos\theta_B \varepsilon_o$.

the crystal pivots A and B. As seen from Fig. 8 (p. 50), this slit has an effective image at S'' and S'''. The range in wavelengths passed was determined by the angle that the slit at S''' subtends at T_o. The slit width was 4 mm and after the width of the target focal spot was taken into consideration the aperture of the detector was made larger than the width of the beam at the detector.

The vertical height of the detector opening was 1 cm. The vertical dimension of the focal spot of the x-ray target was 1 cm for the molybdenum tube and 0.5 cm for the tungsten tube. X-ray target to detector = 159 cm. So

λÅ	$\phi 2$	$\frac{1}{4}\phi^2 \tan \theta_B$
0.710	39.6×10^{-6}	0.64 seconds of arc
0.208	22.2×10^{-6}	0.10 seconds of arc

DETECTION OF X-RAYS

Previous work with this two crystal x-ray spectrometer incorporated an ion chamber and a d.c. amplifier using the Barth circuit as described by Penick.[17] Such a system has two disadvantages; the drift of the d.c. amplifier, and the minimum background determined by the detecting apparatus itself. This background arises chiefly from the grid leak current of the electrometer tube, Johnson noise in the grid resistor and alpha particles coming from the sides of the ion chamber. Such a system for detection works satisfactorily when working with line spectra, but if points on the (much weaker) continuous spectrum are desired for study, the background of this detector prohibits its use.

The problems for this study were to increase the power output

of the x-ray tube, to increase the sensitivity of detection, and to reduce the background. The power output was limited by the type of x-ray tube and power supply available. A xenon filled Geiger counter was therefore developed to increase the ratio of peak to background readings. Several articles in the literature have reported unsuccessful attempts in constructing xenon counters. A Geiger counter seems desirable because there are no problems of stability and the background is external to the detector. It has a minor disadvantage of a finite lifetime of three to four months of daily use. Xenon is desirable in this range of wavelengths as its absorption is considerably greater than argon and other gases used in Geiger counters. The counter can thus be made small, reducing the cosmic ray background and still maintain high sensitivity. A comparison of the sensitivity for the same pressure of argon and xenon is shown in Fig. 9 (p. 53).

A crossection of the Geiger tube is shown in Fig. 10 (p. 54). It is the usual Bell type counter, but longer. The body is of copper. The inside was bored and the corner in the end opposite the window was rounded to facilitate cleaning for refilling. The 7 mil, tungsten, center conductor was brought in through a standard Kovar-glass-Kovar seal, which was soldered in place with silver-copper eutectic. The center conductor was terminated in a small glass bead. The 1 mil aluminum window was sealed to the body by a continuous lead gasket (diamond shape in crossection) between the Al window and the copper body; pressure on the gasket was maintained by a stainless steel ring bolted to the copper body by six bolts and spring lock washers.

Considerable difficulty was encountered at first in obtaining a

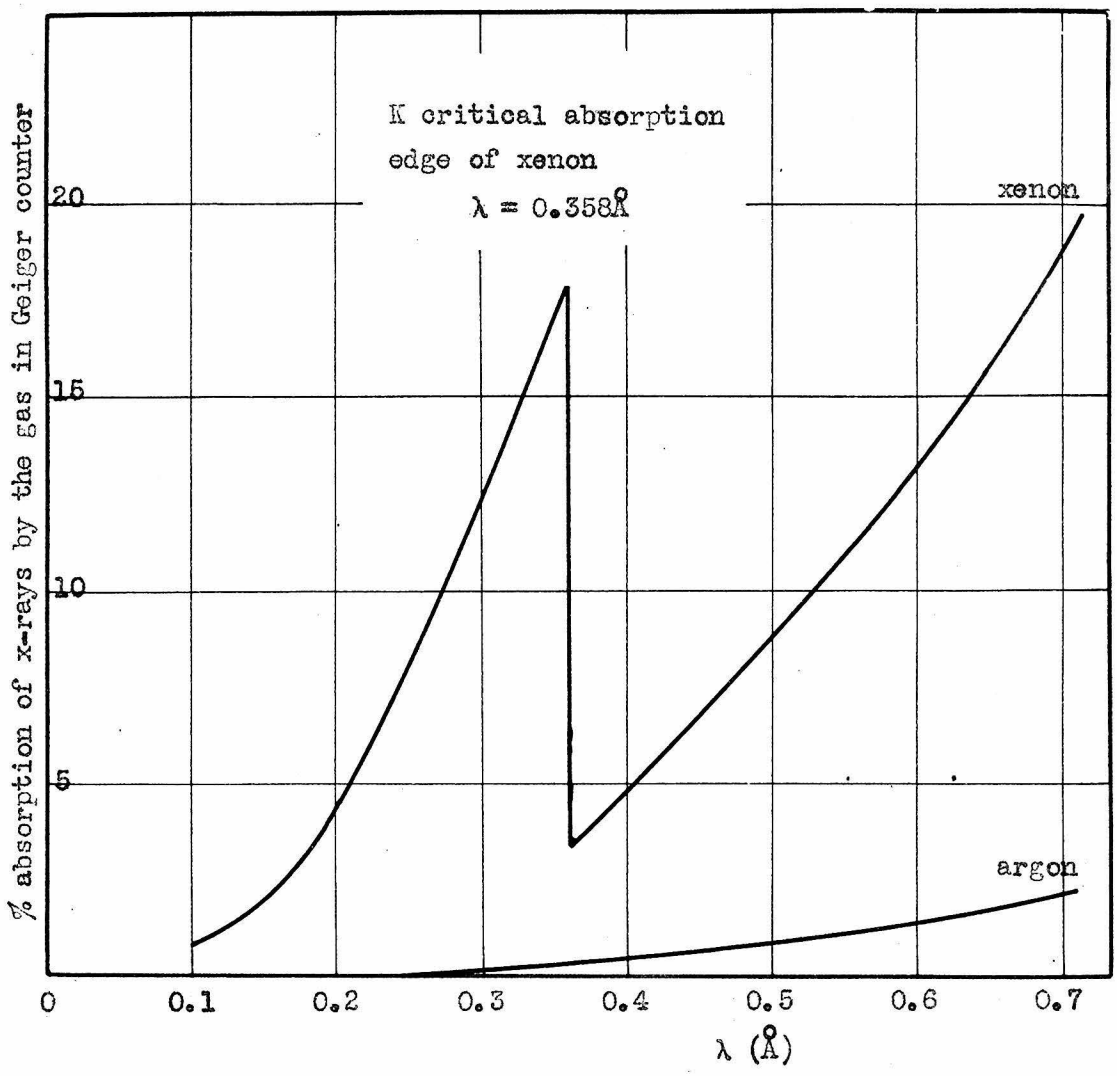

Fig. 9. Calculated absorption of x-rays in a 3 inch path of xenon and argon, both at a pressure of 10 cm. of Hg. Assuming that this absorption is primarily by the photoelectric process, these curves give efficiencies of the counter for these two gases.

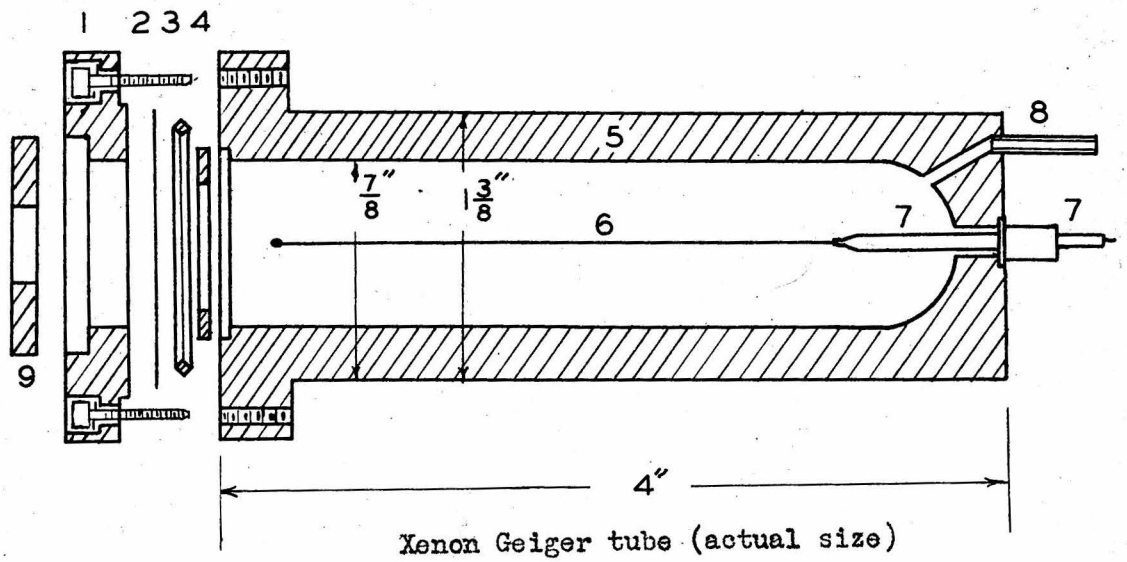

Xenon Geiger tube (actual size)

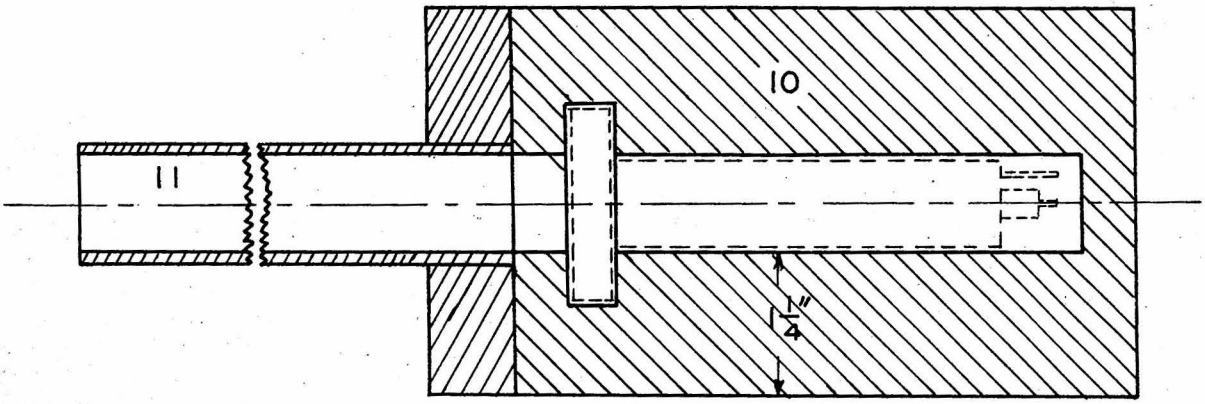

Lead shield for Geiger tube (half size)

Fig. 10. Xenon Geiger tube and lead housing. Components: (1) stainless steel ring damp, (2) 1 mil Al window, (3) continuous lead gasket, (4) copper plate with 1 cm x 2 cm window to support Al window, (5) solid copper body, (6) 7 mil tungsten wire terminated in small glass bead, (7) Kovar-glass-Kovar seal and insulator, (8) copper pumping and filling tube, (9) lead disk with 1 cm x 1 cm window, (10) lead housing split in halves along center line, and (11) $6\frac{1}{2}$ inch lead snout which reduces the solid angle in which the counter receives radiation, thus reducing background.

flat plateau in a plot of the counting rate vs. voltage applied to the Geiger tube. Cleaning the copper cathode with nitric acid and distilled water would result in a good counter when filled with argon, but not with xenon. About 2-3 per cent petroleum ether was used as a quench gas.

The following technique was finally developed in which very satisfactory xenon filled counters of 10 cm pressure and 2-3 per cent petroleum either were obtained. The method of cleaning the tube by baking in hydrogen could not be used because of the low melting point of lead and aluminum. The method of cleaning used was to clean the center conductor by a.c. electrolysis with sodium hydroxide, the copper cathode by baking in hydrogen and the aluminum window with soap and distilled water. The parts were then assembled as quickly as possible and put on the vacuum system for 24 hours. Outgassing was aided by gentle heating. Such a procedure has always resulted in a good counter with a 100^{V} plateau at 1300-1400 volts, and a lifetime of three to four months daily use. An interesting feature was observed that on refilling if only the cathode or anode alone was cleaned, the refilled counter would not operate. Each refill consists of reboring the cathode and replacing the anode. The difficulty encountered by others in constructing a xenon counter seems to lie in the greater sensitivity of xenon to the surface conditions of the cathode and anode, and also according to Korff[18] the quench gas must have an ionization potential lower than that of xenon.

The purpose of the quench gas is to eliminate spurious counts caused by photoelectrons and secondary electrons emitted from the metal

surfaces. Most heavy organic molecules have essentially continuous absorption bands to the ultra-violet radiation produced in Geiger counters. They also have a high probability of decomposing when excited by this ultra-violet radiation. Thus they absorb the photon produced in the ion sheath thus preventing a spurious count. When the xenon ion reaches the cathode, it may liberate a secondary electron which can also cause a spurious count. If a heavy organic molecule that has an ionization potential less than that for xenon (12.08^V) is used as a quench gas, an electron transfer can accompany a collision between xenon and the organic molecule. Now when the organic ion approaches the cathode it can capture an electron, but instead of its excitation energy producing a secondary electron from the wall causing a spurious count, the heavy organic excited molecule decomposes. Part of the fractions in petroleum ether have ionization potentials below 12.0^V allowing this electron transfer.

The response of the counter vs. intensity of the x-ray beam entering it is shown in Fig. 12 (p. 59). In this plot the x-ray spectrometer was set for the MoKα_1 wavelength and the log (counts-per-two-minutes) plotted vs. number of 11 mil aluminum absorbers in the path of the x-ray beam.

Comparing the rocking curves obtained using the ion chamber and d.c. amplifier to those obtained using the xenon counter showed a gain in the ratio of peak to background reading of about 100 times!

A one inch lead housing and 1/8 inch lead snout shown in Fig. 10 (p. 54) reduced the cosmic and x-ray background to about 20 c.p.m. Note that the small dimensions of the counter make the use of this

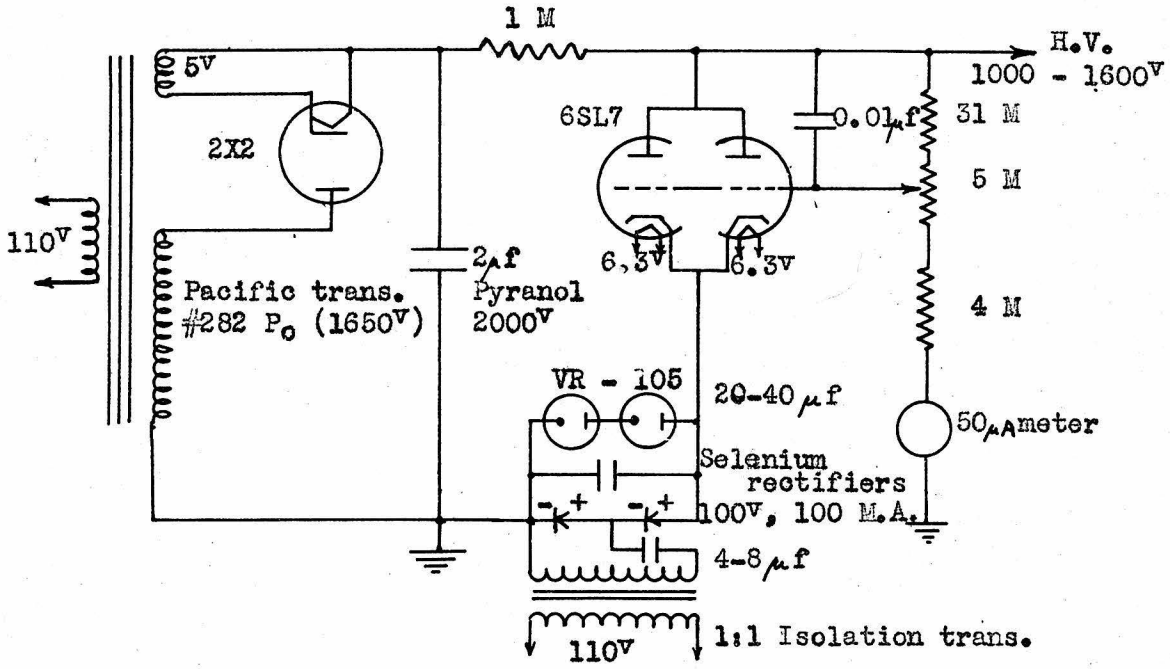

High Voltage Supply

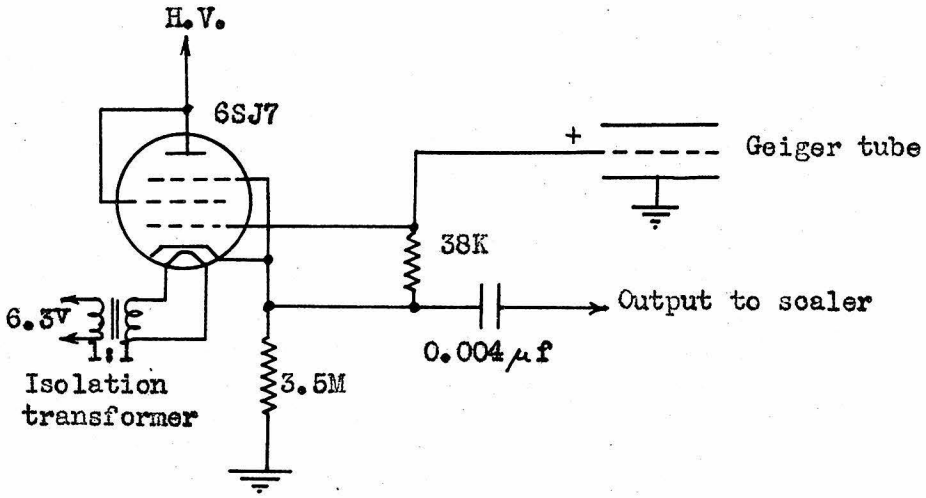

Quench Circuit

Fig. 11. High voltage supply and quench circuit for the xenon Geiger counter.

lead shielding much less cumbersome than would be the case for an ion chamber set-up.

The high voltage supply and the quench circuit for the xenon counter are shown in Fig. 11 (p. 57). The quench circuit is the Neher-Pickering type. The resistance in the RC circuit (C is the capacitance to ground) regulates the time for the charge to leak off the Geiger tube after it has fired; and thus the time the voltage on the Geiger tube is held at its threshold value. Holding the voltage down allows the discharge inside the Geiger tube to be neutralized without producing spurious counts. This cathode-follower type circuit converts a high impedance line to one of low impedance and thus permits the use of a long transmission line between the Geiger tube and quench circuit and the scaler. The negative pulse from the output of the quench circuit is fed to a one stage amplifier and the positive output pulse from the amplifier is fed to the scaler. The scaler[19] has a scale of 64 and drives a "Cyclotron Specialties" counter.

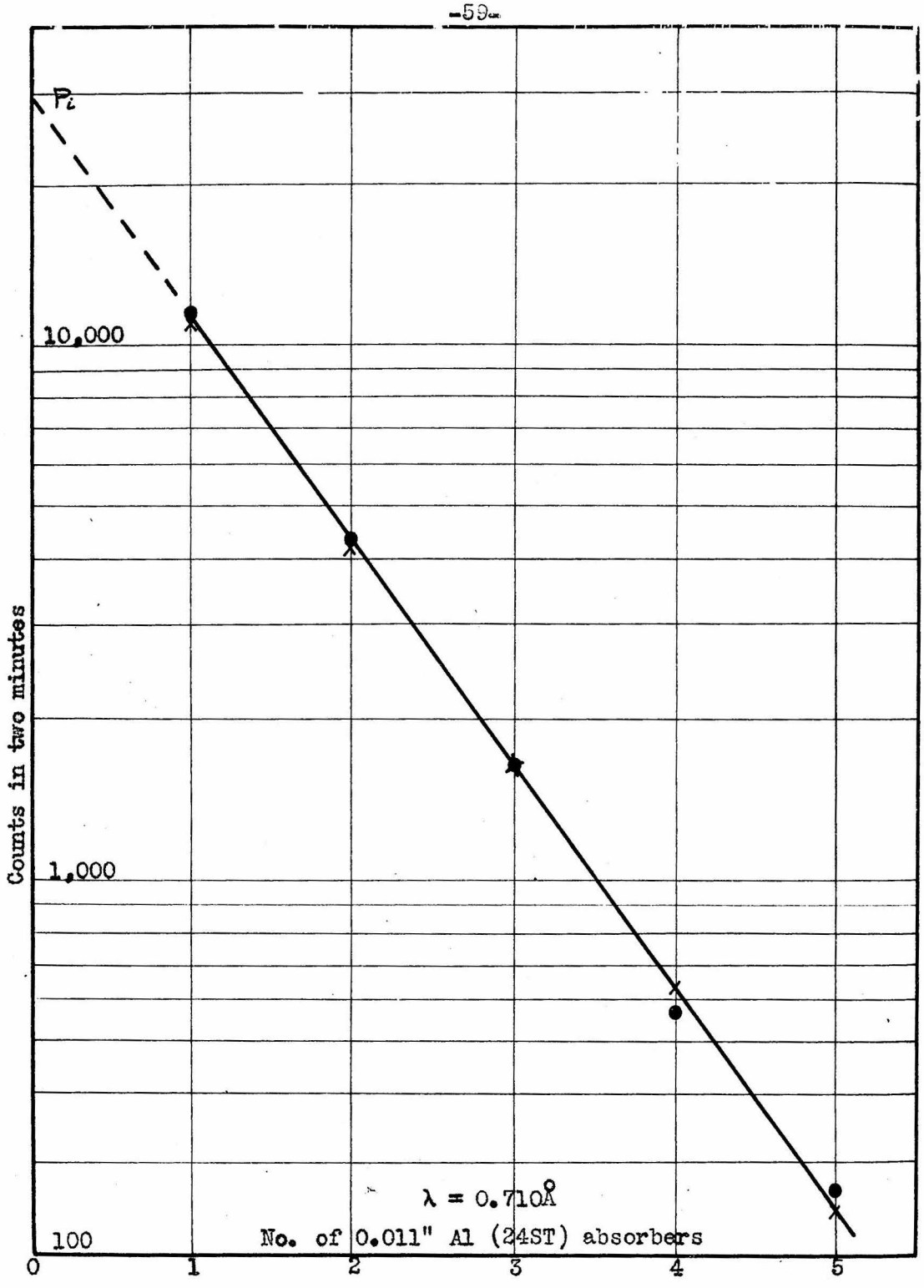

Fig. 12. Typical plot of log of counts in two minutes vs. number of absorbers in the path of the beam used for determining P_i (power in the "straight through" beam). Plots such as this one indicated when the voltage was too high so that wavelengths of $\frac{\lambda}{2}$ were being transmitted in second order reflection for then a plot similar to the above would no longer be a straight line. These also show the linearity of the xenon Geiger counter over the range of counting rates used.

PART V

EXPERIMENTAL RESULTS (A)

Wavelength Determination of the Tungsten $K\alpha_1$ X-ray Line.

Grating Spacing of the (310) Planes of Quartz.

Shapes of the $MoK\alpha_1$ and $WK\alpha_1$ X-ray Lines.

WAVELENGTH AND GRATING CONSTANT DETERMINATION

The wavelength of the tungsten $K\alpha_1$ line is determined by comparing with the molybdenum $K\alpha_1$ line. The $MoK\alpha_1$ line has been determined with such precision that it can be considered as the standard for the Siegbahn scale. When Bragg's law of reflection is satisfied in the first order

$$\lambda = 2d \sin \theta \qquad 4.1$$

The $K\alpha_1$ notation is that of Siegbahn referring to the $K\text{-}L_{III}$ transition. By using the same crystals and experimental set-up to measure the glancing angle for Bragg reflection, θ, for both lines, the wavelength in terms of the wavelength of the $MoK\alpha_1$ line is

$$\lambda_{WK\alpha_1} = \lambda_{MoK\alpha_1} \frac{\sin \theta_{WK\alpha_1}}{\sin \theta_{MoK\alpha_1}} \qquad 4.2$$

As described in previous parts, θ can be measured by determining the angular separation of the centers of the "parallel" and "antiparallel" rocking curves of a two crystal spectrometer. To reduce the errors of the worm wheels, several positions of the wheels were used. It is seen from Fig. 3 (p. 28) that crystal A can diffract the beam either to the right or the left by rotating crystal A through 2θ. For either

position of crystal A, two positions of crystal B are possible for diffraction in both "parallel" and "antiparallel" positions, which are just 180° apart. Thus there are two positions of crystal B when the beam is diffracted to right or left from crystal A. Using all four positions utilizes different portions of the worm wheel and so different corrections for the readings. Such a method reduces the instrumentation error. Each run consists of a measurement of the "parallel" and "antiparallel" rocking curves. In Fig. 6 (p. 45) items (30) and (31) are weights attached to the geared wheels to take the backlash out of the gears. For each run crystal B, together with the detector, was moved somewhat beyond its position for the "parallel" and "antiparallel" rocking curves and in such a direction that when returning crystal B to make the setting the weight is lifted by the crystal pivot wheel. This method keeps any backlash in the gears to a minimum as crystal B is moved consecutively through the "parallel" and "antiparallel" rocking curves.

Fig. 13 (p. 62) shows typical "parallel" and "antiparallel" runs for the molybdenum and tungsten $K_{\alpha 1}$ lines.

Table I (p. 63) gives the results of the θ determinations. The corrections were taken from the graph of Fig. 7 (p. 46).

Using the value for the wavelength of the $MoK_{\alpha 1}$ line[20] as

$$\lambda_{MoK_{\alpha 1}} = 707.831 \text{ x.u. (Siegbahn scale)}$$

and the angles given in Table I, the wavelength for the $WK_{\alpha 1}$ line is

$$\lambda_{WK_{\alpha 1}} = 208.575 \pm 0.008 \text{ x.u. (Siegbahn scale)}$$

Using $\lambda_{MoK_{\alpha 1}}$ above and $\theta_{MoK_{\alpha 1}}$ given in Table I, the grating constant

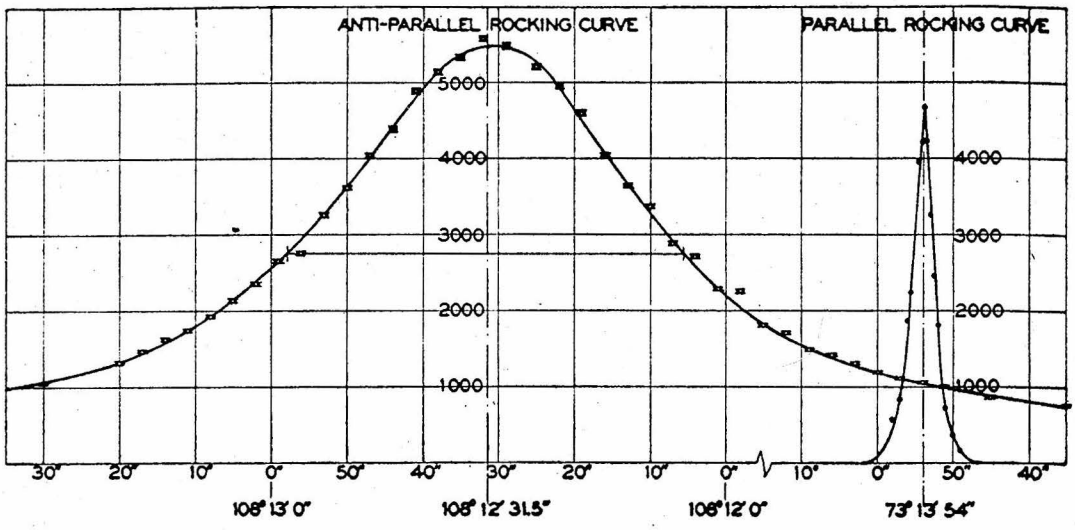

Fig. 13a. Typical two crystal spectrometer rocking curve of molybdenum K_{α_1} line (run No. 2) reflected from (310) planes of quartz in first-order, parallel and antiparallel positions. The ordinate numbers on the parallel and antiparallel rocking curves give the number of counts in two minutes. The vertical heights of the rectangular dots on the antiparallel curve are indicative of the uncertainty of counting (square root of total counts). On the parallel rocking curve the statistical uncertainty is not thus shown.

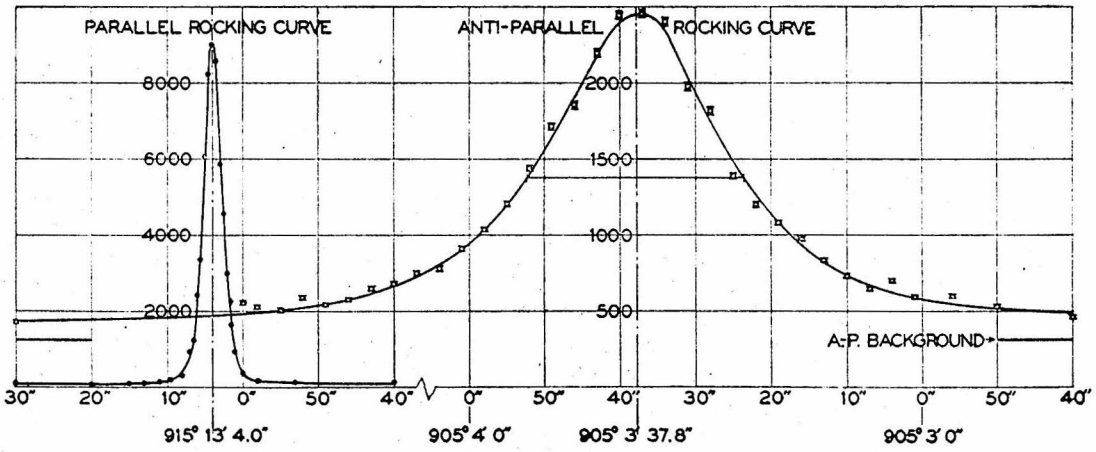

Fig. 13b. Typical two crystal spectrometer rocking curve of tungsten K_{α_1} line (run No. 2) reflected from (310) planes of quartz in first order, parallel, and antiparallel positions. The ordinate numbers on the parallel rocking curve give the number of counts in two minutes, those on the antiparallel curve the number in five minutes. The vertical heights of the rectangular dots on the antiparallel curve are indicative of the statistical uncertainty of counting (square root of total counts). On the parallel rocking curve the statistical uncertainty is not thus shown.

TABLE I. Two crystal spectrometer Bragg angle determinations of Mo K_{α_1} and W K_{α_1} on quartz (310) planes.

Mo K_{α_1} line

Deviation of beam by crystal A to	Run No.	Parallel position reading	Worm wheel correction	Parallel Corrected	Antiparallel position reading	Worm wheel correction	Antiparallel position corrected	2θ	θ Bragg Angle
Left	1	73°13'53.9"	+4.4"	73°13'58.3"	108°12'31.2"	+3.1"	108°12'34.3"	34°58'36.0"	17°29'18.0"
Left	2	73°13'55.4"	+4.4"	73°13'59.8"	108°12'32.7"	+3.1"	108°12'35.8"	34°58'36.0"	17°29'18.0"
Left	3	73°13'55.5"	+4.4"	73°13'59.9"	108°12'32.2"	+3.1"	108°12'35.3"	34°58'35.4"	17°29'17.7"
Left	4	893°14'1.1"	-1.5"	893°13'59.6"	928°12'35.7"	+0.9"	928°12'36.6"	34°58'37.0"	17°29'18.5"
Right	5	928°12'41.0"	+0.9"	928°12'41.9"	893°14'4.2"	-1.5"	893°14'2.7"	34°58'39.2"	17°29'19.6"
Right	6	928°12'38.7"	+0.9"	928°12'39.6"	893°14'8.2"	-1.5"	893°14'6.7"	34°58'32.9"	17°29'17.0"
Right	7	927°58'43.0"	+0.7"	927°58'43.7"	893°0'8.5"	-1.5"	893°0'7.0"	34°58'36.7"	17°29'18.4"

Average value of θ for Mo K_{α_1} on (310) planes of quartz 17°29'18.1" ± 0.3".

W K_{α_1} line

Right	1	95°25'4.6"	+5.3"	95°25'9.9"	85°15'36.7"	-4.2"	85°15'32.5"	10°9'37.4"	5°4'48.7"
Right	2	915°13'4.0"	+1.8"	915°13'5.8"	905°3'37.8"	-9.6"	905°3'28.2"	10°9'37.6"	5°4'48.8"
Right	3	915°13'4.8"	+1.8"	915°13'6.6"	905°3'38.3"	-9.6"	905°3'28.7"	10°9'37.9"	5°4'49.0"
Left	4	905°3'36.6"	-9.6"	905°3'27.0"	915°13'1.2"	+1.8"	915°13'3.0"	10°9'36.0"	5°4'48.0"
Left	5	905°3'34.6"	-9.6"	905°3'25.0"	915°13'2.5"	+1.8"	915°13'4.3"	10°9'39.3"	5°4'49.7"
Left	6	85°3'29.7"	-4.4"	85°3'25.3"	95°12'58.7"	+5.3"	95°13'4.0"	10°9'38.7"	5°4'49.4"
Left	7	85°3'30.4"	-4.4"	85°3'26.0"	95°12'58.8"	+5.3"	95°13'4.1"	10°9'38.1"	5°4'49.1"

Average value of θ for W K_{α_1} on (310) planes of quartz 5°4'49.0" ±0.2".

for the (310) planes of quartz is

$$d = 1177.705 \text{ x.u. (Siegbahn scale)}$$

The room temperature during experiment was $22^\circ \pm 1^\circ$ C. Correcting to 18° C, the usually accepted standard, by applying the thermal expansion coefficient[21] of 14.5×10^{-6} per degree C for expansion normal to the optic axis gives

$$d_{18^\circ} = 1177.657 \pm 0.02 \text{ x.u.}$$

This agrees well with work by Ingelstam who obtained $\lambda_{WK_{\alpha 1}} = 208.571$ x.u.[22] and d = 1177.6 x.u.[23]

ERRORS DUE TO INDEX OF REFRACTION

When the diffracting planes are normal to the crystal faces the index of refraction has no effect on the above results. For, if λ' and θ' are the wavelength and Bragg angle inside the crystal, λ and θ outside, and μ is the index of refraction, $n\lambda' = 2d \sin\theta'$ inside but

$$\mu = \frac{\lambda}{\lambda'} = \frac{\sin\theta}{\sin\theta'} = 1 - \delta$$

and there results

$$\frac{n\lambda}{\mu} = \frac{2d \sin\theta}{\mu}$$

If now the diffracting planes make a small angle α with the normal to the crystal faces, it is shown in Appendix E that the correction for λ when the angle 2θ is measured by determining the angular separation between the "parallel" and "antiparallel" rocking curves is

$$\lambda = 2d \sin\frac{2\theta}{2}\left\{ 1 + \frac{\delta \sin^2\alpha}{\cos\alpha \cos^2\theta} \right\}$$

From the curved crystal spectrometer work it was determined that $\alpha \approx 1^\circ$; therefore $\cos\alpha \simeq 1$, $\sin^2\alpha = 3.04 \times 10^{-4}$ and $\delta = 3.28 \times 10^{-6}\lambda^2$[23]

(when λ is in Angstrom units).

For the $WK_{\alpha 1}$ line

$$\lambda = 2d \sin \frac{2\theta}{2} \left\{ 1 + 4.14 \times 10^{-11} \right\}$$

For the $MoK_{\alpha 1}$ line

$$\lambda = 2d \sin \frac{2\theta}{2} \left\{ 1 + 5.12 \times 10^{-10} \right\}$$

The error due to the index of refraction is negligible compared to the experimental error.

THE ERROR DUE TO VERTICAL DIVERGENCE OF X-RAY BEAM

As shown in Part III the vertical divergence introduces no error in the parallel position. It has been shown experimentally by Allison[15] that for ϕ in the range 4×10^{-3} to 1×10^{-2} vertical divergence has no appreciable effect on position and shape of the antiparallel rocking curve. The usual practice is to keep $\frac{\phi^2}{4} \tan \theta_B$ equal to about 1/2 second of arc or less (see p. 51).

SHAPE OF THE $K_{\alpha 1}$ LINE FOR Mo AND W

It was shown in Part III that the shape of the rocking curve in the "antiparallel" position was essentially that of the spectral line. Eq. 3.37 shows that if the vertical divergence in the x-ray beam is small, then the antiparallel rocking curve will be a witch, provided the spectral line and the parallel rocking curve are witches. For a perfect crystal the theoretical parallel rocking curve is essentially a witch, but it is also so narrow compared to the line width that it will have a small effect in distorting the shape of the spectral line. A test of Eq. 3.37 was made by plotting a witch on top of the

experimental antiparallel rocking curves for the runs in Table I (p. 63), using the half width and peak values of the experimental data (two of the experimental antiparallel rocking curves are shown in Fig. 13 (p. 62)). The calculated curves of a witch fitted very nicely the experimental points. It is thus concluded that the shape of the spectral lines of $MoK_{\alpha 1}$ and $WK_{\alpha 1}$ are essentially that of a witch.

The width at half maximum is used for comparing line widths. The width of the spectral line is very nearly the difference between the half widths of the antiparallel and parallel rocking curves (see Eq. 3.37). These results are given in Table II (p. 67). $W_{\theta_{\#}}$ and $W_{\theta_{\|}}$ are the full widths at half maximum of the antiparallel and parallel rocking curves. The conversion from angular rotation of crystal B to wavelengths is obtained from Eq. 3.33. The wavelength that will be selected by both crystals for a particular setting β of crystal B will be that one which will make both arguments in the numerator zero in Eq. 3.33, thus $W_\theta = 2 \frac{\Delta\lambda}{\lambda} \tan \theta_B$, neglecting ϕ^2 terms.

Compton and Allison[14] pp. 742-746, in a summary of data give $\Delta\lambda$ for the line width of $MoK_{\alpha 1}$ as 0.29 x.u. and $\Delta\lambda$ for $WK_{\alpha 1}$ as 0.15 x.u. Most of the earlier measurements were made with calcite whose dispersion is about a third that of the (310) planes of quartz and whose parallel rocking curve widths are usually 3 to 5 times that of the quartz used here. From this consideration the results given here should be closer to the true shape of the Mo and W $K_{\alpha 1}$ lines than any of these earlier works.

TABLE II

$K_{\alpha 1}$ line widths at half maximum.

$MoK_{\alpha 1}$

Run No.	$W_{\theta_{\#}}$ antiparallel (sec. of arc)	$W_{\theta_{\|\|}}$ parallel (sec. of arc)	$W_{\theta_{\#}} - W_{\theta_{\|\|}}$ (sec. of arc)
1	48.8	3.3	45.5
2	48.9	3.5	45.4
3	49.3	3.5	45.8
4	48.0	2.9	45.1
5	50.4	3.7	46.7
6	49.5	4.0	45.5
7	49.0	3.7	45.3

Average value of the full width at half maximum for the $MoK_{\alpha 1}$ line

$= 45.6'' \pm 0.3''$

$= 0.248 \pm 0.0017$ x. u.

$WK_{\alpha 1}$

Run No.	$W_{\theta_{\#}}$ antiparallel (sec. of arc)	$W_{\theta_{\|\|}}$ parallel (sec. of arc)	$W_{\theta_{\#}} - W_{\theta_{\|\|}}$ (sec. of arc)
2	27.4	2.8	24.6
3	27.1	2.6	24.5
4	27.7	2.8	24.9
5	27.7	2.6	25.1
6	29.4	3.2	26.2
7	29.4	2.8	26.6

Average value of the full width at half maximum for the $WK_{\alpha 1}$ line

$= 25.3'' \pm 0.33''$

$= 0.143 \pm 0.0018$ x. u.

PART VI

EXPERIMENTAL RESULTS (B)

Comparison of the Theoretical and Experimental Diffraction Patterns from the (310) Planes of Quartz.

In Part III it was shown that the rocking curves obtained by the two crystal spectrometer in the "parallel" position depended only upon the nature of the two crystals and not upon the spectral distribution of the radiation, or the height or width of the slits defining the x-ray beam. It was shown there that there is a difference in the diffraction pattern for the normal and parallel polarizations. In this study the detector measures both polarizations simultaneously, so the parallel rocking curve cannot be unfolded to obtain the single crystal diffraction pattern. If only one polarization is considered, it is still impossible to obtain from the two crystal parallel rocking curves the single crystal diffraction pattern. It was shown by Laue[11] that if the two crystal "parallel" rocking curve $P(\beta)$ is symmetrical [$(b = -1)$ for planes parallel to the crystal face], then only if it can be assumed that the single crystal diffraction pattern is symmetrical, is it possible to find the single crystal diffraction patterns by an unfolding method such as the use of Fourier Transforms. But this assumption defeats the original purpose. For the transmission case and the diffracting planes normal to the face $(b = +1)$ the situation is worse because $P(\varphi)$ is not symmetrical unless the single crystal diffraction patterns are symmetrical. This arises from the fact that save for the median ray the angle of incidence on the crystal planes

is not equal to the angle of reflection (see Eq. 4.6). From Eq. 5.23

$$P(\beta) = \frac{\int_{-\infty}^{\infty} \frac{I_H}{I_o}(\varepsilon)\,\frac{I_H}{I_o}(-\beta-\varepsilon)\,d\varepsilon}{\int_{-\infty}^{\infty} \frac{I_H}{I_o}(\varepsilon)\,d\varepsilon} \qquad 6.1$$

and

$$P(-\beta) = \frac{\int_{-\infty}^{\infty} \frac{I_H}{I_o}(\varepsilon)\,\frac{I_H}{I_o}(\beta-\varepsilon)\,d\varepsilon}{\int_{-\infty}^{\infty} \frac{I_H}{I_o}(\varepsilon)\,d\varepsilon}$$

Only if $\frac{I_H}{I_o}(\varepsilon) = \frac{I_H}{I_o}(-\varepsilon)$ is $P(\beta) = P(-\beta)$. It is, therefore, necessary to compare the two crystal "parallel" rocking curves calculated from the single crystal theory with the experimental rocking curves. This avoids making assumptions about the inaccessible single crystal diffraction pattern.

The two crystal "parallel" rocking curves are "normalized" by dividing the measured curve by the power incident on crystal B. The properties of this "normalized" curve that are compared with theory are: R, the area under the "normalized" curve; P(0), its peak value; and W_θ, its half width at half maximum. In Part III these quantities were derived from the theoretical single crystal diffraction patterns given by Eq. 2.22 for the particular set of quartz plates used in this study. They are:

$$\mathrm{Re}\,\frac{\mu_o t_o}{\gamma_o} = \left\{\frac{e^2}{mc^2}\,\frac{d}{2}\,\frac{|F_H|}{V}\right\}\frac{\lambda}{\cos\theta_B}\left[\frac{1+\cos^2 2\theta_B + 2l_o^2\,(1+\cos^4 2\theta_B)}{1+\cos 2\theta_B + l_o^2\,(1+\cos^3 2\theta_B)}\right] \qquad 6.2$$

$$P(0)e^{\frac{\mu_o t_o}{\gamma_o}} = \frac{1}{4}\left[\frac{(1+\cos 2\theta_B) + \frac{3}{4}l_o^2\,(1+\cos^3 2\theta_B)}{(1+\cos 2\theta_B) + l_o^2\,(1+\cos^3 2\theta_B)}\right] \qquad 6.3$$

$$W_\theta \approx 2w_\theta \approx \left\{\frac{2d}{\pi}\frac{e^2}{mc^2}\frac{|F_H|}{V}\right\} \cos\theta_B \lambda \left[\frac{2(1+\ell_o^2\cos^4\theta_B)}{1+2\ell_o^2\cos^4\theta_B} - 1\right]^{\frac{1}{2}} \qquad 6.4$$

where ℓ_o is the term due to the contribution from anomalous scattering

$$\ell_o = c\left[\frac{e^2}{mc^2}\frac{|F_H|}{V} t_o\right] \frac{\lambda}{\cos\theta_B}$$

and c is defined by Eq. 2.18.

The results of the calculations for these three quantities are tabulated in Appendix F. It is shown there that ℓ_o^2 is negligible except for $\lambda = 0.710\text{Å}$ and $\lambda = 0.530\text{Å}$.

As will be shown in the results, the characteristics of the "parallel" rocking curve may vary by as much as 30 per cent depending on the particular portion of the crystal tested. In arriving at the theoretical "parallel" rocking curve it was assumed that the diffraction patterns of both crystals were identical. For the case where they were not the same and for only one polarization

$$P(\beta) = \frac{\int_{-\infty}^{\infty} \frac{I_H^A}{I_o}(\varepsilon)\frac{I_H^B}{I_o}(-\beta-\varepsilon)\,d\varepsilon}{\int_{-\infty}^{\infty} \frac{I_H^A}{I_o}(\varepsilon)\,d\varepsilon}$$

where the superscripts refer to crystals A and B. If the beam is being reflected from different parts of the crystals for each wavelength setting and the diffraction pattern varies from point to point on the crystal, then a study of the $P(\beta)$ curve vs. wavelength may be misleading. The variation in diffraction properties of the crystal from point to point may overshadow the wavelength trend.

The section of the crystals directly above the pivots A and B and at a height defined by the vertical slit system was chosen to be studied as a function of λ. The x-ray beam was approximately 4 mm

wide and 5 mm high at crystal B. Adjustment of the spectrometer so that the diffracted beams passed over the desired points was accomplished as follows: The horizontal defining slits S (see Fig. 3 (p. 28)) were set so that their center was on the line joining pivots A and B; over pivot B was suspended a plumb-bob by a 1/2 mm lead wire. Photographs were taken of the $K_{\alpha 1}$ diffracted beam from crystal A just after passing through slits S and then behind the lead wire which is directly over the axis of pivot B. This gave the position of the beam with respect to the spectrometer. The relative positions of crystal A and the spectrometer table were then adjusted until the beam passed over the two pivots A and B to within a 1/2 mm. Thus to select a wavelength on the continuous spectrum the gears of the spectrometer table were coupled to those of crystal A so that the table moved twice as fast as crystal A, and crystal A rotated to a new position with respect to the incident beam. The new setting of crystal A relative to the setting for the $K_{\alpha 1}$ line gave the wavelength of the central ray for the new setting.

Because of the horizontal divergence of the beam defined by the slits, radiation passing through the spectrometer is not monochromatic. The spread in wavelengths for points on the continuous spectrum was calculated by using Bragg's law and the measured horizontal divergence of the beam as shown in Part IV and Fig. 8 (p. 50). The slits were wide enough to allow the $K_{\alpha 1,2}$ doublet to pass. As the intensity of the line spectra used was so much greater than neighboring points on the continuous spectrum, the spread in wavelengths for the $K_{\alpha 1}$ line tabulated is just the doublet separation.

The technique used for measuring a "parallel" rocking curve was as follows: The wavelength was selected as given above. The "window" curve of the counter was then measured. This was done by moving the counter, which rests in the cradle of the spectrometer (see Fig. 6 (p. 45)), and observing the counting rate; first, with crystal B set near the "parallel" rocking curve peak; and, second, with crystal B only a few seconds beyond positions for any diffraction. This locates the positions for the counter when measuring (1) the "parallel" rocking curve and (2) the "straight through" beam needed for "normalizing" the curve. The "straight through" beam is the incident beam on crystal B less the absorption in crystal B.

As the maximum counting rate of a Geiger counter and scaling circuits is limited, the power in the "straight through" beam was measured by extrapolating a plot of the log of the counting rate vs. the number of absorbers in the incident beam (selected to have the same thickness) to zero absorbers. The errors in this extrapolation are increased as the power in the "straight through" beam is increased because the distance of extrapolation becomes longer. But the errors in measuring the rocking curve are decreased on increasing the power in the incident beam. It was found that the least error would result when the intensity of the "straight through" beam was adjusted so that the extrapolated point for no absorbers was about double the maximum value the detector was capable of handling. This latter value was usually around 7000 c.p.m.

For a given run the power in the "straight through" beam was measured, then the parallel rocking curve, and then the power in the

incident beam again measured. Doubling the points in the "straight through" beam determination helps make the "straight through" beam extrapolation more accurate, and also indicates the stability of the x-ray source during the run. See Fig. 12, p. 59.

For each wavelength several runs were made for the two possible "parallel" positions of crystal B. Let one be called ($\bar{5}10$), then a rotation of 180° gives (510). As the "straight through" beam multiplied by $e^{\frac{\mu_o t_o}{\gamma_o}}$ is equal to the incident beam on crystal B, measured quantities $Re^{\frac{\mu_o t_o}{\gamma_o}}$ and $P(0)e^{\frac{\mu_o t_o}{\gamma_o}}$ can be compared with theory without determining the true absorption of the beam in passing through crystal B.

Fig. 14 (p. 74) shows representative "parallel" rockings at five different wavelengths. A typical set of calculations that were made for each "parallel" rocking curve measured is shown in Appendix G. The calculated results for the observed "parallel" rocking curves are tabulated in Appendix H.

In Table III (p. 75) the average values from the experimental results are tabulated with the calculated quantities derived from Eqs. 6.2, 6.3 and 6.4. The results for $Re^{\frac{\mu_o t_o}{\gamma_o}}$ vs. λ from both theory and experiment are plotted in Fig. 15 (p. 76).

As the diffraction patterns are very narrow, it was difficult to determine the peak value of the curves accurately. The smallest interval of angular rotation of crystal B was 1/4 sec. and as the full width at half maximum was two seconds and less the peak position did not always correspond to angular setting of crystal B. The variation in determining P(0) was sometimes as high as 10 per cent. This did not affect the half width very much as the sides of the curve are

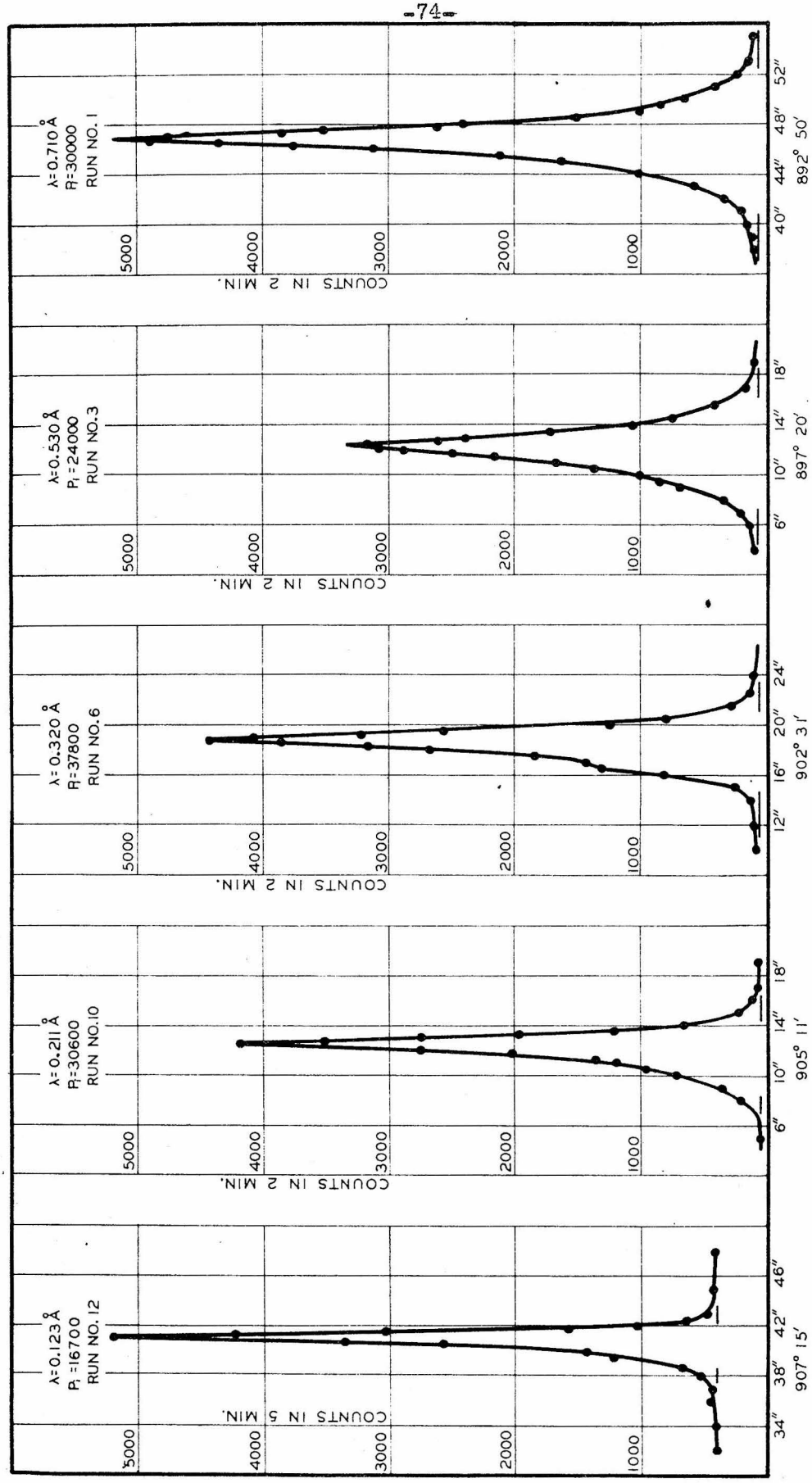

Fig. 14. Experimental rocking curves of the two crystal x-ray spectrometer using the (310) planes of quartz in the first-order, parallel position. P_1 is the number of counts in two minutes of the "straight through" beam used for "normalizing" the curves. The "Run No." designation refers to the table of data in Appendix H for crystal B in Position I.

TABLE III.

Observations on the transmission diffraction patterns from the (310) planes of quartz.

λ(Å)	$Re^{\frac{\mu_o t_o}{\gamma_o}}$ x 10^6 (radians)			$P(0)e^{\frac{\mu_o t_o}{\gamma_o}}$			W_θ (seconds of arc)		
	Obs.		Cal.	Obs.		Cal.	Obs.		Cal.
	(310)	$(\bar{3}1\bar{0})$	(310) or $(\bar{3}1\bar{0})$	(310)	$(\bar{3}1\bar{0})$	(310) or $(\bar{3}1\bar{0})$	(310)	$(\bar{3}1\bar{0})$	(310) or $(\bar{3}1\bar{0})$
0.710 ± .0020*	2.58	2.77	2.30	.172	.161	.246	1.1	1.3	.53
0.530 ± .0074*	2.02	2.12	1.65	.134	.136	.2498	1.2	1.2	.42
0.320 ± .0076*	1.50	1.51	1.00	.116	.111	.250	1.1	1.0	.26
0.210 ± .002**	1.30	1.63	0.657	.123	.128	.250	0.73	0.92	.17
0.123 ± .0084**	0.89	1.04	0.389	.115	0.890	.250	0.54	0.88	.10

*Molybdenum tube used for the x-ray source.

**Tungsten tube used for the x-ray source.

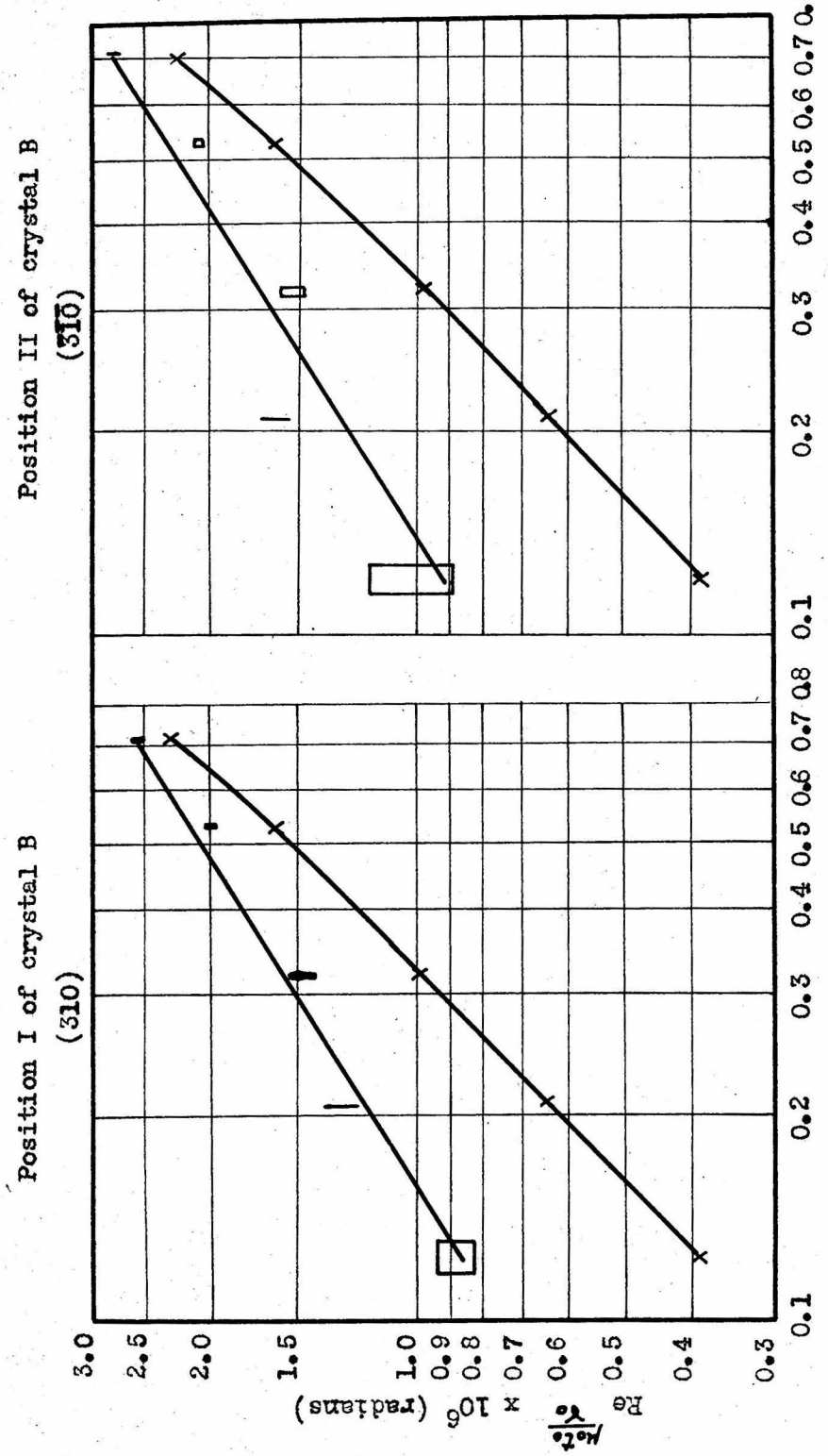

Fig. 15. Log of integrated reflecting power vs. log of the wavelength plot to determine the dependence of the integrating reflecting power on the wavelength. A comparison of theory with experiment of the integrated reflecting power of the (310) planes of quartz as measured by the two crystal x-ray spectrometer. The width of the rectangle for the experimental points gives the range of wavelengths transmitted by the spectrometer at each wavelength setting. The height of the rectangle gives the spread in the experimental data.

relatively steep. The area was measured by a planimeter. Five determinations of the area were made for each curve with a "probable" error of less than 0.37 per cent.

The data in Table IV (p. 78) show that moving the x-ray beam 6 mm along the face of crystal B can change the characteristics of the two crystal rocking curve by as much as 30 per cent. Referring to Fig. 15 (p. 76) the two points for $\lambda < 0.25\text{Å}$ were determined with the tungsten x-ray tube. For the three points $\lambda > 0.25\text{Å}$ a molybdenum tube was used. The inability to adjust the diffracted beam so that it passes over exactly the same points of both crystals A and B when either x-ray tube was used may account for the irregularity between these two sets of data.

From Fig. 15 (p. 76) it is seen that the measured integrated reflecting power for these crystals does not decrease as fast as that predicted by the theory. Referring to Eqs. 6.2, 6.3 and 6.4, the terms in the brackets are due to the anomalous dispersion and the effect of the two crystal spectrometer on the single crystal diffraction patterns. In Appendix F it is shown that the numerical value of these brackets is very nearly equal to unity. Thus the integrated reflecting power as measured by the two crystal spectrometer is essentially that of a single crystal.

In Part II it was shown that for a mosaic crystal of small blocks whose dimension $t_0 < 10^{-3}$ cm, the integrated reflecting power should decrease with wavelength according to λ^2. This is not the case here. In Table III (p. 75) it is seen that the results from theory and experiment are fairly close for $\lambda = 0.710\text{Å}$, but for shorter wavelength, the

TABLE IV.

	Position I of crystal B (310)			Position II of crystal B ($\overline{3}10$)		
Δd(mm)	$Re^{\frac{\mu_o t_o}{\gamma_o}} \times 10^6$ (radians)	$P(0)e^{\frac{\mu_o t_o}{\gamma_o}}$	W_θ (Sec. of Arc)	$Re^{\frac{\mu_o t_o}{\gamma_o}} \times 10^6$ (radians)	$P(0)e^{\frac{\mu_o t_o}{\gamma_o}}$	W_θ (Sec. of Arc)
3	2.51	.175	1.03	2.65	.158	1.2
0	2.58	.172	1.1	2.77	.161	1.3
-1	2.48	.160	1.25			
-3	3.29	.185	1.5	2.54	.154	1.3

The above table shows the effect of moving the x-ray diffracted beam from crystal A to different points along the face of crystal B. $\lambda = .710\text{Å}$. The width of the beam is approximately 1.5 mm at crystal B. is the horizontal displacement of the x-ray beam from the pivot axis of crystal B along the crystal face.

results of the perfect crystal theory for the integrated reflecting power and half width decrease more rapidly than the experimental results. It is also noted that the values of the normalized peaks of the "parallel" rocking curves are lower than the calculated values.

These facts might be explained by a structure in the crystal composed of fairly large blocks whose angular deviation is very small. For the long wavelengths the width of the diffraction pattern for a perfect crystal is larger than the angular deviation of the blocks, and the crystal as a whole acts very nearly like a perfect crystal. For shorter wavelengths the width of the diffraction pattern approaches the same magnitude as the angular deviation in the orientation of the blocks. Thus the resulting width and integrated reflecting power would not decrease as fast as predicted by the theory of a perfect crystal for the pattern becomes dominated by the angular deviation in the orientation of the blocks. The peak of the curve is thus lower than predicted by theory as the diffracted power is spread over a larger angular range.

Such a structure would also indicate variation of the "parallel" rocking curves from point to point on the crystals and also slight irregularities* on the side of the parallel rocking curves which were observed to change as the beam was moved to different parts of crystal B.

The results of this experiment show that the integrated reflecting power and half width of the diffraction pattern for the (310) planes of quartz are not proportional to the first power of the wavelength as

*Subsidiary reflections were also observed symmetrically placed about the (310) parallel position rocking curves. A study was made of these reflections as a function of wavelength (see Appendix I), but at present they are unexplained.

predicted by theory but are proportional to a power of the wavelength slightly less than unity. These results are entirely different from those found by David A Lind[2] who observed that the integrated reflecting power for a crystal, cut from the same block as the two used here, but in the stressed condition as found in the curved crystal gamma ray spectrometer, decreased as λ^2.

REFERENCES

(1) J. W. M. DuMond, Rev. Sci. Inst. (1947) 18, 626

(2) David A. Lind, Ph. D. Thesis, Calif. Inst. of Tech. June, 1948

(3) S. K. Allison, Phys. Rev. (1932) 41, 1

(4) S. G. Parratt, Phys. Rev. (1932) 41, 561

(5) William H. Zachariasen, "Theory of Diffraction in Crystals", John Wiley and Sons, Inc., Chapman and Hall, Ltd. (1945)

(6) M. v. Laue, "Rontgenstrahl-Interferenzen", Leipzig, Akademische Verlagsgesellschaft, 1941

(7) Leon Brillouin, "Wave Propagation in Periodic Structures", McGraw and Hill Book Company (1946)

(8) H. Hönl, Zeitschr. f. Phys. (1933) 84, 1
Ann. der Phys. (5) (1933) 18, 625

(9) M. Schwarzschild, Phys. Rev. (1928) 32, 162

(10) R. C. Spencer, Phys. Rev. (1931) 38, 618

(11) M. v. Laue, Zeitschr. f. Physik (1931) 72, 472

(12) S. P. Smith, Phys. Rev. (1934) 46, 343

(13) J. W. M. DuMond and A. Hoyt, Phys. Rev. (1930) 36, 1702

(14) Compton and Allison, "X-Ray in Theory and Experiment" Van Nostrand Co., Inc., New York (1935)

(15) S. K. Allison, Phys. Rev. (1933) 44, 63

(16) J. W. M. DuMond and D. Marlow, R. S. I. (1937) 8, 112

(17) D. B. Penick, R. S. I., (1935) 6, 115

(18) S. A. Korff, "Electron and Nuclear Counters", Van Nostrand, New York, (1946) pp. 89-118

(19) W. A. Higinbotham, James Gallagher, and Mathew Sands, R. S. I. (1947) 10, 706

(20) M. Siegbahn, "Spectroskopie der Rontgenstrahlen", Julius Springer, Berlin (1931) 2nd Edition, p. 179

(21) A. H. Jay, Proc. Roy Soc. (1933) 142, 237

(22) E. Engelstam, (4) (1936) No. 5, Nova Acta Reg. Soc. Sci., Upsal.

(23) E. Engelstam, Arkiv. f. Mat., Astro. o. Fys. 27B, No. 4 (1939)

(24) Sven Elg, Zeits. f. Phys. (1937) 106, 315

(25) R. Brill, C. Hermann, and Cl. Peters, Ann. der. Physik, (1942) 41, 233

APPENDIX A.

The following calculations for the volume of the unit cell and the structure factor for the (310) planes of quartz used the crystal structure data from Brill, Hermann, and Peters(25)

a. Volume of the unit cell.

Quartz has a hexagonal crystal structure with the unit cell as

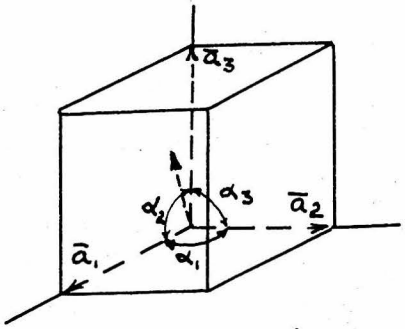

$$V = (\bar{a}_1\bar{a}_2\bar{a}_3) = a_1a_2a_3\left[1 + \cos\alpha_1\cos\alpha_2\cos\alpha_3 - \cos^2\alpha_1 - \cos^2\alpha_2 - \cos^2\alpha_3\right]^{\frac{1}{2}}$$

$$a_1 = a_2 = 4.903\ \text{Å}$$

$$a_3 = 5.393\ \text{Å}$$

$$\alpha_1 = \measuredangle(\bar{a}_2,\bar{a}_3) = 90^\circ, \cos\alpha_1 = 0$$

$$\alpha_2 = \measuredangle(\bar{a}_1,\bar{a}_3) = 90^\circ, \cos\alpha_2 = 0$$

$$\alpha_3 = \measuredangle(a_2,a_1) = 120^\circ, \cos\alpha_3 = -\tfrac{1}{2}$$

$$V = (4.903)^2 \times 5.393\left[1 - \tfrac{1}{4}\right]^{\frac{1}{2}}$$

$$V = 112\ \text{Å}^3$$

b. Structure factor of the (310) planes of quartz.

(Terms due to anomalous dispersion not included here)

$$F_H = \sum f_k^o\, e^{2\pi i(\bar{B}_H\cdot\bar{r}_k)}$$

$$= \sum f_k^o\, e^{2\pi i(h_1x_1 + h_2x_2 + h_3x_3)}$$

f_k^o is the atomic structure factor (no anomalous dispersion) for the k^{th} atom of the unit cell. The position vector of the k^{th} atom is

$$\bar{r}_k = x_1\bar{a}_1 + x_2\bar{a}_2 + x_3\bar{a}_2$$

and

$$\bar{B}_H = h_1\bar{b}_1 + h_2\bar{b}_2 + h_3\bar{b}_3$$

Using $\bar{b}_i \cdot \bar{a}_j = \delta_{ij}$ and $(h_1h_2h_3) = (310)$

$$\bar{B}_H \cdot \bar{r}_k = 3x_1 + 1x_2 + 0x_3$$

The unit cell contains 3 Si atoms and 6 O atoms.

$$\text{so } F_H = f_{Si}^o \sum_{Si} e^{2\pi i(3x_1+x_2)} + f_O^o \sum_O e^{2\pi i(3x_1+x_2)}$$

x_1, x_2, x_3 were determined from Brill, Hermann, Peters[25] data.

$$u = 0.465 \pm .003$$

$$x = 0.415 \pm .003$$

$$y = 0.272 \pm .003$$

$$z = 0.120 \pm .002$$

as shown in the following tables.

For the 3 Silcon atoms:

Atom No.	x_1,x_2,x_3	x_1	x_2	x_3	$\bar{B}_H \cdot \bar{r}_k$	$2\pi \bar{B}_H \cdot \bar{r}_k$ (in degrees)
1	(u,0,0)	0.465	0	0	1.395	142°
2	($\bar{u}$,$\bar{u}$,1/3)	-0.465	-0.465	.333	-1.860	-309.5°
3	(0,u,2/3)	0	0.465	.667	0.465	167°

For the 6 Oxygen atoms:

Atom No.	x_1,x_2,x_3	x_1	x_2	x_3	$\bar{B}_H \cdot \bar{r}_k$	$2\pi \bar{B}_H \cdot \bar{r}_k$ (in degrees)
1	x,y,z	0.415	0.272	0.120	1.517	186°
2	y-x,$\bar{x}$,1/3 z	-0.143	-0.415	0.453	-0.844	-303.5°
3	$\bar{y}$,x-y,2/3 z	-0.272	0.143	0.787	0.673	-242°
4	x-y,$\bar{y}$,$\bar{z}$	0.143	0.272	0.120	0.157	56.5°
5	y,x,2/3-z	0.272	0.415	0.547	1.231	83.1°
6	$\bar{x}$,y-x,1/3 - z	-0.415	-0.143	0.213	-1.388	-139.5°

$$\sum e^{2\pi i \bar{B}_H \cdot \bar{r}_k} = \sum \cos(2\pi \bar{B}_H \cdot \bar{r}_k) + i(\sin 2\pi \bar{B}_H \cdot \bar{r}_k)$$

For Si:

Atom No.	$\cos(2\pi \bar{B}_H \cdot \bar{r}_k)$	$\sin(2\pi \bar{B}_H \cdot \bar{r}_k)$
1	-.788	.616
2	.636	.772
3	-.974	.225

$$\sum_{Si} e^{2\pi i(\bar{B}_H \cdot \bar{r}_k)} = -1.126 + i\ 1.613$$

For Oxygen:

Atom No.	$\cos(2\pi \bar{B}_H \cdot \bar{r}_k)$	$\sin(2\pi \bar{B}_H \cdot \bar{r}_k)$
1	-.996	-.105
2	.552	.834
3	-.460	.883
4	.552	.834
5	.120	.993
6	-.766	-.643

$$\sum_{O} e^{2\pi i(\bar{B}_H \cdot \bar{r}_k)} = -1.006 + i\ 2.776$$

From Compton and Allison[14] p. 781

$$f^o_{Si} = 6.89$$

$$f^o_{O} = 2.73$$

Therefore

$$F_H = -10.49 + i\ 18.68$$

$$|F_H| = 21.4$$

APPENDIX B.

Calculations of the Fourier Coefficients ψ_H' and ψ_H''. See p. 16 of text.

$$\psi_{H'} = -\frac{4\pi e^2}{m\omega_o^2}\frac{1}{V}\sum_k (f_k^o + 2\xi_K^k)e^{2\pi i\,\bar{B}_H\cdot\bar{r}_k}$$

$$\psi_{H''} = -\frac{4\pi e^2}{m\omega_o^2}\frac{1}{V}\sum_k 2\eta_K^k\, e^{2\pi i\,\bar{B}_H\cdot\bar{r}_k}$$

From Hönl[8] the values of 2ξ and 2η for the K shell electrons are

$$2\xi_K = \frac{2^7 e^{-4}}{9}\left\{\frac{4x^2}{(1-\Delta)^2}\ln\left|1-\frac{1}{x^2}\right| - \frac{1}{(1-\Delta)^3}\left(2x^2+x^3\ln\left|\frac{1-x}{1+x}\right|\right)\right\}$$

$$2\eta_K = \frac{2^7 e^{-4}}{9}\left\{\frac{4x^2}{(1-\Delta)^2} - \frac{x^3}{(1-\Delta)^3}\right\}$$

where $x = \frac{\lambda}{\lambda_K}$. The critical absorption edges for the L, M --- etc. shells are so much greater than the wavelengths used that the anomalous contribution from these electrons is neglected. Using the results of Honl the following table was calculated:

λ(Å)	$x = \frac{\lambda}{\lambda_K}$ (Si)	$2\eta_K$	$2\xi_K$	$x = \frac{\lambda}{\lambda_K}$	$2\eta_K$ (O)	$2\xi_K$
.710	0.105	0.0670	0.091	0.0302	.00605	.0121
.530	0.0787	0.0376	0.063	0.0225	.00352	.0052
.320	0.0476	0.0139		0.0136	.00124	
.211	0.0313	0.00590		0.00898	.000525	
.123	0.0183	0.00252		0.00523	.000224	

Si($\Delta = 0.276$, $\lambda_K = 6.73$Å) O($\Delta = 0.30$, $\lambda_K = 23.5$Å)

Summing over each type of atom gives

$$\psi_{H''} = -\frac{4\pi e^2}{m\omega_o^2}\frac{1}{V}\left[2\eta_K^{Si}\sum_{Si} e^{2\pi i(\bar{B}_H\cdot\bar{r}_k)} + 2\eta_K^{O}\sum_{O} e^{2\pi i(\bar{B}_H\cdot\bar{r}_k)}\right]$$

$$= -\frac{4e^2}{m\omega_o^2}\frac{1}{V}\left[a+ib\right]$$

The summations are calculated in Appendix A.

λ(Å)	a	b	$c \times 10^3$	$\chi \times 10^2$	$\chi^2 \times 10^4$
.710	-0.0815	0.125	6.98	6.99	48.8
.530	-0.0455	0.0703	3.90	3.91	15.3
.320	-0.0169	0.0237	1.35	1.36	1.85
.211	-0.00717	0.0110	0.613	0.613	0.376
.123	-0.00296	0.00468	0.259	0.260	0.0675

Where

$$\psi_H' = -\frac{4\pi e^2}{m\omega_o^2}\frac{1}{V}(-10.49 + i\ 18.68);\ \xi \text{ terms neglected compared to } f_k^o$$

$$c = \frac{\psi_{H\sigma}'\psi_{H\sigma}'' + \psi_{H\iota}'\psi_{H\iota}''}{|\psi_H'|^2}$$

$$\chi = \left|\frac{\psi_H''}{\psi_H'}\right|$$

APPENDIX C.

Relationship between the angle of scattering and the angle of incidence for an x-ray beam diffracted by a crystal with plane parallel faces.

The simple Laue symmetrical transmission case is given as an example. The condition for constructive interference inside the crystal when the incident beam deviates slightly from Bragg's condition of reflection is given by Laue's vector equation

$$\bar{\beta}_H = \bar{\beta}_o + \bar{B}_H$$

where $\bar{\beta}_o$ and $\bar{\beta}_H$ (the incident and diffracted wave vectors inside the crystal) do not necessarily make the same angle with B_H. Let the incident ray outside the crystal make an angle θ with respect to the diffraction planes (for this special case the normal to the face of the crystal and the diffracting planes are parallel). The scattering angle is measured with respect to the crystal planes at the emerging face. The corresponding angles θ' and θ'_s, inside the crystal, are measured similarly; see the following sketch:

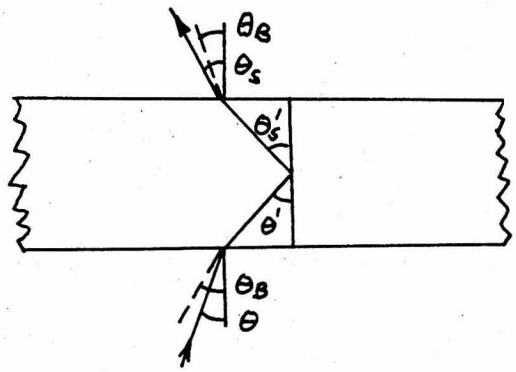

The angles of incidence and scattering are given by

$$\bar{B}_H \cdot \bar{\beta}_H = \bar{B}_H \cdot \bar{\beta}_o + \bar{B}_H \cdot \bar{B}_H$$

OR

$$\beta_H \sin \theta'_s + \beta_o \sin \theta' = B_H$$

For the symmetrical Laue case $B_H = 2 k_o \sin \theta_B$, θ_B is measured outside the crystal; k_o is the magnitude of the wave vector outside the crystal, and is related to the wave vectors inside the crystal by the indices of refraction. The index of refraction is not necessarily the same for the incident and diffracted waves inside the crystal when diffraction occurs (see Part II).

$$\beta_H = k_o (1+\delta_H)$$

$$\beta_o = k_o (1 + \delta_o)$$

So $(1 + \delta_H) \sin \theta_s' + (1 + \delta_o) \sin \theta' = 2 \sin \theta_B$

Using Snell's law

$$\mu = (1 + \delta) = \frac{\sin \theta}{\sin \theta'}$$

$$\sin \theta_s + \sin \theta = 2 \sin \theta_B$$

OR $$2 \sin \frac{\theta_s + \theta}{2} \cos \frac{(\theta_s - \theta)}{2} = 2 \sin \theta_B$$

dropping $(\theta_s - \theta)^2$ terms

$$\sin \frac{(\theta_s+\theta)}{2} = \sin \theta_B$$

or $$\theta_s = 2\theta_B - \theta$$

For the general case where the diffracting planes making some angle with the normal to the surface of the crystals Zachariasen[5] gives for θ_s

$$\theta_s = \theta_B - b (\theta - \theta_B)$$

b is defined in Part II; $b = +1$ for the diffracting planes normal to the surface and $b = -1$ for the planes parallel to the surface.

The angle of incidence is equal to the angle of scattering only when $\theta = \theta_B$ or $b = -1$.

APPENDIX D.

Fold of two witches.

The problem is to integrate

$$I(y) = \int_{-\infty}^{\infty} f_1(x) \cdot f_2(x-y)dy$$

where $$f_1(x) = \frac{I_1}{1+\frac{x^2}{a^2}} \; ; \quad f_2(x) = \frac{I_2}{1+\frac{x^2}{b^2}}$$

$$I(y) = I_1 I_2 a^2 b^2 \int_{-\infty}^{\infty} \frac{1}{a^2+x^2} \cdot \frac{1}{b^2+(x^2-y^2)} dx$$

$$= I_1 I_2 a^2 b^2 \int_{-\infty}^{\infty} \left[\frac{Ax+B}{a^2+x^2} + \frac{Cx+D}{b^2+(x-y)^2} \right] dx$$

where $$A = \frac{2y}{\left[b^2+a^2+y^2\right]^2 - 4a^2b^2}$$

$$B = \frac{b^2+y^2-a^2}{\left[b^2+a^2+y^2\right]^2 - 4a^2b^2}$$

$$C = \frac{3y^2-(b^2-a^2)}{\left[b^2+a^2+y^2\right]^2 - 4a^2b^2}$$

$$I(y) = I_1 I_2 a^2 a^2 \left\{ \frac{A}{2} \ln \frac{1+\frac{x^2}{a^2}}{1+\frac{(x-y)^2}{b^2}} \Bigg|_{-\infty}^{\infty} + \left[\frac{B}{a} + \frac{Cy}{b} + \frac{D}{b} \right] \pi \right\}$$

$$= I_1 I_2 a^2 b^2 \left\{ 0(\text{for y finite}) + \left[\frac{B}{a} + \frac{Cy}{b} + \frac{D}{b} \right] \pi \right\}$$

Substituting for B, C, and D,

$$I(y) = \frac{I_1 I_2 ab}{a+b} \; \frac{\pi}{1+\left(\frac{y}{a+b}\right)^2}$$

The fold of two witches gives another witch, whose half width is the sum of the half widths of the two witches folded together.

APPENDIX E.

Index of refraction correction to Bragg's law.

Let the diffracting planes make a small angle with the normal to the crystal faces as shown in the figure below. The angle between crystal settings for Bragg reflection in the parallel and antiparallel positions for the crystal x-ray spectrometer will be $(\theta_1+\theta_2)$

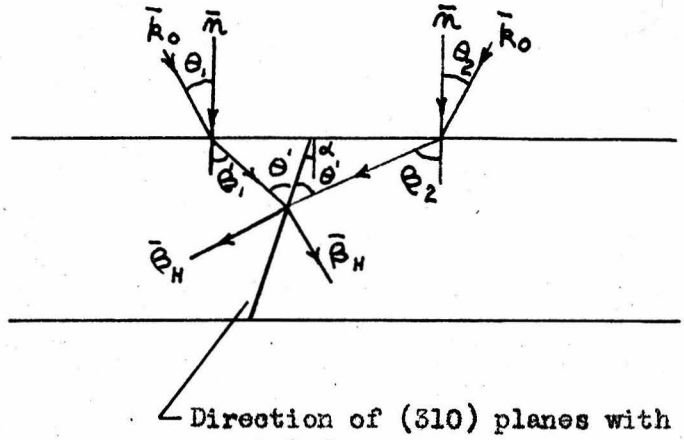

Direction of (310) planes with respect to crystal faces.

When Bragg's law of reflection is satisfied inside the crystal

$$\lambda' = 2d \sin\theta' \qquad \text{E.1}$$

The index of refraction is related to the wavelengths and sine of the angles θ and β by

$$\mu = 1 - \delta = \frac{\lambda}{\lambda'} = \frac{\sin\theta}{\sin\beta} \qquad \text{E.2}$$

and

$$\cos\beta \approx \frac{\cos\theta}{\mu}\left(1 - \frac{\delta}{\cos^2\theta}\right)$$

From Eq. E.1 θ_1 is related to λ by

$$\lambda = \mu\lambda' = \mu\, 2d \sin\theta' = \mu\, 2d \sin(\beta_1+\alpha)$$

where $\theta' = \beta + \alpha$

$$\lambda = 2d\left[\sin\beta_1\cos\alpha + \cos\beta_1\sin\alpha\right]\mu$$

Making the substitutions from E.2

$$\lambda = 2d\left[\sin\theta_1\cos\alpha + \sin\alpha\cos\theta_1\left(1 - \frac{\delta}{\cos^2\theta_1}\right)\right]$$

$$\lambda = 2d\left[\sin(\theta_1+\alpha)\right]\left\{1 - \frac{\delta\sin\alpha}{\cos\theta_1(\sin(\theta_1+\alpha))}\right\} \qquad \text{E.3}$$

The relation connecting θ_2 and λ where

$$\theta' = \beta_2 - \alpha, \text{ is similarly}$$

$$\lambda = 2d \sin(\theta_2 - \alpha)\left\{ 1 + \frac{\delta \sin \alpha}{\sin(\theta_2 - \alpha) \cos \theta_2} \right\} \qquad \text{E.4}$$

Adding Eqs. E.3 and E.4 gives

$$2\lambda = 2d \left\{ \sin(\theta_1 + \alpha) + \sin(\theta_2 - \alpha) + \delta \sin\alpha \left(\frac{1}{\cos \theta_2} - \frac{1}{\cos \theta_2} \right) \right\}$$

$$2\lambda = 2d \left\{ 2 \sin \frac{\theta_1 + \theta_2}{2} \cos\left(\frac{\theta_1 - \theta_2}{2} + \alpha \right) + \frac{\delta \sin\alpha (\cos \theta_1 - \cos \theta_2)}{\cos^2\theta} \right\}$$

$$\text{let } \phi = \frac{\theta_1 - \theta_2}{2}$$

$$2\lambda = 2d \left\{ 2 \sin \frac{\theta_1 + \theta_2}{2} \cos (\phi + \alpha) - 2\delta \frac{\sin \alpha \sin \frac{\theta_1 + \theta_2}{2} \sin \phi}{\cos^2 \theta} \right\}$$

$$\lambda = 2d \sin \frac{\theta_1 + \theta_2}{2} \left\{ \cos (\phi + \alpha) - \delta \frac{\sin \alpha \sin \phi}{\cos^2 \theta} \right\} \qquad \text{E.5}$$

From the figure

$$\beta_2 - \alpha = \beta_1 + \alpha$$

or $\cos(\beta_2 - \alpha) = \cos (\beta_1 + \alpha)$. Expanding and using

$$\cos \beta \approx \frac{1}{\mu} \cos \theta \left(1 - \frac{\delta}{\cos^2 \theta}\right)$$

$$\cos \beta_2 \cos\alpha + \sin \beta_2 \sin\alpha = \cos \beta_1 \cos\alpha - \sin \beta_1 \sin \alpha$$

$$\cos \theta_2 \left(1 - \frac{\delta}{\cos^2 \theta_2}\right) \cos \alpha + \sin \theta_2 \sin\alpha = \cos \theta_1 \left(1 - \frac{\delta}{\cos^2 \theta_1}\right) \cos \alpha - \sin \theta_1 \sin \alpha$$

$$\cos \theta_2 \cos\alpha + \sin \theta_2 \sin\alpha - \frac{\delta}{\cos \theta_2} \cos\alpha = \cos\theta_1 \cos \alpha - \sin\theta_1 \sin\alpha - \frac{\delta \cos \alpha}{\cos \theta_1}$$

$$-\cos(\theta_2 - \alpha) + \cos(\theta_1 + \alpha) = -\delta \cos\alpha \left[\frac{1}{\cos \theta_2} - \frac{1}{\cos \theta_1} \right]$$

$$2 \sin \frac{\theta_1 + \theta_2}{2} \sin \left(\frac{\theta_1 - \theta_2}{2} + \alpha \right) = \left(\frac{\cos \theta_2 - \cos \theta_1}{\cos^2\theta} \right) \cos\alpha$$

$$2 \sin \frac{\theta_1 + \theta_2}{2} \sin \left(\frac{\theta_1 - \theta_2}{2} + \alpha \right) = -\cos \frac{2 \sin \frac{\theta_2 + \theta_1}{2} \sin \frac{\theta_2 - \theta_1}{2}}{\cos^2 \theta}$$

So $$\sin(\phi+\alpha) = -\delta \frac{\cos\alpha \sin\phi}{\cos^2\theta}$$

$$\sin\phi\cos\alpha + \cos\phi \sin\alpha = -\delta \frac{\cos\alpha \sin\phi}{\cos^2\theta}$$

$$\sin\left(\cos\alpha + \frac{\cos\alpha}{\cos^2\theta}\right) = -\cos\phi \sin\alpha$$

but

$\phi = 1^\circ$; ϕ small, $\cos\phi \approx 1$

so

$$\sin\phi \approx -\tan\alpha\left(1 - \frac{\delta}{\cos^2\theta}\right) \qquad \text{E.6}$$

$$\cos(\phi+\alpha) = \left[1 - \sin^2(\phi+\alpha)\right]^{\frac{1}{2}} = 1 - \frac{\delta^2 \cos\alpha \tan^2\alpha}{\cos^4 0}\left(1 - \delta^2_{(\cdot)}\right)^2 + \cdots$$

$$\cos(\phi+\alpha) \approx 1 - \delta^2 \frac{\cos\alpha \tan^2\alpha}{\cos^4\theta} \qquad \text{E.7}$$

Substituting Eqs. E.5 and E.6 in Eq. E.7 gives

$$\lambda = 2d \sin\left(\frac{\theta_1 + \theta_2}{2}\right)\left\{1 + \frac{\delta \sin^2\alpha}{\cos \cos^2\theta}\right\} \qquad \text{E.8}$$

as Bragg's equation and the correction term due to index of refraction when the diffracting planes make a small angle α to the normal to the crystal faces.

APPENDIX F.

Calculations of $Re^{\frac{\mu_o t_o}{\gamma_o}}$, $P(0)e^{\frac{\mu_o t_o}{\gamma_o}}$, W_θ from the theoretical results derived in Part III.

Atomic and crystal constants used are:

$\frac{e^2}{mc^2} = 2.82 \times 10^{-13}$ cm.

$d = 1.177 \times 10^{-8}$ cm. (310) lattice spacing.

$|F_H| = 21.4$, structure factor.

$V = 112 \times 10^{-24}$ cm^3, volume of the unit cell.

$t_o = 0.10$ cm , thickness of the crystal plates.

a. Anomalous scattering contribution term

$$\ell_o = cA(K = 1)$$

c has been calculated in Appendix B.

$$A(K = 1) = \left(\frac{e^2}{mc^2} \frac{|F_H|}{V} t_o\right) \frac{\lambda}{\cos \theta_B} = 53.5 \frac{\lambda}{\cos \theta_B}$$

λ(Å)	$\cos \theta_B$	$A(K = 1)$	$c \times 10^3$	$\ell_o = cA(K = 1)$	ℓ_o^2
.710	.954	39.73	6.98	0.277	0.0767
.530	.974	29.1	3.90	0.113	0.0128
.320	.991	17.3	1.35	0.0234	0.000547
.211	.996	11.18	0.613	0.00686	0.0000471
.123	.999	6.60	0.259	0.00171	0.00000292

b. Integrated reflecting power as measured by the two crystal spectrometer.

$$Re^{\frac{\mu_o t_o}{\gamma_o}} = \left\{\frac{e^2}{mc^2} \frac{d}{2} \frac{|F_H|}{V}\right\} \frac{\lambda}{\cos \theta_B} \left[\frac{1+\cos^2 2\theta_B + 2\ell_o^2 (1+\cos^4 2\theta_B)}{1+\cos 2\theta_B + \ell_o^2 (1+\cos^3 2\theta_B)}\right]$$

$$\text{let } f_R(\theta_B, \ell) = \left[\frac{1+\cos^2 2\theta_B + 2\ell_o^2(1+\cos^4 2\theta_B)}{1+\cos 2\theta_B + \ell_o^2(1+\cos^3 2\theta_B)}\right]$$

$$\left\{\frac{e^2}{mc^2} \frac{d}{2} \frac{|F_H|}{V}\right\} = 317.5$$

$\lambda(\text{Å})$	$\cos\theta_B$	$f_R(\theta_B, \ell_o)$	$\text{Re}\ \frac{\mu_o t_o}{\gamma_o} \times 10^6$
.710	.954	.977	2.30
.530	.974	.964	1.65
.320	.991	.980	1.00
.211	.996	.994	0.657
.123	.999	.997	0.389

c. Ratio of the peak of the two crystal "parallel" rocking curve to the power of the beam incident on crystal B.

$$P(0)e^{\frac{\mu_o t_o}{\gamma_o}} = \frac{1}{4}\left[\frac{1+\cos\theta_B+3/4\,\ell_o^2(1+\cos^3 2\theta_B)}{1+\cos 2\theta_B+\ell_o^2(1+\cos^3 2\theta_B)}\right]$$

$$= \frac{1}{4} f_P(\theta_B, \ell_o)$$

$\lambda(\text{Å})$	$f_P(\theta_B, \ell_o)$	$P(0)e^{\frac{\mu_o t_o}{\gamma_o}}$
.710	.987	.246
.530	.999	.2498
.320	1.00	.250
.211	1.00	.250
.123	1.00	.250

d. Half width at half maximum of the two crystal parallel rocking curves.

$$W_\theta \approx 2w_\theta \approx \frac{10^6}{4.848}\left\{\frac{2d}{\pi}\frac{e^2}{mc^2}\frac{|F_H|}{V}\right\}\cos\theta_B\lambda\left[\frac{2\,(1+\ell_o^2(\cos^4\theta_B))}{1+2\,\ell_o^2\cos^4\theta_B}-1\right]^{\frac{1}{2}}$$

= seconds of arc

$$\text{Let } f_{W_\theta}(\theta_B, \ell_o) = \left[\frac{2(1+\ell_o^2(\cos^4\theta_B))}{1+2\,\ell_o^2\cos^4\theta_B}-1\right]^{\frac{1}{2}}$$

$$\left\{\frac{2d}{\pi}\frac{e^2}{mc^2}\frac{|F_H|}{V}\right\} = 403$$

$\lambda(\text{Å})$	$\cos\theta_B$	$f_W(\theta_B, \ell_o)$	$W_\theta(\text{sec})$
.710	.954	.942	.530
.530	.974	.990	.424
.320	.991	1.00	.264
.211	.996	1.00	.172
.123	.999	1.00	.103

APPENDIX G.

Sample calculations for $\mathrm{Re}^{\frac{\mu_o t_o}{\gamma_o}}$, $P(0)e^{\frac{\mu_o t_o}{\gamma_o}}$, and W_θ from the experimental data.

The two crystal "parallel" rocking curves were plotted on large millimeter graph paper (75 cm wide) with the definitions as follow:

A = area of "parallel" rocking curve in cm^2

M = counts/min per cm (ordinate)

N = seconds of arc per cm (abscissa)

P_i = counts/min in "straight through" beam

1 second of arc = 4.848×10^{-6} radians

Then

$$\mathrm{Re}^{\frac{\mu_o t_o}{\gamma_o}} = \frac{A \times M \times N \times 4.848 \times 10^{-6}}{P_i}$$

$$= \frac{cm^2 \times \frac{\text{counts}}{\text{min}} \; \frac{1}{cm} \times \frac{\text{seconds of arc}}{cm} \times \frac{\text{radians}}{\text{seconds of arc}}}{\text{counts/min}}$$

= radians

For the first run, No. I, Position I of crystal B, in Appendix G

M = 200 counts/two min per cm

N = 2 seconds of arc/cm

The area was measured with a planimeter. Its readings read twice the area.

Area measurements

Run No.	2A	Δx_i^2	$.673\frac{\sqrt{\Sigma \Delta x_i}}{n}$
1	77.5	.21	
2	77.5	.21	
3	78.2	.14	
4	79.0	.96	
5	78.2	.14	
	390.4	1.56	$.673 \times 0.25 = .216$

Average $2A = 78.08 \pm .28\%$

$A = 39.04$ cm $\pm .28\%$

From Fig. 12, p. 59, $P_i = 30{,}000$ c.p.2m.

From the "parallel" rocking curve

$$P(0)e^{\frac{\mu_o t_o}{\gamma_o}} = \frac{5054-60}{P_i}$$

$$\frac{P_o(0)}{2} = 2497 + 60 = 2557$$

$$Re^{\frac{\mu_o t_o}{\gamma_o}} = 2.52 \times 10^{-6} \text{ radians}$$

$$P(0)e^{\frac{\mu_o t_o}{\gamma_o}} = .167$$

$$W_\theta = 1.10 \text{ seconds of arc.}$$

APPENDIX H.

Experimental results for $Re^{\frac{\mu_o t_o}{\gamma_o}}$, $P(0)e^{\frac{\mu_o t_o}{\gamma_o}}$, and W_θ.

		Position 1 of crystal B (310)			Position 2 of crystal B ($\bar{3}\bar{1}0$)		
Run No.	λ (Å)	$Re^{\frac{\mu_o t_o}{\gamma_o}} 10^6$	$P(0)e^{\frac{\mu_o t_o}{\gamma_o}}$	W_θ(sec)	$Re^{\frac{\mu_o t_o}{\gamma_o}} 10^6$	$P(0)e^{\frac{\mu_o t_o}{\gamma_o}}$	W_θ(sec)
1	.710 ± .0020	2.52	.167	1.10	2.65	.164	1.3
2		2.64	.177	1.10	2.89	.157	1.45
3	.530 ± .0074	1.97	.137	1.05	2.12	.136	1.2
4		2.06	.130	1.35	2.11	.136	1.2
5	.320 ± .0076	1.54	.115	1.2	1.58	.111	1.1
6		1.46	.116	1.0	1.43	.110	0.95
7	.211 ± .002	1.20	.118	.85	1.54	.123	.85
8		1.27	.114	.65	1.69	.122	1.1
9		1.33	.123	.73	1.65	.131	0.8
10		1.38	.136	0.70			
11	.123 ± .0084	0.91	.103	0.70	0.87	.910	0.75
12		0.81	.115	0.50	1.21	0.87	1.00
13		0.94	.127	0.50			

Experimental results of moving the diffracted x-ray beam from crystal A to different positions on crystal B. λ = .710Å. Δd is the horizontal displacement of the beam from the axis of crystal B.

	Position 1 of crystal B (310)			Position 2 of crystal B (310)		
Δd(mm)	$Re^{\frac{\mu_o t_o}{\gamma_o}} 10^6$	$P(0)e^{\frac{\mu_o t_o}{\gamma_o}}$	W_θ (sec.)	$Re^{\frac{\mu_o t_o}{\gamma_o}} 10^6$	$P(0)e^{\frac{\mu_o t_o}{\gamma_o}}$	W_θ (sec.)
3	2.40	.177	0.95	2.65	.158	1.2
3	2.62	.172	1.10			
-3	3.36	.188	1.45	2.62	.155	1.45
-3	3.22	.185	1.5	2.44	.152	1.2
-1	2.44	.160	1.25			
-1	2.51	.159	1.25			

APPENDIX I.

Observations on multiple "parallel" rocking curves.

During the process of finding the parallel positions of crystals A and B for the (310) planes, it was observed that for a given wavelength conditions for diffraction occurred for several positions of crystal B "off parallel" from the parallel setting for the (310) planes. These "off parallel" rocking curves were symmetrical about the parallel rocking curve for the (310) planes, (let us call the center position), that is, if one "off parallel" rocking curve was found at a certain angular rotation of crystal B from the center position, a similar "off parallel" rocking curve would be found by rotating crystal B through the same angle from the center position in the opposite direction. When two "off parallel" rocking curves occurred on one side, the second was at twice the angular rotation of crystal B from the center position as was the first "off parallel" rocking curve. The third was just three times; etc. The number increased as the wavelength decreased.

The amazing part was that on rotating either crystal A or crystal B through 180° the angular spacing between these "off parallel" rocking curves changed. For one combination of crystals A and B the spacing was approximately 38" and in the other it was 8'57". Let arrows give the directions of crystals A and B as shown:

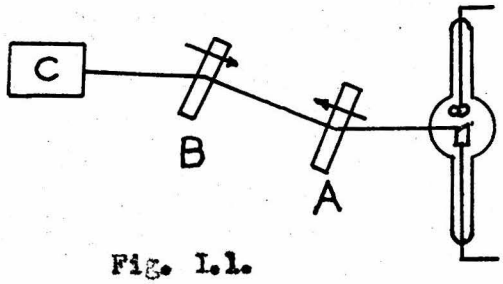

Fig. I.1.

As long as the arrows point in opposite directions (inward or outward) the spacing between the positions of the "off parallel" rocking curves remained the same. But now if the arrows point in the same direction the spacing changes to the other value.

A careful study was made of a large angular region on both sides of the central position for several wavelengths. The region where the "off parallel" rocking curve disappeared on reversing either crystal A or B was carefully studied and nothing was observed above background.

The following table gives the observed positions of crystal B for parallelism of the (310) planes with crystal A, and the positions of crystal B for the observed "off parallel" rocking curves. The magnitude of the peaks of these rocking curves is also given but can only be compared at each wavelength as the sensitivity of the counter changes with wavelength and the x-ray beam intensity was not the same for the different wavelengths.

The effect of these multiple parallel positions was eliminated in the wavelength determination given in Part V. As the "antiparallel" rocking curve is 2' or arc or less, the arrangement to give the 9' spacing was always used. When crystal B was rotated 180° to select a new setting of the worm wheel crystal A was rotated 180° so that the 9' spacing still existed.

TABLE I-1

Positions → ← or ← → of crystals. See Fig. I.1

λ(Å)	Settings (θ) Magnitude	Side Reflections		(Central position)	Side Reflections		Ave. Angular Spacing
.710	θ c.p.2m						
.350	θ c.p.2m (Bkgd. 50)		901°30'33" 2209	901°31'9" 5122	901°3'43¼" 3250		36½"
.210	θ c.p.2m (Bkgd. 50)		905°2'53" 725	905°3'34" 7700	905°4'16½" 3551		41 3/4"
.123	θ c.p.5m (Bkgd.400)	907°14'23¾" 540	907°15'3/4" 934	907°15'39½" 4479	907°16'16" 1872	907°16'54½" 1430	907°17'33" 530	38"

Positions ← ← or → → of the crystals.

.710	θ c.p.2m						
.350	θ c.p.2m (Bkgd. 50)		81°22'5½" 1431	81°31'2" 2894	81°39'57½" 1725		8'56"
.210	θ c.p.2m (Bkgd. 50)		84°54'33" 2614	85°3'29" 7400	85°12'29½" 2857		8'58"
.123	θ c.p.5m (Bkgd. 300)	86°57'40" 486	87°6'37¼" 1000	87°15'33½" 3000	87°24'33" 948	87°33'28¾" 900	8'57"